

4

DUE FILE COPY

GL-TR-89-0081
ENVIRONMENTAL RESEARCH PAPERS, NO. 1026

AD-A223 291

Feasibility Study for an Atmospheric Density Specification Satellite

T.L. KILLEEN
A.G. BURNS
B.C. KENNEDY
R.G. ROBLE
F.A. MARCOS



13 March 1989



Approved for public release; distribution unlimited.



IONOSPHERIC PHYSICS DIVISION

PROJECT 4643

GEOPHYSICS LABORATORY

HANSCOM AFB, MA 01731-5000


DTIC
JUN 03 1990
E D

90 06 25 165

"This technical report has been reviewed and is approved for publication"


WILLIAM K. VICKERY
Acting Branch Chief

FOR THE COMMANDER


ROBERT A. SKRIVANEK
Division Director

Qualified requestors may obtain additional copies from Defense Technical Information Center. All others should apply to the National Technical Information Service.

If your address has changed, or if you wish to be removed from the mailing list, or if the addressee is no longer employed by your organization, please notify AFGL/DAA, Hanscom AFB, MA 01731. This will assist us in maintaining current mailing list.

Do not return copies of this report unless contractual obligations or notice on a specific document requires that it be returned.

UNCLASSIFIED

SECURITY CLASSIFICATION OF THIS PAGE

REPORT DOCUMENTATION PAGE				Form Approved OMB No. 0704-0188	
1a. REPORT SECURITY CLASSIFICATION Unclassified			1b. RESTRICTIVE MARKINGS		
2a. SECURITY CLASSIFICATION AUTHORITY			3. DISTRIBUTION / AVAILABILITY OF REPORT Approved for public release; distribution unlimited.		
2b. DECLASSIFICATION / DOWNGRADING SCHEDULE					
4. PERFORMING ORGANIZATION REPORT NUMBER(S) GL-TR-89-0081 ERP, No. 1026			5. MONITORING ORGANIZATION REPORT NUMBER(S)		
6a. NAME OF PERFORMING ORGANIZATION Geophysics Laboratory		6b. OFFICE SYMBOL (If applicable) LIS		7a. NAME OF MONITORING ORGANIZATION	
6c. ADDRESS (City, State, and ZIP Code) Hanscom AFB Massachusetts 01731-5000			7b. ADDRESS (City, State, and ZIP Code)		
8a. NAME OF FUNDING / SPONSORING ORGANIZATION		8b. OFFICE SYMBOL (If applicable)		9. PROCUREMENT INSTRUMENT IDENTIFICATION NUMBER	
8c. ADDRESS (City, State, and ZIP Code)			10. SOURCE OF FUNDING NUMBERS		
PROGRAM ELEMENT NO. 62101F		PROJECT NO. 4643		TASK NO. 14	WORK UNIT ACCESSION NO. 01
11. TITLE (Include Security Classification) Feasibility Study for an Atmospheric Density Specification Satellite					
12. PERSONAL AUTHOR(S) Killeen, T.L.*, Burns, A.G.*, Kennedy, B.C.*, Roble, R.G.**, and Marcos, F.A.					
13a. TYPE OF REPORT Scientific Interim		13b. TIME COVERED FROM _____ TO _____		14. DATE OF REPORT (Year, Month, Day) 1989 March 13	
15. PAGE COUNT 86					
16. SUPPLEMENTARY NOTATION * Space Physics Research Laboratory, University of Michigan, Ann Arbor, MI 48109 ** High Altitude Observatory, NCAR, Boulder, CO 80302					
17. COSATI CODES			18. SUBJECT TERMS (Continue on reverse if necessary and identify by block number)		
FIELD	GROUP	SUB-GROUP	Atmospheric density, Satellite measurements, Upper atmosphere, Density models, GINMS, etc.		
04	01				
22	03				
19. ABSTRACT (Continue on reverse if necessary and identify by block number) The purpose of the Atmospheric Density Specification (ADS) mission (AFGL-705) is to generate a coordinated and comprehensive global data set of lower thermospheric state variables (density, temperature, and wind) in the altitude range 100 - 300 km. This data set will be analyzed by a team of scientists including experimentalists and theoreticians to improve the performance of the density specification models of this region of the atmosphere, which currently provide density predictions to a typical accuracy of ~15 percent. The instrument complement of the proposed mission includes an ion/neutral mass spectrometer capable of determining absolute neutral densities to ~5 percent, an electrostatic triaxial accelerometer for satellite drag and cross-track wind determination, a Fabry-Perot interferometer for the determination of altitude profiles of vector winds, temperatures and composition, and an ion mass spectrometer capable of determining neutral winds and ion neutral constituent abundances. This study addresses the scientific underpinnings for density specification, orbital lifetimes and geometries, instrument configurations, and theoretical modeling requirements to evaluate the utility of the					
20. DISTRIBUTION/AVAILABILITY OF ABSTRACT <input checked="" type="checkbox"/> UNCLASSIFIED/UNLIMITED <input type="checkbox"/> SAME AS RPT. <input type="checkbox"/> DTIC USERS			21. ABSTRACT SECURITY CLASSIFICATION Unclassified		
22a. NAME OF RESPONSIBLE INDIVIDUAL Frank A. Marcos			22b. TELEPHONE (Include Area Code) (617) 377-3037		22c. OFFICE SYMBOL LIS

DD FORM 1473, JUN 86

Previous editions are obsolete.

SECURITY CLASSIFICATION OF THIS PAGE

UNCLASSIFIED

UNCLASSIFIED

SECURITY CLASSIFICATION OF THIS PAGE

proposed ADS data base for leading towards a reduction in the errors of the density specification models for both total density and density variability. The approach studied involves heavy use of a numerical thermospheric general circulation model (TGCM). The stated goal of the program is to achieve a model rms error of $\sim \pm 5$ percent in total density, with a similar and simultaneous improvement in the operational satellite drag models. This feasibility study describes supporting programs together with data analysis and theoretical modeling tasks that are recommended to complement the ADS mission so that this goal will be met.

UNCLASSIFIED

SECURITY CLASSIFICATION OF THIS PAGE

Accession For	
NTIS GRA&I	<input checked="" type="checkbox"/>
DTIC TAB	<input type="checkbox"/>
Unannounced	<input type="checkbox"/>
Justification	
By	
Distribution/	
Availability Codes	
Dist	
Special	
A-1	



Contents

1. INTRODUCTION	1
2. THE LOWER THERMOSPHERE: REVIEW OF PRESENT UNDERSTANDING	4
2.1 Control of Thermospheric Composition and Density	5
2.2 Energy Budget	15
2.2.1 Global Mean Energy Budget	15
2.2.2 Perturbations About the Global Mean	19
2.3 Dynamical Considerations	21
2.4 Gravity Wave and Planetary Wave Forcing	26
2.5 Summary of the Theoretical Considerations Pertaining to Lower Thermosphere Density Specification	37
3. REVIEW OF MODELING TECHNIQUES FOR DENSITY	38
3.1 Semi-Empirical Models	38
3.1.1 Inherent Accuracy of Contributing Sensors	41
3.1.2 Errors in the Extrapolation Procedures	43
3.1.3 Limited Temporal and Spatial Resolution	43
3.1.4 Limited Experimental Coverage and/or Unmodeled and Unpredicted Systematic Variations	44
3.1.5 Inherent Stochastic Nature of Atmospheric Variability	46
3.1.6 Summary of Future Improvements	46
3.2 Dynamical Models TGCMS	46
3.2.1 Current Performance of the NCAR-TGCM for Density Specification	48
4. AFGL DENSITY SPECIFICATION WORKSHOP RECOMMENDATIONS	51
4.1 Status of Semi-Empirical Models	54
4.2 Workshop Recommendation for Density Specification Program	54

Contents

5. MISSION PAYLOAD AND OBSERVABLES	55
5.1 Instrumentation	55
5.1.1 SETA	55
5.1.2 QINMS	56
5.1.3 CADS	56
5.1.4 FPI	56
5.1.4.1 FPI Instrument Description	57
5.1.4.2 Fabry-Perot Interferometer	57
5.1.4.3 Scanning Telescope Optical Design	59
5.1.4.4 Electronics	60
5.1.5 FPI Sensitivity	60
5.1.6 FPI Error Analysis	62
5.1.6.1 Statistical Errors	62
5.1.6.2 Systematic Errors	62
5.1.7 IPDPH	64
5.1.8 EUVS	64
5.1.9 FPI-DENS	64
5.2 Spacecraft and Orbital Parameters	67
5.3 Cross Calibration	67
5.4 Orbit Selection	67
5.4.1 Orbital Motion	68
5.4.2 Satellite Lifetime	69
6. ADS ANTICIPATED DATA RESOURCES AND UTILITY	72
7. CONCLUSIONS	73
7.1 Requirements	74
7.2 Implementation	75
REFERENCES	77

Illustrations

1. Global Cartesian Plots (Latitude and Longitude) of the Major Forcing Terms Controlling the Thermospheric Density at 120 km Altitude from NCAR-TGCM Calculations	11
2. As for Figure 1, Except that the Altitude of the Calculations is 320 km	12
3. Polar Plots of the Total Density and Density Forcing Terms	13
4. Calculated Log_{10} Profiles of Thermospheric Heating Rates ($\text{ergs g}^{-1}\text{s}^{-1}$) for (a) Solar Minimum and (b) Solar Maximum Conditions	17
5. Calculated Log_{10} Profiles of Neutral Gas Heating and Cooling Rates ($\text{ergs g}^{-1}\text{sec}^{-1}$) for (a) Solar Minimum and (b) Solar Maximum Conditions	18
6. Climatological Upper Thermospheric Neutral Wind Map for UT Bins Centered at 07:00, 09:00, and 11:00 hrs UT (Top to Bottom)	23
7. Comparison Between DE-2 Equatorial Upper Thermospheric Zonal Wind Averages (Wharton et al., 1984) and the Predictions of the NCAR-TGCM	24
8. Contours Giving the Probability of Occurrence of a Fluctuation Amplitude as Large or Larger than the Ordinate at a Particular Magnetic Latitude (Abcissa) for (a) Long Wavelength (400-4000 km) Waves and (b) Short Wavelength (40-400 km) Waves	27
9. Calculated Vertical Wind Perturbations at 300 km from the NCAR-TGCM for a Model Run Simulating a Discrete Geomagnetic Storm	28
10. Measured Variations in Specific Spatial Scales as Measured Using the SETA Instrument for Orbit 151	30
11. As for Figure 10, Except for Orbit 309	31
12. Power Spectrum for SETA Measured Density Fluctuations During Julian Day 79094-95	32
13. As for Figure 12, Except for Julian Day 79084	33
14. Integral Power Spectrum, Illustrating the Percentage Power Remaining at Scales Smaller than the Abcissa for the SETA Measurements from Julian Day 79094-5	35

Illustrations

15. As for Figure 14, Except for Julian Day 79084	36
16. Comparison Between Measurements of Total Density on the AE-C Spacecraft Using the MESA, OSS and NACE Instruments	42
17. Comparison Between Calculations from the NCAR-TGCM and the MSIS-83 Models for the March 22, 1979 Substorms (Roble et al., 1987)	45
18. (a) Calculated Standard Deviations from the Mean as a Function of Latitude for the Geomagnetically Quiet Two Day Period Centered on Julian Day 81325	49
(b) Same Comparison for the 3-Day Geomagnetically Active Period Centered on Julian Day 82328	50
19. (a) Calculated Relative Errors Obtained by Ratioing the TGCM and MSIS-86 Model Predictions to the Measured Atomic Oxygen Densities on a Point-by-Point Basis, Binning by Latitude and Obtaining the Standard Deviation About the Mean Ratio for Each Bin	52
(b) Same Comparison for the 3-Day Geomagnetically Active Period Centered on Julian Day 82328	53
20. Optical Schematic of ADS Fabry-Perot Interferometer	58
21. Baffle Schematic for ADS Fabry-Perot Interferometer	58
22. ADS Fabry-Perot Interferometer Spectrogram Output	59
23. Electronic Functional Block Diagram for the ADS Fabry-Perot Interferometer	61
24. Errors on Derived Winds and Temperatures for the ADS Fabry-Perot Interferometer	63
25. Changes in Spectral Signature of the O ₂ (0-0) Atmospheric Band Due to Changes in Rotational Temperature	65
26. Number of 0.22 Seconds Integration Times Necessary to Achieve a 1° Rotational Temperature Error in the Daytime Thermosphere as a Function of Altitude Using the ADS-FPI	66
27. Orbital Decay Histories	70
28. Satellite Lifetime Versus Initial Eccentricity	71
29. Instrument Schematic	72

Tables

1. Global Mean Thermospheric Energy Budget	16
2. Density Ratio to MSIS-86 for N ₂ , O and He when Ap<11	39
3. NCAR-TGCM Inputs and Outputs (Version 4)	47
4. ADS Mission Complement	55
5. ADS-FPI Instrument Sensitivity	60
6. Spacecraft and Orbit Parameters	67

Feasibility Study for an Atmospheric Density Specification Satellite

1. INTRODUCTION

Rapid progress in understanding and theoretically modeling the state variables of the Earth's upper atmosphere (temperature, density, wind, and composition) has been sustained over the past decade, with several coordinated experimental programs, such as the NASA Atmosphere Explorer (AE) and Dynamics Explorer (DE) missions and the U.S. Air Force Space Test Program, providing important global-scale experimental data sets in various altitude regions. The fundamental theoretical understanding of the upper atmosphere has greatly benefitted from these programs and a new generation of sophisticated numerical models (thermospheric general circulation models, TGCs) has been tested and constrained by the global data sets thereby obtained. The morphological description of the structure of the upper atmosphere has also improved due to the continued development and enhancement of semi-empirical models, such as the Mass Spectrometer-Incoherent Scatter (MSIS) model (Hedin, 1983¹; 1987²; 1988³) and the earlier Jacchia models based on satellite

(Received for publication 8 March 1989)

1. Hedin, A.E. (1983) A revised thermospheric model based on mass spectrometer and incoherent scatter data: MSIS-83, *J. Geophys. Res.* **88**:10170-10188.
2. Hedin, A.E. (1987) MSIS-86 thermospheric model, *J. Geophys. Res.* **92**:4649-4662.
3. Hedin, A.E. (1988) CIRA-88, Chapter 1, The empirical model atmosphere: Atmospheric model in the region 90 to 2000 km, in press, Pergamon Press.

drag measurements (Jacchia, 1965⁴; 1971⁵; 1977⁶). The U.S. Air Force operational models of thermospheric density and temperature are currently based on such semi-empirical models, which reflect the mean behavior of the thermosphere as described by the large bodies of data from the various previous experimental programs. The semi-empirical models use analytical functions to fit to randomly-selected subsets of the available data and spectral coefficients are generated that can be used conveniently to reconstitute thermospheric densities and temperatures as a function of space, time, and geomagnetic and solar activity levels.

Unfortunately, the combination of progress in scientific understanding and progress in quantitative semi-empirical modeling described briefly above has not yet led to operational models of thermospheric density (providing mean values or standard deviations about the mean) with accuracies of much better than ~15 percent in the altitude range 100-300 km (Hedin, 1987²). Furthermore, recent efforts to improve the accuracy of the operational models by incorporating additional experimental data (such as the DE neutral compositional data set) into the semi-empirical models have not markedly improved the situation (Marcos, 1985⁷, 1987⁸; Hedin, 1987²; Hedin and Mayr, 1987⁹). The operational model accuracies are somewhat better at low latitudes and for geomagnetic quiet times (typically ~12-15 percent), but density uncertainties at high latitudes during geomagnetic storm periods often exceed ~50 percent. The U.S. Air Force has several requirements for ~5 percent accuracy or better in thermospheric density specification (mean density and variability), and therefore current capabilities of the operational models are not sufficient for many purposes. The reasons for the rather unsatisfactory performance of the operational models are complex and are discussed below in some detail. In general, however, it may be stated that the semi-empirical models themselves are limited by several factors including: 1) the inherent accuracy (or lack thereof) of the contributing sensors providing data for the model fitting procedures, 2) possible errors or inappropriate assumptions in the extrapolation procedures used to interpolate between data points and to extend the range of the empirical model to altitude regions where the data are sparse, 3) limited temporal and spatial resolution in the formulation of the empirical model (for example, MSIS-86 uses 3-hourly Kp values to determine the geomagnetic activity effect that observations show can be much more rapid in reality), 4) limited experimental coverage, and 5) the inherent stochastic nature of atmospheric variability, which might be expected to provide a fundamental limit on the accuracy with which any given geophysical situation can be quantitatively modeled. Any serious attempt to

-
4. Jacchia, L.G. (1964) Static diffusion models of the upper atmosphere with empirical temperature profiles, *Smithsonian Astrophys. Obs. Spec. Rpt. No. 170*, also published in *Smithsonian Contrib. Astrophys.* **8**:215-257, 1965.
 5. Jacchia, L.G. (1971) Revised static models of the thermosphere and exosphere with empirical temperature profiles, *Smithsonian Astrophys. Observ. Spec. Rpt. No.* 332.
 6. Jacchia, L.G. (1977) Thermospheric temperature, density and composition: New models, *Smithsonian Astrophys. Obs. Spec. Rpt. No.* 375.
 7. Marcos, F.A. (1985) Requirements for improved thermospheric neutral density models, Paper AAS85-312, AAS/AIAA Astrodynamics Specialist Conference Proceedings, Vail, CO.
 8. Marcos, F.A. (1987) Accuracy of satellite drag models, Paper AAS 87-552, AAS/AIAA Astrodynamics Specialist Conference Proceedings, Kalispell, MO.
 9. Hedin, A.E. and Mayr, H.G. (1987) Characteristics of wavelike fluctuations in Dynamics Explorer neutral composition data, *J. Geophys. Res.* **92**:11159-11172.

improve the accuracy of semi-empirical models of thermospheric density will have to discuss the relative importance of these various factors.

Because of the lack of significant improvement in the performance of the operational models, it has become evident that a new approach is needed to make headway in this area. Possible avenues include the upgrading of semi-empirical models such as MSIS by additional critical evaluation of existing data sets, incorporating new data sets, and increasing the spatial and temporal resolution. While such improvements to semi-empirical models are discussed below, this report concentrates on the benefits that would accrue from a different type of approach involving coordinated experimental and numerical modeling efforts specifically designed to improve the operational models of upper mesospheric and lower thermospheric density, temperature, and wind. The two major elements of this program are: 1) a spacecraft mission with a low-altitude perigee (~140 km) designed to make redundant and absolutely-calibrated measurements of density, composition, temperature, and wind, with orbital characteristics that enable the required comprehensive coverage of the essential state variables in space and time, and 2) use of the "first-principles" theoretical modeling approach espoused by the National Center for Atmospheric Research (NCAR) thermosphere general circulation model (TGCM). Numerical models, such as the NCAR-TGCM, are, in principle, capable of detailed predictions of thermospheric "weather" at high temporal and spatial resolution. Such a theoretical modeling approach for thermospheric density prediction would be analogous to the manner in which tropospheric general circulation models are used routinely for weather forecasting and hindcasting. The anticipated results of using the combination of these two program elements are discussed in detail in this report. In particular, the benefits of the proposed program are compared critically with estimated improvements that would be realizable with relatively straightforward modifications of the existing semi-empirical models to increase their spatial and temporal resolution.

The spacecraft component of the proposed program is the Air Force Geophysics Laboratory (AFGL) Atmospheric Density Specification (ADS) mission with a payload including the following space-qualified instruments: a quadrupole ion/neutral mass spectrometer (QINMS), a neutral composition and density sensor (CADS), a satellite electrostatic triaxial accelerometer (SETA) and a Fabry-Perot interferometer (FPI). The experimental techniques and the nature of the observables to be measured are described below, together with a discussion of the requirements for additional information from other programs pertaining to the input of energy and momentum into the Earth's upper atmosphere. The basic ADS instrument complement provides for the precise and absolutely calibrated measurement of all thermospheric state variables along the ADS orbital track. The accelerometer provides absolute *in situ* measurements of density, satellite drag, and cross-track winds, as well as a calibration capability for the QINMS and CADS sensors. The QINMS sensor provides measurements of neutral density, neutral composition, ion density and ion composition. The CADS sensor provides absolute measurements of neutral density, temperature and composition, as well as the neutral wind velocity along the satellite vector. The FPI instrument provides altitude profiles of vector neutral winds, temperatures, and volume emission rates of excited species. As can be noted, there is a degree of redundancy in the experimental measurements of the thermospheric state variables. This redundancy is essential for the ADS mission concept in order to cross-calibrate and intercompare the different observational techniques to provide real confidence in the stated absolute accuracy of the measurements.

Global-scale absolute measurements of thermospheric state variables from ADS will provide a self-consistent and rigorous test of both the numerical and semi-empirical models, leading to an improvement in their predictive capability. Recent experience with the NASA Dynamics Explorer (DE) program has clearly shown how a well-integrated spacecraft mission, providing observational coverage of all the important parameters, can lead rapidly to significant new understanding and modeling capabilities - for the DE case at upper thermospheric altitudes. In this report, we estimate potential improvements in density specification models to be attained in view of our current and evolving theoretical understanding of the lower thermospheric region and the nature of the anticipated ADS data base. Our confidence in the estimates of future improvements for lower-thermosphere density specification is based on a critical evaluation of the available and evolving modeling capability, the likelihood of the creation of a successful ADS data base, and experience gained over the past several years with analogous experimental and theoretical modeling initiatives in the upper thermosphere. The organization of this report is as follows. Section 2 contains a discussion of the current scientific understanding of the domain in question, namely the lower thermosphere between 100 and 200 km. Emphasis is given to the outstanding scientific questions that relate to the control of atmospheric density. Section 3 contains a summary of the capability of both the numerical (first principles) models and the semi-empirical models to predict atmospheric densities. A discussion of future developments and current limitations of the various modeling approaches is also given here, together with a summary of the basic observational requirements for significant future progress in this area. In Section 4, the recommendations of a recent workshop on thermospheric density specification held at AFGL in October 1987 are discussed. In Section 5, the ADS mission concept and proposed payload is described, together with orbital and lifetime considerations and desirable enhancements to the basic payload. Section 6 describes the nature of the data base to be obtained by the ADS instruments, as well as the desired complementary sources of information necessary to quantify the inputs of energy and momentum to the thermosphere. Section 7 contains a discussion of the improvements in modeling techniques and capabilities to be anticipated as a result of the ADS program and presents the major conclusions and recommendations of this study.

2. THE LOWER THERMOSPHERE: REVIEW OF SCIENTIFIC PROBLEMS AND PRESENT UNDERSTANDING

While the prime focus of this report is to lead towards an improved description of total mass density in the lower thermosphere, it is clear from theoretical considerations that mean densities, as well as density perturbations, are inextricably linked in a causal sense to dynamical, compositional, and thermal structures in the atmosphere and are, therefore, dependent on the entire range of thermal, chemical, dynamical, and radiative processes occurring in the thermospheric gases.

Although a full scientific understanding of the physics and chemistry of the domain may not be necessary for a wholly *empirical* approach to density specification, such an understanding is essential for any approach involving either numerical models or semi-empirical models. For a numerical model, physical understanding is an obvious prerequisite to the appropriate formulation of the governing equations and their boundary conditions. For a semi-empirical model, any data extrapolation technique used to interpolate between measured data points and to extend the range of

the model from data-rich regions to data-sparse regions requires a mathematical formulation having some physical meaning in the real atmosphere. Because of the high cost (relative to meteorological instruments, for example) of deployment of instruments designed to measure the density of the upper atmosphere, the vast nature of the domain in question, and the complexity and variability of the thermospheric medium, a successful *purely empirical* model is almost certainly out of the question for the present and the foreseeable future. All the data-based models discussed in this report and in current use are semi-empirical; that is, there is some physical treatment used to extrapolate from the available data (such as the assumption of diffusive equilibrium or a Bates model form to the thermal structure, etc.). Thus, even this class of model is dependent in a very direct way on the validity of the scientifically-based assumptions used in the data extrapolation and fitting procedures. We therefore start the discussion by reviewing our basic scientific understanding of the lower thermosphere and by pointing out some of the significant experimental uncertainties that limit that understanding. In the following discussion, the major points requiring attention within the proposed Air Force density program are italicized for emphasis. A short summary of the principal theoretical considerations is given at the end of the section.

2.1 Control of Thermospheric Composition and Density

The governing (or "primitive") equations of the thermosphere are basically given by appropriate expressions for the conservation of mass, momentum, and energy for the gas as a whole, as well as for the individual species within the gas. These equations may be derived by taking the first three moments of the Boltzmann transfer equation (that is, Schunk¹⁰), where certain assumptions are generally made regarding the form of the viscous stress tensor and the heat flux vector (from higher order moments) to close the set of equations. The conservation equations are coupled and require appropriate boundary conditions and information on a number of transport parameters (such as coefficients of viscosity, thermal conduction, and eddy diffusion) for their solution. The transport parameters are obtained either experimentally or from considerations of gas kinetic theory. This theoretical formulation is considered to be sufficiently accurate for all practical purposes involving neutral densities and composition, although some of the assumptions are questionable in certain domains (generally high altitudes) involving ionospheric and magnetospheric plasma populations.

The basic mechanisms that control the composition and thereby the total density of the thermosphere are perhaps best appreciated by considering the individual species continuity equation. Although we are mainly interested here with total density, a knowledge of thermospheric composition is required for a complete specification of the region. Moreover, without a knowledge of composition (mean molecular mass), it is impossible to extrapolate total density from one location to another in the vertical direction without incurring significant error. It is therefore important to understand the processes responsible for the control of thermospheric composition.

In the altitude range of interest, the three major neutral species are O, O₂, and N₂, with O being lighter than the mean mass and O₂ and N₂ being heavier than the mean mass. Above the turbopause (near 105-110 km altitude), the process of molecular diffusion tends to return the major constituents

10. Schunk, R.W. (1975) Transport equations for Aeronomy, *Planet. Space Sci.* **23**:437.

towards individual "diffusive equilibrium" profiles given by their respective masses. Since molecular nitrogen is largely chemically inert, it maintains a profile that resembles one of diffusive equilibrium, but one that can also be perturbed significantly by dynamical and thermal processes. Atomic and molecular oxygen, on the other hand, are controlled by both chemical production and loss (photodissociation and recombination) as well as by dynamical and diffusive processes. The assumption of diffusive equilibrium (i.e. zero diffusive flux) may not always be justified (Mayr et al., 1978¹¹; Burns et al., 1988¹²; Rees et al., 1988¹³), even in a relatively quiet atmosphere and for inert species, such as molecular nitrogen.

The continuity equation for a single thermospheric species may be written in terms of the partial derivative with time of the mass mixing ratio, Ψ_i , of the i^{th} species. We use horizontal spherical coordinates and a log pressure vertical coordinate (λ, ϕ, z), where λ = longitude, ϕ = latitude and $z = \ln(P_0/P)$, P is the pressure, and P_0 (= 50 μ Pa) is a reference pressure, to write the following vector equation for the mass mixing ratio of each species (this is the form used in NCAR-TGCM, see Dickinson et al.¹⁴)

$$\begin{aligned} \frac{\partial \tilde{\Psi}}{\partial t} = & - \frac{e^z}{\tau} \frac{\partial}{\partial z} \left[\frac{\bar{m}}{m_{N_2}} \left(\frac{T_{00}}{T} \right)^{0.25} \frac{L}{\bar{\alpha}} \tilde{\Psi} \right] \\ & + e^z \frac{\partial}{\partial z} \left[K(z) e^{-z} \frac{\partial \tilde{\Psi}}{\partial z} \right] - \left[\vec{V} \cdot \nabla \tilde{\Psi} + w \frac{\partial \tilde{\Psi}}{\partial z} \right] + \tilde{S} - \tilde{R} \end{aligned} \quad (1)$$

The terms on the right hand side of this equation represent, respectively, the changes in the composition due to molecular diffusion, eddy diffusion, horizontal and vertical advection, and chemical production and loss. The vector mass mixing ratio is given by $\tilde{\Psi} = (Y_{O_2}, Y_O)$ and Ψ_i is defined by:

$$\Psi_i = \frac{n_i m_i}{\sum_j n_j m_j} \quad (2)$$

\vec{V} = the horizontal velocity vector; u = the eastward neutral velocity; v = the northward neutral velocity; w = the vertical neutral velocity; T = temperature; n_i is the number density of the i^{th} species, and m_i is the mass of the i^{th} species. Other parameters include D , the molecular diffusion coefficient given by

-
11. Mayr, H.G., Harris, I., and Spencer, N.W. (1978) Some properties of upper atmosphere dynamics, *Rev. Geophys. and Space Phys.* **16**:539.
 12. Burns, A.G., Killeen, T.L., and Roble, R.G. (1989) Processes responsible for the compositional structure of the thermosphere, *J. Geophys. Res.* **94**:3670-3686.
 13. Rees, D., Fuller-Rowell, T.J., and Rishbeth, H. (1988) The use of mass spectrometer measurements to derive thermospheric temperature and density, *Planet. Space Sci.* **36** 281-290.
 14. Dickinson, R.E., Ridley, E.C., and Roble, R.G. (1984) Thermospheric general circulation with coupled dynamics and composition, *J. Atmos. Sci.* **41**:205-219.

$$D = D_0 \left[\frac{P_{00}}{P} \right] \left[\frac{T}{T_{00}} \right]^{1.75} \quad (3)$$

where D_0 is a characteristic diffusion coefficient at pressure P_{00} and temperature T_{00} ($= 2 \times 10^{-9} \text{ cm}^2 \text{ s}^{-1}$), H_0 is the characteristic molecular nitrogen scale height at $T_{00} = 273\text{K}$ ($= 8.63 \text{ km}$), J_{O_2} is the molecular oxygen photodissociation rate; k is a rate coefficient for three-body ($O + O + M \rightarrow O_2 + M$) recombination of atomic oxygen given by $k = 3.8 \times 10^{-30} \exp(-170/T)/T$ for $M = O_2$ (Johnson, 1968¹⁵) and $k = 4.8 \times 10^{-33}$ for $M = N_2$ (Campbell and Gray, 1973¹⁶). $K(z)$ is the eddy diffusion coefficient, \bar{m} the mean mass, P_{00} is the atmospheric pressure at the ground ($= 10^5 \text{ Pa}$), $T_{00} = 273\text{K}$, τ is the diffusion time scale. The mixing ratio of N_2 is defined as

$$\Psi_{N_2} = 1 - \Psi_{O_2} - \Psi_O \quad (4)$$

Photodissociation provides a source of O given by:

$$\tilde{S} = J_{O_2} \begin{bmatrix} -\Psi_{O_2} \\ +\Psi_{O_2} \end{bmatrix} \quad (5)$$

and three body recombination provides a source of O_2 and a sink of O. The α_{ij} in the first term on the right hand side of Eq. (1) are given by:

$$\begin{aligned} \alpha_{11} &= -[\phi_{13} + (\phi_{12} - \phi_{13}) \cdot \Psi_2] \\ \alpha_{22} &= -[\phi_{23} + (\phi_{21} - \phi_{23}) \cdot \Psi_1] \\ \alpha_{12} &= (\phi_{12} - \phi_{13}) \cdot \Psi_1 \\ \alpha_{13} &= (\phi_{21} - \phi_{23}) \cdot \Psi_2 \end{aligned} \quad (6)$$

where the subscript 1 denotes O_2 ; 2 denotes O; and 3 denotes N_2 . The ϕ_{ij} are defined by:

$$\phi_{ij} = \left(\frac{D}{D_{ij}} \right) \left(\frac{m_3}{m_j} \right) \quad (7)$$

where D_{ij} is the mutual diffusion coefficients given by Colegrove.¹⁷ The matrix operator \mathbf{L} has elements:

-
15. Johnson, H.S. (1968) Gas phase kinetics of neutral oxygen species, NBS-NSRSDS-20, U.S. Government Printing Office, Washington, DC.
 16. Campbell, I.M. and Gray, C.N. (1973) Rate constants for $O(^3P)$ recombination and association with $N(^4S)$, *Chem. Phys. Lett.* **18**:607-609.
 17. Colegrove, F.D. (1966) Atmospheric composition in the lower thermosphere, *J. Atmos. Terr. Phys.* **37**:1563-1570.

$$L_{ij} = \delta_{ij} \left(\frac{d}{dz} - \epsilon_{ij} \right) \quad (8)$$

where δ_{ij} is the delta function and ϵ_{ij} is defined by

$$\epsilon_{ii} = 1 - \frac{m_i}{\bar{m}} - \frac{1}{\bar{m}} \left[\frac{\partial \bar{m}}{\partial z} \right] \quad (9)$$

The L matrix defines diffusive equilibrium solutions through the equation $\mathbf{L}\tilde{\Psi} = 0$. Departures from diffusive equilibrium are driven by the hydrodynamic transport and the chemical terms in Eq. (1). The equation for total mass continuity can be obtained by summing the individual species continuity equation over all species, leading to:

$$\frac{\partial \rho}{\partial t} + \rho \nabla \cdot \vec{U} + \vec{V} \cdot \nabla \rho + w \frac{\partial \rho}{\partial z} = 0 \quad (10)$$

where ρ is the total mass density and \vec{U} is the total mass-averaged vector velocity and the equation is couched in ordinary cartesian coordinates. The terms on the left hand side of the equation are the local time rate of change of total density, velocity divergence, horizontal advection and vertical advection. In this report we use calculations of the individual terms from the NCAR-TGCM to illustrate the importance of vertical and horizontal winds for the advective control of thermospheric density.

It can be seen from an examination of the above equations that the time dependent mass mixing ratios of thermospheric species are controlled mainly by dynamical (transport) processes, including the advective effects of horizontal and vertical winds, molecular and eddy diffusion. The specification of thermospheric density may be treated conveniently as separable into two parts: 1) the mean density structure that would exist if there were no transport processes operating (that is, the zero flux or diffusive equilibrium solution to the coupled continuity and momentum equations) and 2) perturbations from the mean due to transport processes. The information required to specify the mean density structure as well as the departures from the mean as a function of local time, latitude, longitude, UT, elapsed time, geomagnetic activity, etc. is discussed in the following paragraphs.

First, considering a static atmosphere above the turbopause, the mean density structure at a given location and time is simply determined by the sum of the various individual equilibrium species distributions and is, therefore, primarily dependent on the mean temperature lapse rate which is established, in turn, by the balance among the various mean thermospheric heating and cooling terms (principally, the competition between solar UV/EUV heating and downward thermal conduction). *Thus, to obtain a full understanding of mean thermospheric densities as a function of location, time, season, and solar activity (location in the solar cycle), a detailed knowledge of the mean thermospheric heat sources and sinks is required.* Clearly, a corollary to the above would be a statement that the global mean density profile in the thermosphere is dependent on the globally-averaged energy sources and sinks. The conservation of energy equation (third moment of the Boltzmann transfer equation), therefore, contains the essential physical relationships governing the mean density structure.

Secondly, density perturbations about the mean occur regularly as a function of local time, location, storm time, etc. Such perturbations can, in principle, be modeled rigorously using the conservation equations given above. In general, the chemical sources and sinks appearing in Eq. (1) are of great significance for the O/O_2 ratio but are not very important for total density, since the number of oxygen atoms is conserved. Similarly, the processes of molecular and eddy diffusion, which are of significance for the establishment of the individual species density profiles, are not critically important for total density perturbations. Variations in density are, therefore, caused primarily by dynamical perturbations (for example, the advective effects of vertical and horizontal winds) that are induced, in turn, by either heat or momentum sources. The equation governing thermospheric winds is the conservation of momentum equation (second moment of the Boltzmann transfer equation).

The thermospheric wind systems can be large in scale, such as planetary waves, tides, and the diurnal "breathing" motions of the thermosphere in response to the solar UV/EUV heat sources (upward winds during the daytime and downward winds at night). They can also be small in scale, such as: 1) gravity waves that may propagate far from the region of creation or 2) localized regions of upwelling (caused by local heating) that act as source regions for gravity waves. The large scale day-to-night and summer-to-winter thermospheric flows induced by differential heating give rise to the principal large-scale day-to-night and summer-to-winter horizontal density differences observed in satellite data and in semi-empirical models. The small scale perturbations are correlated with fluctuations in the geomagnetic activity level and are principally responsible for the inherent difficulty in accurately specifying "point" thermospheric density. *In general, therefore, an understanding of density perturbations in the thermosphere requires a full description and understanding of thermospheric motions of all scales and their causes.*

The importance of the quantitative understanding of thermospheric heat sources and sinks and wind systems, emphasized above, leads naturally to the conclusion that the appropriate modeling tool for the study of mean atmospheric density structure and fluctuations about the mean is the thermosphere general circulation model (TGCM) which has the inherent capability of self-consistently calculating density perturbations and neutral wind systems on a global, 3-dimensional, time-dependent basis from fundamental physical principles. Two TGCMs are currently highly developed: the National Center for Atmospheric Research (NCAR) TGCM (Dickinson et al., 1981¹⁸, 1984¹⁴; Roble et al., 1982¹⁹, 1983²⁰; Roble and Ridley, 1987²¹) and the University College London

-
18. Dickinson, R.E., Ridley, E.C., and Roble, R.G. (1981) A three-dimensional, time-dependent general circulation model of the thermosphere, *J. Geophys. Res.* **86**:1499-1512.
 19. Roble, R.G., Dickinson, R.E., and Ridley, E.C. (1982) Global circulation and temperature structure of the thermosphere with high-latitude plasma convection, *J. Geophys. Res.* **87**:1599-1614.
 20. Roble, R.G., Dickinson, R.E., Ridley, E.C., Emery, B.A., Hays, P.B., Killeen, T.L., and Spencer, N.W. (1983) The high latitude circulation and temperature structure of the thermosphere near solstice, *Planet. Space Sci.* **31**:1479-1499.
 21. Roble, R.G. and Ridley, E.C. (1987) An auroral model for the NCAR thermospheric general circulation model, *Annales Geophysicae* **5**:369-382.

TGCM (Fuller-Rowell and Rees, 1980²²; Fuller-Rowell et al., 1987²³). These models use a variety of prescriptions and parameterizations based on geophysical and solar indexes to describe the thermospheric energy inputs and solve the coupled governing equations discussed earlier to calculate all the thermospheric state variables (temperature, density, composition and wind) on a global time dependent grid. Of course, confidence in the reliability of TGCM output fields can only come from extensive model validation using a variety of experimental data sets and case studies. This process of validation is ongoing at the present time, and has already led to some notable successes, particularly at F-region altitudes where DE data have been available to constrain and test the TGCM formulation. In this report, we use calculations from specific model runs of the National Center for Atmospheric Research (NCAR) TGCM to illustrate the current capability of that model to predict thermospheric density.

As discussed above, perturbations in thermospheric densities are largely controlled by the advective effects of thermospheric motions, whereas the mean density structure is controlled largely by the net effect of thermospheric heat sources and sinks. The thermal and dynamical forcings are, of course, strongly coupled through the energy and momentum equations. Thus, for example, a local heat deficit (with respect to a global mean) causes downward motions that tend to reduce the local density, but also lead to subsequent adiabatic heating through compression of the thermospheric gas. It is clear that, for such a non-linear problem, self-consistent numerical techniques, such as those employed in the NCAR-TGCM, offer the only real means of understanding the complicated inter-relationships. Other important models exist, but these (in general) use various levels of questionable approximations to the governing equations to linearize the problem.

A sense of the quantitative relationship among the various direct causal mechanisms that control thermospheric density may be obtained by examination of the NCAR-TGCM calculations shown in Figures 1, 2, and 3, using the diagnostic package of Killeen and Roble.^{24,25} Model calculations of the horizontal advection (Figure 1a) and vertical advection (Figure 1b) density forcing terms [terms 3 and 4 in Eq. (10)] are shown at an altitude of 120 km for a TGCM run corresponding to geophysical conditions of December solstice, solar maximum, with a prescription for tidal forcing at the lower boundary due to Fesen et al.²⁶ The terms are plotted as a function of latitude and longitude for a given UT (21:00 hrs) and are given in units of gms/cm³-sec. The individual forcing terms are

-
22. Fuller-Rowell, T.J. and Rees, D. (1980) A three-dimensional, time-dependent global model of the thermosphere, *J. Atmos. Sci.* **37**:2545-2657.
 23. Fuller-Rowell, T.J., Quegan, S., Rees, D., Moffett, R.J., and Bailey, G.J. (1987) Interactions between neutral thermospheric composition and the polar ionosphere using a coupled ionosphere-thermosphere model, *J. Geophys. Res.* **92**:7744-7748.
 24. Killeen, T.L. and Roble, R.G. (1984) An analysis of the high latitude thermospheric wind pattern calculated by a thermospheric general circulation model, 1, Momentum forcing, *J. Geophys. Res.* **89**:7509-7522.
 25. Killeen, T.L. and Roble, R.G. (1986) An analysis of the high latitude thermospheric wind pattern calculated by a thermospheric general circulation model, 2, Neutral Parcel trajectories, *J. Geophys. Res.* **91**:11291-11307.
 26. Fesen, C.S., Dickinson, R.E., and Roble, R.G. (1986) Simulation of thermospheric tides at equinox with the NCAR thermospheric general circulation model, *J. Geophys. Res.* **91**:4471-4489.

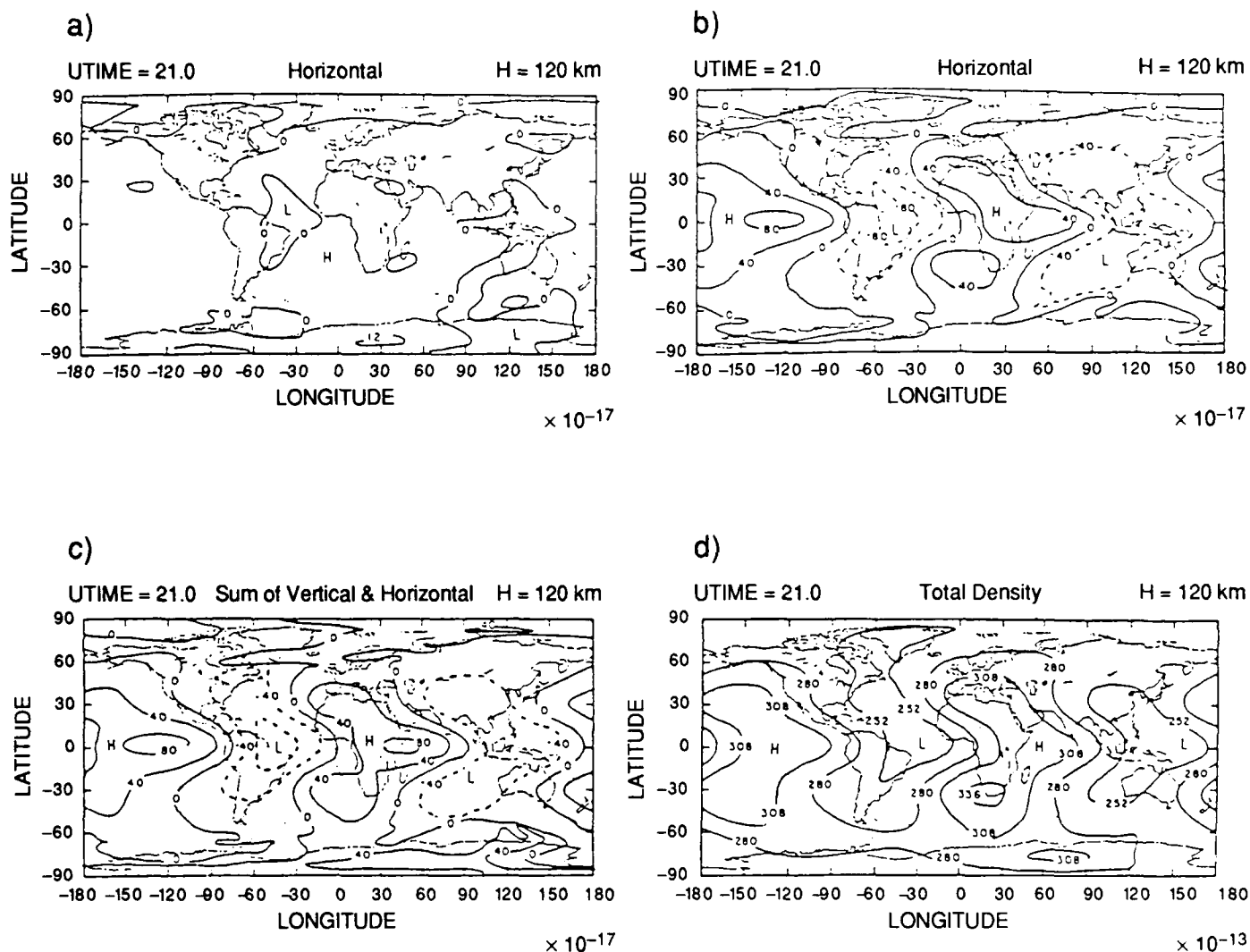


Figure 1. Global cartesian plots (latitude and longitude) of the major forcing terms controlling the thermospheric density at 120 km altitude from NCAR-TGCM calculations. The units used for the forcing terms are $\text{gms cm}^{-3} \text{sec}^{-1} (\times 10^{-20})$ and the terms are a) horizontal advection, b) vertical advection, c) total rate of change in thermospheric density, respectively. Figure 1d shows the calculated total density at this altitude. The model run was for moderate steady geomagnetic activity and solar maximum UV and EUV insolation. The results shown are for a single UT (21:00 hrs).

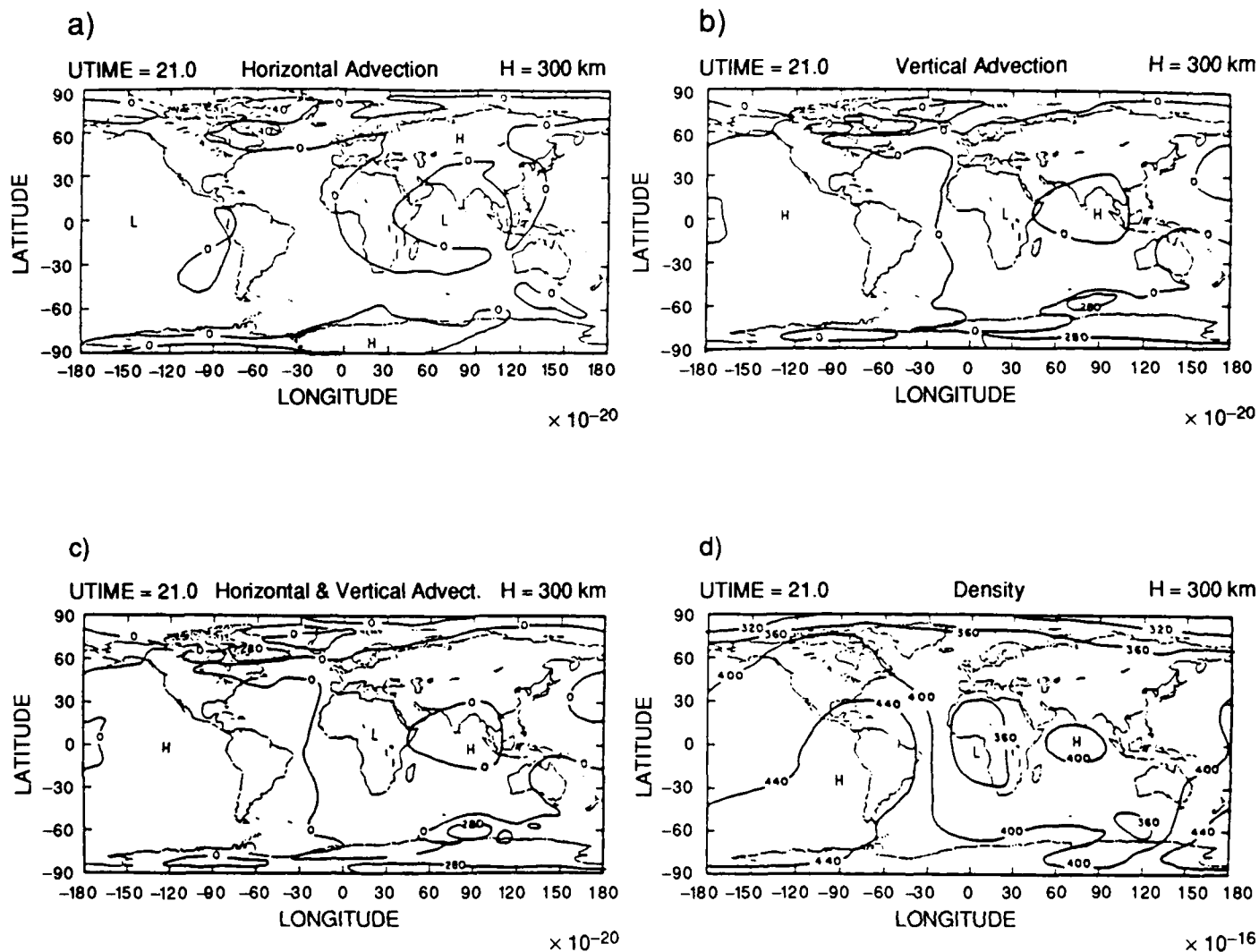


Figure 2. As for Figure 1, except that the altitude of the calculations is 320 km.

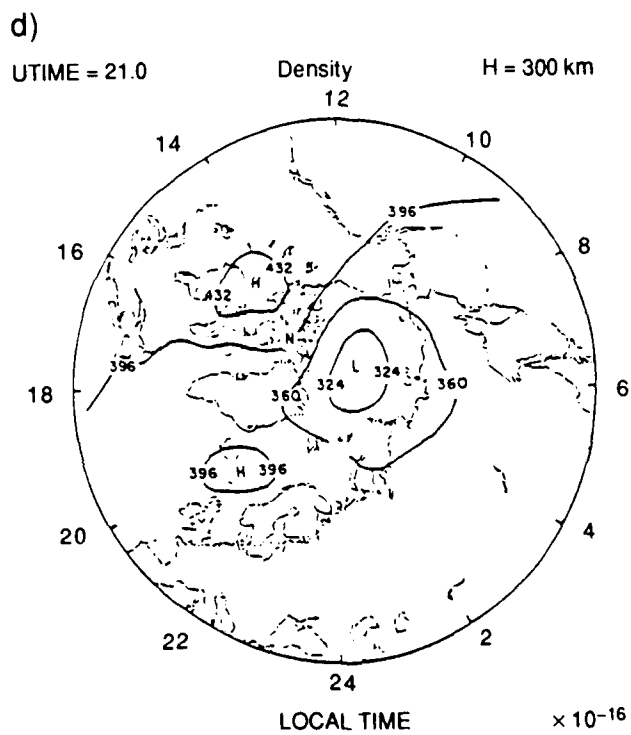
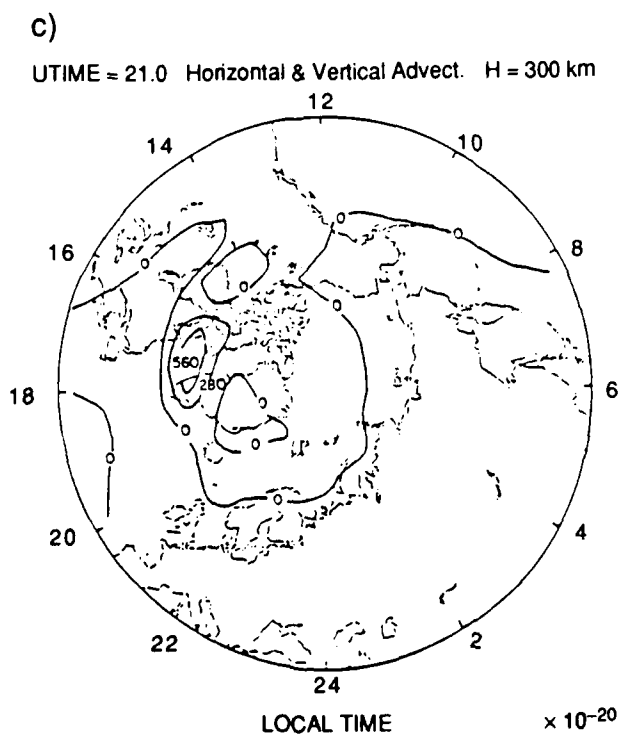
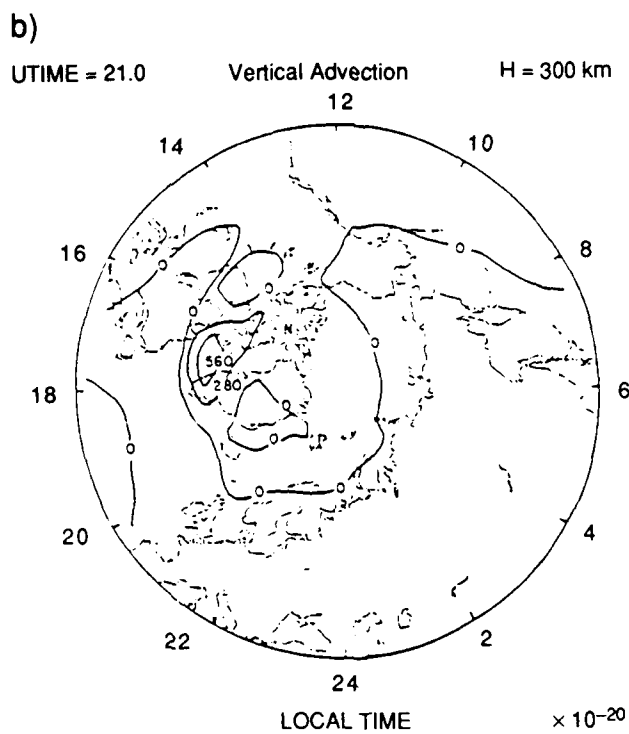
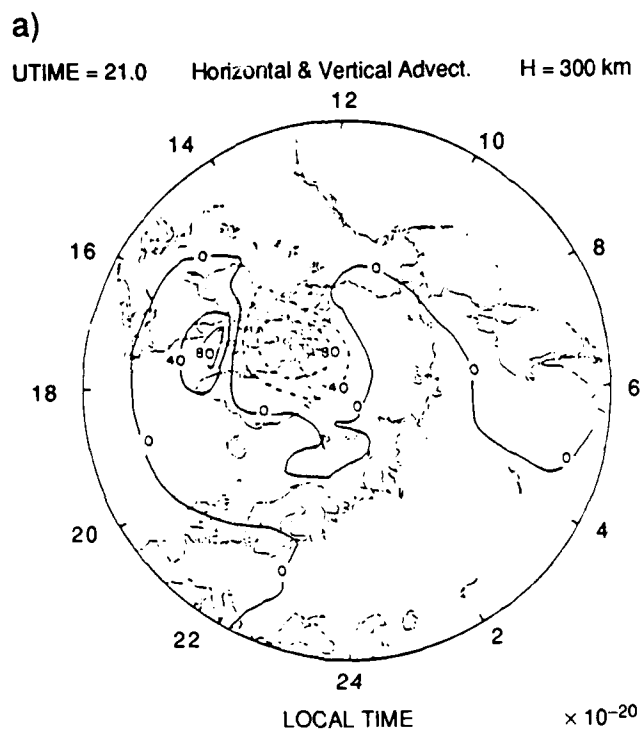


Figure 3. Polar plots of the total density and density forcing terms.

compared with the calculated time rate of change of density at this altitude (Figure 1c) and the total density itself (Figure 1d) given in units of gms/cm^3 . The TGCM run is for the diurnally-reproducible case, that is, the inputs of energy and momentum to the model vary diurnally due only to the diurnally-changing geometrical relationship between the sun and the earth. It can be seen from examination of Figure 1d that, at these altitudes, the global morphology of density is governed largely by the semi-diurnal and diurnal tides. The semidiurnal signature in total density is particularly evident at low latitudes and is clearly governed by the vertical advection term shown in Figure 1b, the horizontal advection term being generally of smaller magnitude (cf Figures 1b and 1c). The calculated density structure is obviously very dependent on the details of the phases and amplitudes of the tides used in the TGCM run. As discussed by Fesen et al.²⁶, the current understanding of global tidal motions is relatively poor and more lower thermospheric measurements of neutral winds, temperatures, and densities are required from networks of ground-based instruments as well as from spaceborne techniques (for example, from the proposed ADS spacecraft). The tidal specification used in the TGCM run illustrated in Figures 1 - 3 may not be realistic in detail, but it does clearly serve to illustrate the strong dependency of thermospheric density on the tides.

The density structure at higher altitudes is further complicated by the strong influence of high-latitude heating. Figure 2 shows the calculated global density structure and the major density forcing terms at an altitude of 300 km using the same TGCM run as for the calculation shown in Figure 1. The semi-diurnal tide is still evident in the total densities, although it is appreciably damped by the dissipative effects of viscosity and ion drag. At these altitudes, the inclusion of tidal forcing is necessary to simulate the observed post-midnight pressure bulge, seen in Figure 2d at equatorial latitudes near 75° E longitude (that is, in the post-midnight sector). Once again, at these altitudes, the effects of vertical winds driven by local heating and cooling processes dominate the calculated density structure. There is a region of relatively high density in the post noon sector at low latitudes and a complementary region of relatively low densities during the nighttime hours at mid- and low-latitudes.

To highlight the important high-latitude density forcing processes, Figure 3 shows the calculated term analysis for the northern polar regions at an altitude of 300 km. The same forcing terms as before are plotted in polar coordinates (latitude and local solar time) from the North pole to 40° N latitude. The density perturbations due to high-latitude effects are clearly evident in the calculations shown in Figure 3d. The density forcing terms (Figures 3a and 3b) have a relatively complicated morphology dependent on the spatial variation of the horizontal and vertical wind systems established by the various high-latitude sources of momentum and energy. The vertical advection term (Figure 3b) has a pattern governed by the vertical winds produced by Joule heating in the auroral zone. The horizontal advection term has a similar but spatially more extensive form governed by the large upper thermospheric horizontal winds. Regions of negative and positive forcing for both the advection terms are evident. The spatial variation of total density (Figure 3d) is relatively smooth by comparison to the more structured individual forcing terms. This is a consequence of the tendency of the neutral atmosphere to integrate out small-scale forcing perturbations because the forces require relatively long time scales to have a significant effect (several hours at these altitudes for moderate geomagnetic activity). The largest perturbations in the total density fields are seen in the auroral regions where strong Joule heating causes large upward winds that are only partially compensated for by divergent horizontal winds. Similar analysis of TGCM model runs for geomagnetic storm times

indicates that the density forcing terms can be much larger, leading to significant and relatively rapid variations of total density such as those reported by Roble et al.²⁷ and Forbes et al.²⁸ from a study of SETA accelerometer data.

2.2 Energy Budget

2.2.1 GLOBAL MEAN ENERGY BUDGET

As mentioned above, the total energy deposited in the thermosphere directly determines the global mean density structure by establishing the temperature lapse rate. Although there are numerous sources and sinks of energy to the thermosphere^{29,30}, the principal source is ultimately due to the absorption of solar UV and EUV radiation and the principal sink is downward thermal conduction towards the cold mesopause. A second important source of energy, caused by magnetospheric-ionospheric coupling, is Joule heating from the dissipation of ionospheric current. The global-mean Joule heating energy source is generally commensurate with and, at times, may be significantly greater than the globally-averaged solar UV and EUV source. Joule heating is a very episodic, patchy, and intrinsically variable phenomenon that is proportional to the square of the magnitude of the vector difference between the ion and neutral mass bulk flow velocities, where the ions are driven into motion by electric fields associated with the solar wind-magnetosphere dynamo interaction. Joule heating, therefore, is dependent on the bulk flow properties of the solar wind, the interplanetary magnetic field magnitude and orientation, the general level of geomagnetic and solar activity, and the time-history of magnetospheric forcing combined with inertial effects in the neutral gas. *A time-dependent specification of magnetospheric energy, particle and momentum inputs will be necessary to accurately model the thermospheric density response to Joule heating.*

The energy deposited in the thermosphere is partitioned and distributed by physical and chemical processes that feed the energy into the neutral gas through a large number of channels. These channels include: neutral heating from photoelectrons; O₂ absorption in the Schumann-Runge continuum and bands; excess energy from exothermic ion-neutral and neutral-neutral chemical reactions; thermal electron, ion, and neutral collisions; O₃ absorption in the Hartley bands; energy liberation during atomic oxygen recombination; cooling from molecular and eddy thermal conduction; NO and CO₂ radiation. A recent comprehensive review of the global mean energy balance

-
27. Roble, R.G., Forbes, J.M., and Marcos, F.A. (1987) Thermospheric dynamics during the March 22, 1979 magnetic storm, *J. Geophys. Res.* **92**:6045-6068.
 28. Forbes, J.M., Roble, R.G., and Marcos, F.A. (1987) Thermospheric dynamics during the March 22, 1979, Magnetic storm 2. Comparisons of model predictions with observations, *J. Geophys. Res.* **92**:6069-6081.
 29. Roble, R.G., Killeen, T.L., Carignan, G.R., Spencer, N.W., Heelis, R.A., Reiff, P.H., Winningham, J.D., and Evans, D.S. (1988) Thermospheric dynamics during 21/22 November 1981: Dynamics Explorer measurements and TGCN predictions, *J. Geophys. Res.* **93**:209.
 30. Killeen, T.L. (1987) Energetics and dynamics of the earth's thermosphere, *Rev. Geophys.* **25**:433-454.

of the thermosphere was given by Roble et al.³¹ Figures 4 and 5, taken from this paper, illustrate the general characteristic shape of the calculated global mean vertical profiles of thermospheric heating and cooling rates, respectively, for both solar maximum and solar minimum conditions. The precise specification of these profiles depends on a thorough knowledge of many aeronomical chemical processes - for example, quenching rates of metastable states, ion-neutral collision rates and specific reaction rates, photodissociation rates for molecular oxygen, etc. The profiles are also critically dependent on the specification of the solar UV and EUV fluxes to the top of the atmosphere. Unfortunately, these fluxes have not been measured directly very often (notably on the Atmosphere Explorer spacecraft^{32,33}), and they therefore represent a major potential source of ongoing uncertainty for the specification of global mean energy inputs and global mean densities. The TGCM models generally use the Hinteregger fluxes as model input, scaled by indirect "proxy" indices, such as the F10.7 cm flux index, to estimate the radiative UV-EUV flux input to the thermosphere. A summary of the calculated global mean thermospheric energy budget in a columnar sense is given in Table 1, taken from Roble et al.³¹

Table 1. Global Mean Thermospheric Energy Budget

	Energy (10^{11} W)	
	Solar Minimum	Solar Maximum
Input solar energy absorbed		
EUV	2.1	6.33
S-R continuum	12.0	15.20
Neutral gas heating		
S-R continuum	4.17	5.59
S-R bands	0.98	0.96
Neutral-neutral chemistry	0.60	1.99
Ion-neutral chemistry	0.29	0.80
Electron-ion collisions	0.14	0.57
O(¹ D) quenching	0.17	0.33
O recombination	0.29	0.38
O ₃ absorption	0.29	0.32
Aurora (direct particle)	0.01	0.01
Joule	0.70	0.71
Total heating	7.64	11.66
IR Cooling		
CO ₂	5.87	5.95
NO	0.41	3.05
O(³ P)	0.23	0.36
Total IR cooling	6.51	9.36
S-R indicates Schumann-Runge.		

-
31. Roble, R.G., Ridley, E.C., and Dickinson, R.E. (1987) On the global mean structure of the thermosphere, *J. Geophys. Res.* **92**:8745-8758.
 32. Hinteregger, H.E. (1981) Representations of solar EUV fluxes for aeronomical applications, *Adv. Space Res.* **1**:39.
 33. Hinteregger, H.E., Fukui, K., and Gilson, B.R. (1981) Observational, reference and model data on solar EUV, from measurements on AE-E, *Geophys. Res. Lett.* **8**:1147.

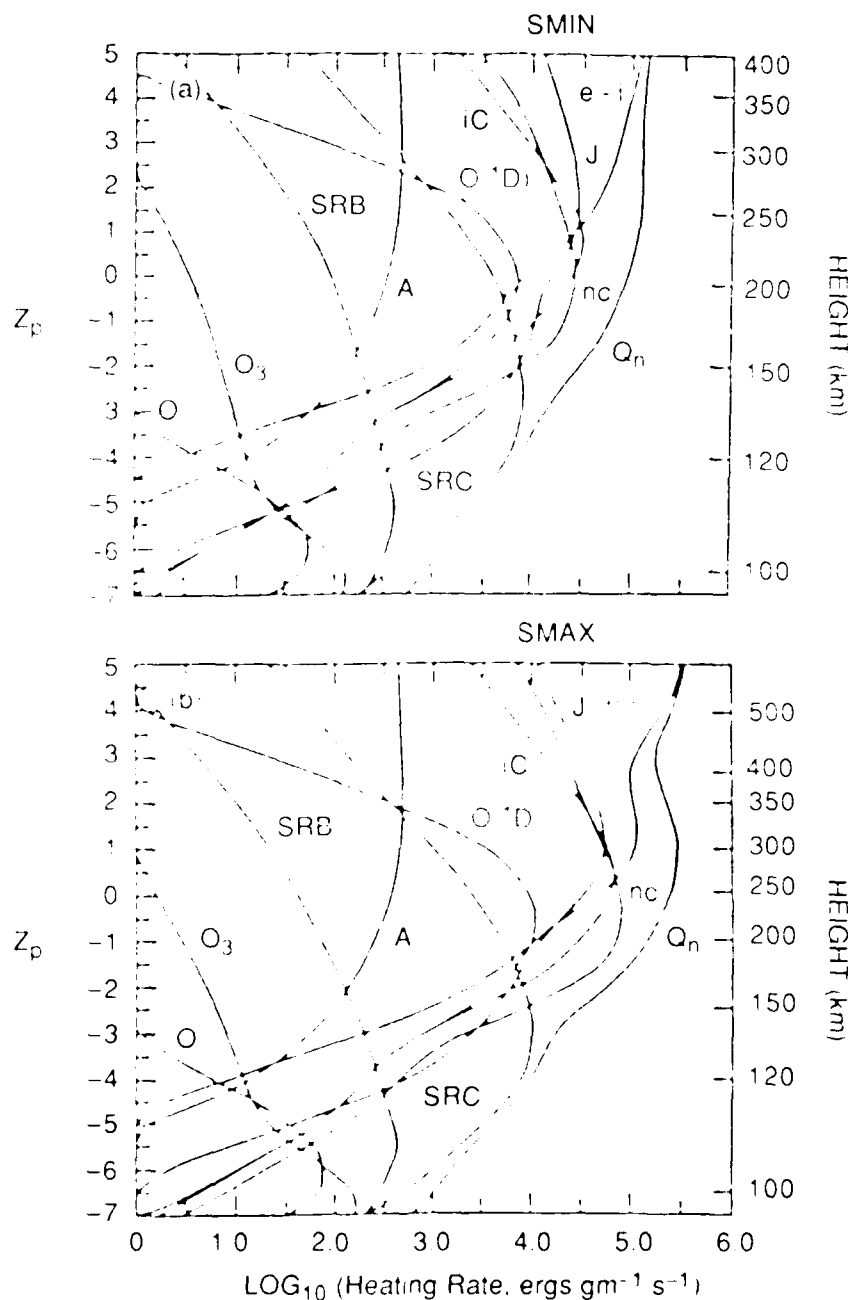


Figure 4. Calculated \log_{10} profiles of thermospheric heating rates ($\text{ergs g}^{-1} \text{s}^{-1}$) for (a) solar minimum and (b) solar maximum conditions. Q_n is the total neutral heating rate; $e-i$ is heating by collisions between thermal electrons, ions, and neutrals; IC is heating from exothermic ion-neutral chemistry; nc is heating from exothermic neutral-neutral chemistry; J is joule heating from the superimposed electric field; A is heating from auroral particles; $O(1D)$ is heating from quenching of $O(1D)$; SRC and SRB are heating from O_2 absorption in the Schumann-Runge continuum and bands, respectively; O is heating from atomic oxygen recombination; and O_3 is heating from absorption of solar radiation in the Hartley bands of Ozone. Taken from Roble et al.³¹

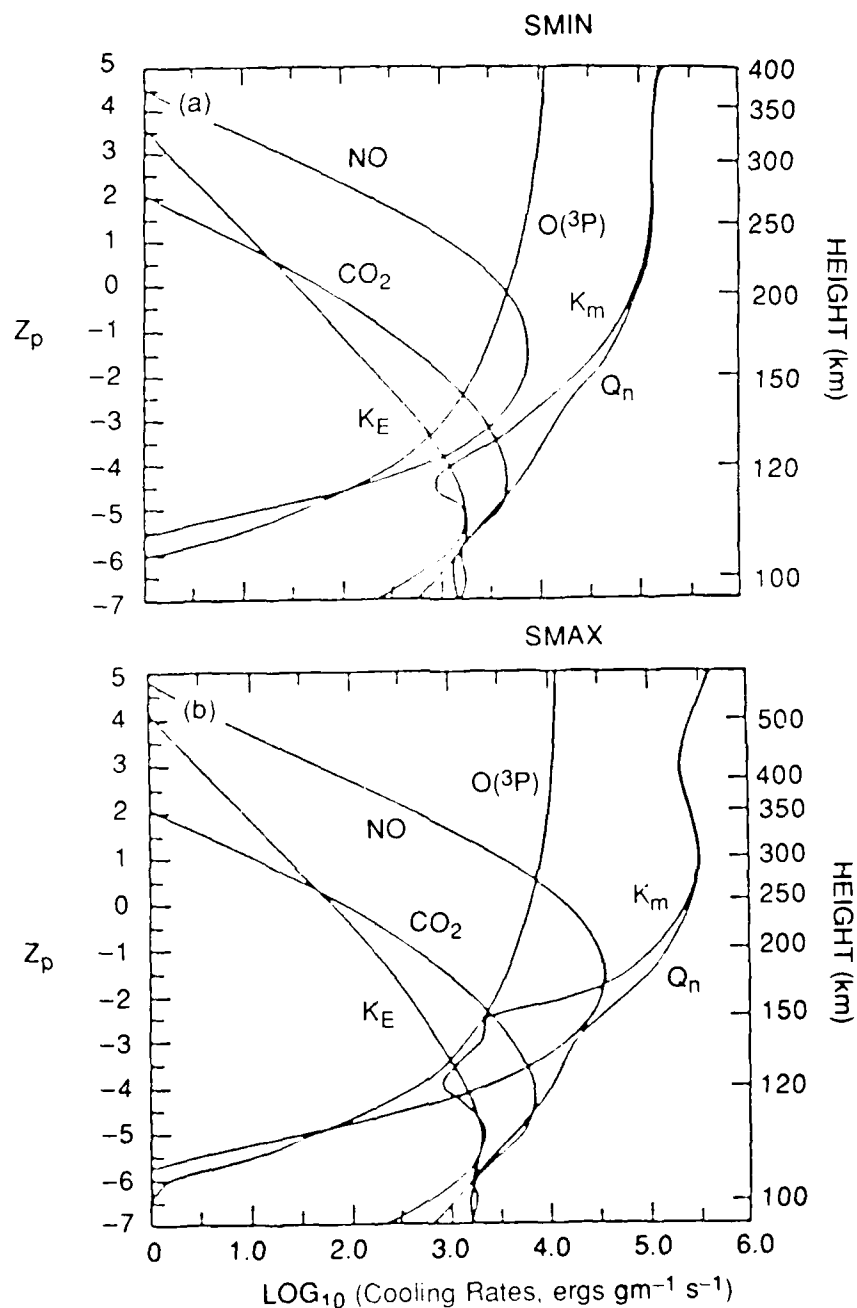


Figure 5. Calculated \log_{10} profiles of neutral gas heating and cooling rates ($\text{ergs g}^{-1} \text{sec}^{-1}$) for (a) solar minimum and (b) solar maximum conditions. Q_n is the total neutral gas heating rate; K_m is the cooling rate by downward molecular thermal conduction and K_E is that by eddy thermal conduction; NO is radiative cooling from the $5.3\text{-}\mu\text{m}$ emission from nitric oxide; CO_2 is radiative cooling from the $15\text{-}\mu\text{m}$ emission from carbon dioxide; and $\text{O}(^3\text{P})$ is cooling from the fine structure of atomic oxygen. Taken from Roble et al.⁴³

The study of Roble et al.³¹ indicated that the combination of the calculated thermospheric heating and cooling rates shown in Figures 4 and 5 and Table 1 was able to accurately match the global mean thermospheric and ionospheric structure given by semi-empirical models of the thermosphere and ionosphere. This match is an impressive step forward, and suggests that the major physical processes controlling thermospheric global mean behavior have been identified and, to first order, quantified on a global mean basis. Roble et al.³¹ noted, however, that there remains a problem with the uniqueness of the set of reaction rates chosen for the study, and they pointed to the need to further quantify several key chemical reaction rates involved in the thermal balance. These include the critical cooling rates from the IR emissions of NO and CO₂ and the chemistry of atomic nitrogen metastable atoms. These processes have an important influence on the thermal balance and at the present provide "tunable" parameters that are adjusted to bring the calculated thermal structure into agreement with the global mean structure embedded within the semi-empirical models. Thus there exists a fundamental framework for the understanding of the dominant thermal processes responsible for establishing the global mean thermal balance in the thermosphere, but this framework requires additional work to quantify the individual processes. *We conclude here that theoretical and experimental (laboratory) work as well as aeronomical studies should be continued to quantify a number of important reaction rates - notably those involving atomic oxygen.*

2.2.2 PERTURBATIONS ABOUT THE GLOBAL MEAN

Perturbations about the global mean for the energy inputs to the thermosphere occur as a function of location and time. The energy perturbations lead to vertical and horizontal winds which then act to change thermospheric density. The high latitude sources of energy (Joule and particle heating) are very variable and, therefore, accurately parameterizing the time-dependent solar and geomagnetic energy inputs remains one of the major sources of potential inaccuracy. Various studies have shown that predictions based on TGCM calculations can vary considerably as a function of the set of indexes chosen to represent the energy input. The most commonly used index for solar UV-EUV variations is the F10.7 cm solar radio flux. While the F10.7 index has the advantage of being routinely obtained and readily available, it has also been shown (by comparison with the limited direct solar UV-EUV radiance measurements) to have shortcomings in terms of matching real UV-EUV fluxes.³⁴ It is clear that the deployment of a more direct experimental technique (that is, spaceborne observations of the input solar spectrum) would represent a significant advance over the present use of indirect indices. Such observations over a limited part of the spectrum will be made routinely when the planned solar X-ray imager is deployed on the GOES-NEXT spacecraft. *We conclude that continued efforts to improve the utility of proxy variables for the solar EUV and UV fluxes are required and, more importantly, there needs to be a well-calibrated direct solar flux monitor in the long term to provide real-time information on the solar input to the thermosphere.* We discuss below the possible addition of a solar flux monitor to the ADS mission complement to address this need.

The geomagnetic variations in the thermosphere are caused by changes in the solar wind magnetosphere dynamo, which may conveniently be characterized by the magnitude of the cross-

34. Lean, J. (1987) Solar-Ultraviolet irradiance variations: A review, *J. Geophys. Res.* **92**:839-868.

polar cap electrostatic potential, and by changes in the pattern and intensity of auroral particle precipitation. Indexes used to provide parameterizations for the time-dependent geomagnetic energy input include the global Kp index, the AE index and the NOAA/TIROS Precipitation Activity Index (Foster et al., 1986³⁵; Fuller-Rowell and Evans, 1987³⁶). TGCM simulations using these indexes in comparisons with DE-2 satellite data have indicated that they provide good first-order descriptors for the time-dependent energy input to the high-latitude thermosphere (Rees et al., 1980³⁷, 1983³⁸, 1985a³⁹, b⁴⁰, 1986⁴¹, 1987⁴²; Roble et al., 1982¹⁹, 1983²⁰, 1984⁴³, 1987c⁴⁴, 1988²⁹; Hays et al., 1984⁴⁵; and Killeen et al., 1986²⁵). Of the currently available geomagnetic indices, the NOAA/TIROS index is to be preferred since it is derived from essentially real-time measurements of electron precipitation from the TIROS spacecraft. The NOAA/TIROS index is based on the local measurements (along the track of the TIROS spacecraft) combined with the use of a statistical data base to infer global

-
35. Foster, J.C., Holt, J.M., Musgrave, R.G., and Evans, D.S. (1986) Ionospheric convection associated with discrete levels of particle precipitation, *Geophys. Res. Lett.* **13**:656-659.
 36. Fuller-Rowell, T.J., and Evans, D.S. (1987) Height integrated Pedersen and Hall conductivity patterns inferred from the TIROS/NOAA satellite data, *J. Geophys. Res.* **92**:7606.
 37. Rees, D., Fuller-Rowell, T.J., and Smith, R.W. (1980) Measurements of high latitude thermospheric winds by rocket and ground-based techniques and their interpretation using a three-dimensional time-dependent dynamical model, *Planet. Space Sci.* **28**:919-932.
 38. Rees, D., Fuller-Rowell, T.J., Gordon, R., Killeen, T.L., Hays, P.B., Wharton, L.E., and Spencer, N.W. (1983) A comparison of wind observations of the upper thermosphere from the Dynamics Explorer satellite with the predictions of a global time-dependent model, *Planet. Space Sci.* **31**:1299-1314.
 39. Rees, D., Gordon, R., Fuller-Rowell, T.J., Smith, M., Carignan, G.R., Killeen, T.L., Hays, P.B., and Spencer, N.W. (1985a) The composition, structure, temperature and dynamics of the upper thermosphere in the polar regions during October to December, 1981, *Planet. Space Sci.* **33**:617-666.
 40. Rees, D., Fuller-Rowell, T.J., Smith, M.F., Gordon, R., Killeen, T.L., Hays, P.B., Spencer, N.W., Wharton, L.E., and Maynard, N.C. (1985b) The westward thermospheric jet-stream of the evening auroral oval, *Planet. Space Sci.* **33**:425-456.
 41. Rees, D., Fuller-Rowell, T.J., Gordon, R., Heppner, J.P., Maynard, N.C., Spencer, N.W., Wharton, L.E., Hays, P.B., and Killeen, T.L. (1986) A theoretical and empirical study of the response of the high-latitude thermosphere to the sense of the "Y" component of the interplanetary magnetic field, *Planet. Space Sci.* **34**:1-40.
 42. Rees, D., Fuller-Rowell, T.J., Quegan, S., Moffett, R.J., and Bailey, G.J. (1987) Thermospheric dynamics: Understanding the unusual disturbances by means of simulations with a fully-coupled global thermosphere/high-latitude ionosphere model, *Annales Geophysicae* **5**:303-328.
 43. Roble, R.G., Emery, B.A., Dickinson, R.E., Ridley, E.C., Killeen, T.L., Hays, P.B., Carignan, G.R., and Spencer, N.W. (1984) Thermospheric circulation, temperature and compositional structure of the Southern Hemisphere polar cap during October-November, 1981, *J. Geophys. Res.* **89**:9057-9068.
 44. Roble, R.G., Emery, B.A., Reid, G.C., Solomon, S., Garcia, R.R., Evans, D.S., Killeen, T.L., Hays, P.B., Heelis, R.A., Hanson, W.B., Winningham, J.D., Spencer, N.W., and Brace, L.H. (1987c) Joule heating in the mesosphere and lower thermosphere during the 13 July 1982 solar proton event, *J. Geophys. Res.* **92**:6083-6090.
 45. Hays, P.B., Killeen, T.L., Spencer, N.W., Wharton, L.E., Roble, R.G., Emery, B.E., Fuller-Rowell, T.J., Rees, D., Frank, L.A., and Craven, J.D. (1984) Observations of the dynamics of the polar thermosphere, *J. Geophys. Res.* **89**:5597-5612.

patterns of particle precipitation. The statistical data base is, in essence, a semi-empirical model obtained from analysis of the entire set of NOAA/TIROS observations over a long period of time. A similar and powerful semi-empirical model of the high-latitude energetic particle input has been established using the DMSP particle data (Hardy et al., 1987⁴⁶). It has not yet been used to generate a global index of energy input for use in numerical modeling.

The NOAA/TIROS index is of great value in that direct measurements of the important variables (precipitating electron fluxes) are involved, but it has the obvious shortcoming that local measurements are extrapolated to provide a global description using assumptions that tend to average out spatial structure in the precipitation. An alternative or supplement to the use of the geomagnetic indices is the possible use of global-scale auroral images obtained from space. Such images have been obtained from various spacecraft, including HILAT, DE-1, and VIKING. Analysis of the images has indicated that the morphology of the aurora can be very complex in space and time and, consequently, any estimate of global particle energy input based on binned and averaged satellite particle data can be significantly in error. Recent modeling work (M.H. Rees, private communication) has indicated that ratios of auroral intensities at different wavelengths may be used to provide detailed estimates of the spatial dependency of the auroral energy input.

From the above discussion, it is clear that an improvement in the parameterization of the high-latitude geomagnetic energy input is desirable for improved density specification. A new technique might involve using both DMSP and TIROS data to provide near real-time particle indexes that have more realistic spatial information. Ideally the particle data would be extended and enhanced by using global images of the aurora in different wavelength regions and a model to calculate energy influxes from the measured intensity ratios. *We conclude that use of the DMSP and NOAA/TIROS measurements should continue to improve the reliability of global indexes of particle precipitation. If possible, the use of intensity ratios derived from global auroral imagery and a model of auroral emission production rates would be recommended to improve the description of the spatial variations of the particulate energy input to the thermosphere.*

2.3 Dynamical Considerations

As discussed above, neutral winds play a key role in the control of thermospheric density variations because of the importance of the advective terms in the total mass continuity equation. Neutral winds are also of importance for the computation of drag and lift forces on space structures, since both of these forces are proportional to the square of the relative velocity. For winds reaching 1 km/sec, the maximum uncertainty in calculating aerodynamic drag or lift, due to ignorance of wind velocity, can be as high as 50 percent, a worst case difference being between a 1 km/sec head wind or tail wind, at an orbital velocity of 8 km/sec. Also, density information derived from spacecraft measurements of drag (using accelerometers) or composition (from retarding potential analyzers) is dependent on a knowledge of wind. *In general, one requires a neutral wind accuracy of ~20-30 m/sec to*

46. Hardy, D.A., Gussenhoven, M.S., Raistrick, R., and McNeil, W.J. (1987) Statistical and functional representations of the pattern of auroral energy flux, number flux, and conductivity. *J. Geophys. Res.* **92**:12275-12294.

get a 1 percent accuracy for density or composition. Since the Air Force density specification program has a need for accuracies in the few percent range, a knowledge of wind velocities on a global scale to this kind of accuracy is essential.

Neutral winds have been measured at upper thermospheric altitudes in the past from the LOGACS satellite experiment (DeVries, 1972⁴⁷; Wu et al., 1974⁴⁸; Straus, 1978⁴⁹), the AFGL SETA instrument (Marcos and Forbes, 1985⁵⁰; Forbes et al., 1987²⁸) and the Dynamics Explorer-2 spacecraft (for example, Killeen and Roble, 1988⁵¹) as well as from a chain of ground-based Fabry-Perot interferometers [for example, see recent reviews by (Hernandez and Killeen, 1988⁵²) and (Killeen, 1987³⁰)]. The Dynamics Explorer-2 mission duration was from August 1981 to February 1983, a period of high solar activity. The wind measurements from DE-2 during this period have led to a detailed "climatological" record of the mean upper thermospheric wind system at solar maximum for high latitudes (for example, Killeen et al.⁵³) and for low latitudes (Wharton et al., 1984⁵⁴). The growing neutral wind data base at upper thermospheric altitude, and in particular the DE-2 measurements, have been a major contributor to and stimulus for the recent development of the TGCMs by providing global-scale tests of the model predictions, thereby leading to refinement of the model inputs and procedures. Examples of the level of agreement that has been possible between global-scale wind observations and model predictions are shown in Figures 6 and 7, taken from Killeen et al.⁵³ The first of these figures shows the monthly-mean measured upper thermospheric winds in the polar regions from DE-2 and the network of ground-based Fabry-Perot interferometers and a comparison with the calculations of the NCAR-TGCM for a diurnally-reproducible (steady geomagnetic and magnetospheric forcing) model run. There is good agreement between the model and the averaged experimental data as a function of UT for this case, corresponding to December 1981 (solar maximum conditions). Figure 7 shows a comparison of the measured zonal winds from DE-2 at equatorial latitudes with the corresponding NCAR-TGCM calculations (labelled VSH, see below). Successful and encouraging comparisons, such as these, have served to critically test the TGCM

-
47. DeVries, L.L. (1972) Structure and motion of the thermosphere shown by density data from the Low-G Accelerometer Calibration System (LOGACS), *Space Res.* **12**:867-879.
 48. Wu, S.T., Matsushita, S., and DeVries, L.L. (1974) An analysis of the upper atmospheric wind observed by LOGACS, *Planet. Space Sci.* **22**:1036.
 49. Straus, J.M. (1978) Dynamics of the thermosphere at high latitudes, *Rev. Geophys. Space Phys.* **16**:183-194.
 50. Marcos, F.A. and Forbes, J.M. (1985) Thermospheric winds from the satellite electrostatic triaxial accelerometer (SETA) system, *J. Geophys. Res.* **90**:6543-6552.
 51. Killeen, T.L. and Roble, R.G. (1988) Thermosphere Dynamics: Contributions from the first five years of the Dynamics Explorer Program, *Rev. Geophys.* **26**:329-367.
 52. Hernandez, G. and Killeen, T.L. (1987) Optical measurements of winds and temperatures in the upper atmosphere, in CIRA-86, *COSPAR International Reference Atmosphere*, Pergamon Press, in press.
 53. Killeen, T.L., Smith, R.W., Spencer, N.W., Meriwether, J.W., Rees, D., Hernandez, G., Hays, P.B., Cogger, L.L., Sipler, D.P., Biondi M.A., and Tepley, C.A. (1986) Mean neutral circulation in the winter polar F-region, *J. Geophys. Res.* **91**:1633-1649.
 54. Wharton, L.E., Spencer, N.W., and Mayr, H.G. (1984) The Earth's thermospheric superrotation from Dynamics Explorer 2, *Geophys. Res. Lett.* **11**:531-533.

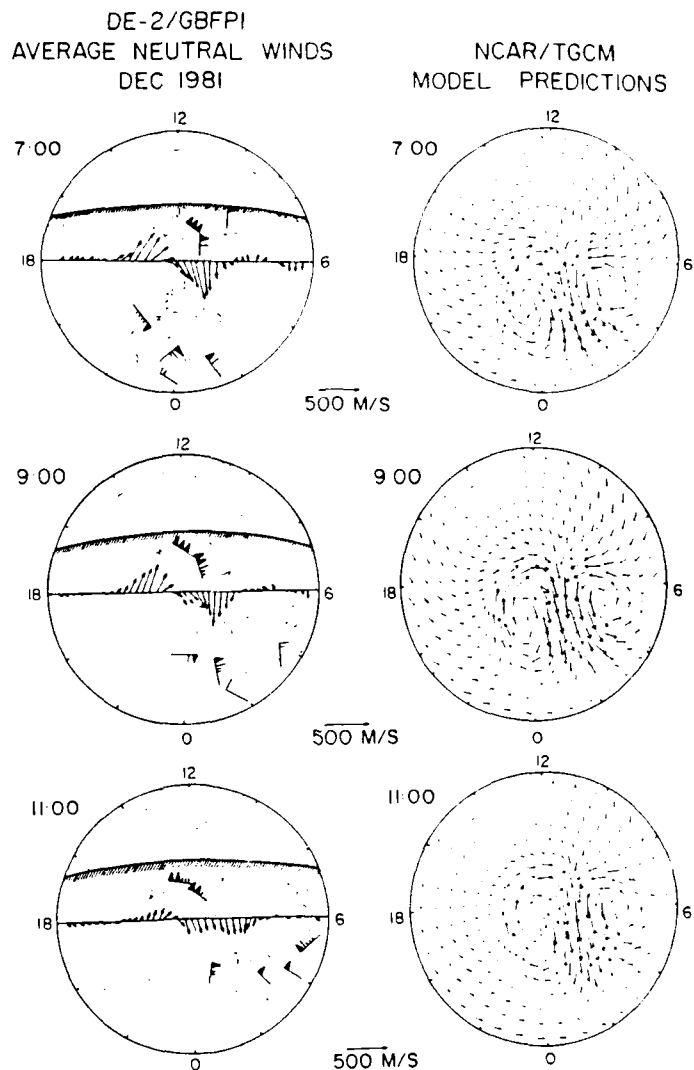


Figure 6. Climatological upper thermospheric neutral wind map for UT bins centered at 07:00, 09:00, and 11:00 hrs UT (top to bottom). The left hand side shows the DE-2 and ground-based Fabry-Perot (GBFPI) UT-averaged measurements plotted in geographic polar coordinates (latitude and LT) for the month of December 1981 (solar maximum). The satellite-averaged winds are given by the arrows. The GBFPI wind measurements are plotted as standard meteorological symbols, with the thermospheric scale defined in text: barb = 100 m/sec; long line = 50 m/sec; and, short line = 10 m/sec. The curved line is the solar terminator. The left hand side illustrates the NCAR-TGCM predictions for the midpoint of the particular UT bin. Model winds are plotted according to the same scale as the satellite winds. Figure taken from Killeen et al.²⁵ (1986).

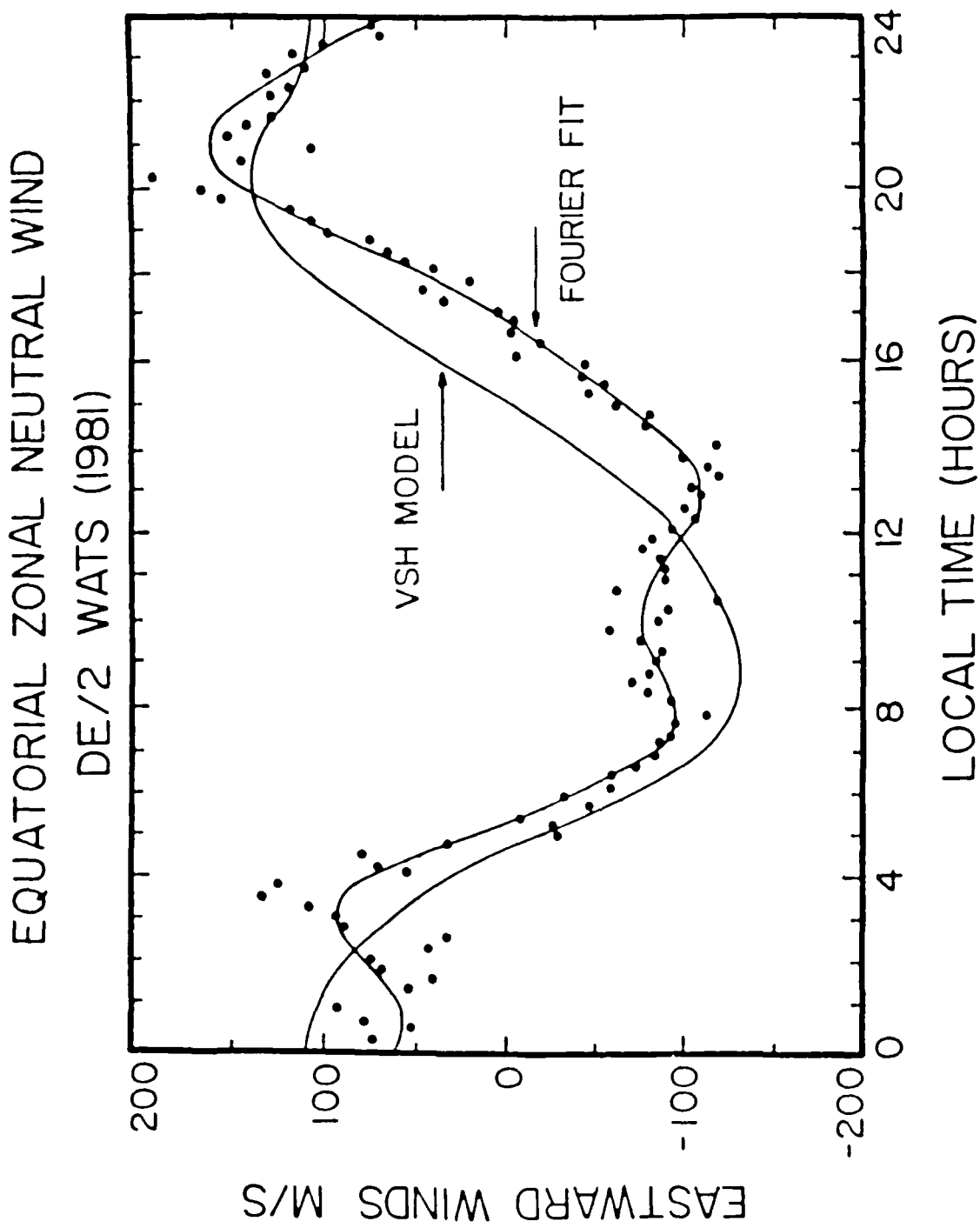


Figure 7. Comparison between DE-2 equatorial upper thermospheric zonal wind averages (Wharton et al. 54) and the predictions of the NCAR-TGCM. Figure taken from Killeen et al. 55

55. Killeen, T.L., Roble, R.G., and Spencer, N.W. (1987) A computer model of global thermospheric winds and temperatures, *Adv. Space Res.* 7:10207:10215.

performance on the global scale, leading to a significant and demonstrable improvement in the model capability.

- The experimental description of the dynamics of the lower thermosphere region is much less well defined than that for the upper thermosphere and, as a consequence, our confidence in the theoretical predictions of the dynamics of the region between 100-200 km is relatively poor. In this region, the most comprehensive source of experimental data has come from the ground based neutral and incoherent scatter radars⁵⁶ and from rocket vapor trail experiments (for example, Heppner and Miller⁵⁷), but these results have not yet led, for example, to a quantitative understanding of the importance of the geomagnetic effect at these altitudes.^{58,59,60}

In the lower thermosphere, the influence on thermospheric winds, composition, and density of tidal structures propagating upwards from below is known to be profound. The major diurnal and semi-diurnal tides produced by ozone and water vapor absorption in the stratosphere and mesosphere are clearly of importance, but their detailed amplitude and phase structures have not yet been described to the point where accurate TGCM parameterizations are possible. A first step to incorporate tides into the NCAR-TGCM formulation was taken by Fesen et al.²⁶ In this study, the tides were introduced into the model equations by modulating the geopotential at the lower boundary. This was done through an iterative series of guesses for the relative amplitudes and phases of the tides that converged when the TGCM diurnal wind calculations at low latitudes resembled those reported from Arecibo radar data. Although this study was an important step, the tidal forcings are still not sufficiently well understood or quantified to enable satisfactory TGCM inputs, although the framework does exist for their incorporation in the model. *It is evident that a large and comprehensive global data base on winds in the 100-200 km region will be necessary to arrive at the required description of the tides.* In this regard, the NSF CEDAR (Coupling, Energetics and Dynamics of Atmospheric Regions) program, which involves the synergistic use of optical and radar data from many ground locations, will be of future importance since the quantification of tidal phases and amplitudes is one of the major objectives within this national program. Spaceborne observations of winds in the lower thermosphere are, however, essential to fill in the necessarily limited ground-based grid and extend the CEDAR results. It is anticipated that a combination of CEDAR measurements of tidal structures from the ground and ADS wind observations in the 140 km region will allow for the required global specification of thermospheric tidal forcing.

-
- 56. Manson, A.H., et al. (1985) Mean winds of the upper middle atmosphere (60-110 km): a global distribution from radar systems (MF, meteor, VHF), Handbook for MAP, 16, 239-253.
 - 57. Heppner, J.P. and Miller, M.L. (1982) Thermospheric winds at high latitudes from chemical releases, *J. Geophys. Res.* **87**:2633-2647.
 - 58. Johnson, R.M. and Luhmann, J.G. (1985a) Neutral wind spectra at the auroral mesopause: Geomagnetic effect?, *J. Geophys. Res.* **90**:1735-1743.
 - 59. Johnson, R.M. and Luhmann, J.G. (1985b) High-latitude mesopause neutral winds and geomagnetic activity: A cross-correlation analysis, *J. Geophys. Res.* **90**:8501-8506.
 - 60. Johnson, R.M., Wickwar, V.B., Roble, R.G., and Luhmann, J.G. (1987) Lower thermospheric winds at high-latitude: Chatanika radar observations, *Annales Geophysicae* **5**:383-405.

2.4 Gravity Wave and Planetary Wave Forcing

The tides in the thermosphere, discussed above, are only one example of a whole family of waves that can propagate in the neutral medium. There exists a spectrum of waves that has been extensively studied theoretically (for example, Hunsucker⁶¹, Mayr et al.^{62,63}). These perturbations are known to have significant effects on the ionosphere and on thermospheric density structures. For example, Traveling Ionospheric Disturbances (TIDs) have been studied for some time and have been shown to be related to waves in the thermosphere.⁶⁴ Wavelike fluctuations in neutral thermosphere density data have also been reported from many *in situ* experiments [for example, Forbes and Marcos⁶⁵, Prolss and von Zahn⁶⁶, Hedin and Mayr⁹]. The propagation velocities of these waves are found to be of the order of 200-1000 m/s for large scale (100 km) waves and less than 200 m/s for medium scale (200 km) waves.

Recent statistical analyses of wave activity have been carried out by Potter et al. (1976)⁶⁷ and Hedin and Mayr⁹, using Atmosphere Explorer and Dynamics Explorer data, respectively. In both cases the wave activity was found to maximize at high geomagnetic latitudes, due to the existence of wave sources associated with geomagnetic heating and momentum forcing. Figure 8, taken from the Hedin and Mayr study, illustrates contours describing the measured probability of occurrence of a thermospheric species density fluctuation amplitude for a) longer wavelength waves (400-4000 km) and b) shorter wavelength waves (50-400 km) as a function of geomagnetic latitude. The contours represent the percentage of the time that percentage fluctuation amplitudes given by the ordinate occur. It can be seen that, for all individual species shown, the occurrence probability maximizes at high latitudes, with appreciable amplitude fluctuations occurring a large percentage of the time.

Figure 9 demonstrates the capability of the NCAR-TGCM to calculate the global-scale propagation of thermospheric waves in the planetary wave part of the spectrum (wavelengths of the order of thousands of km). In this figure, the calculated vertical wind perturbations are shown as a function of time during and following a simulated geomagnetic storm event. As discussed above, vertical winds lead directly to density variations through vertical advection. For this time-dependent model run, the geomagnetic storm was simulated by the impulsive (1-hour duration) insertion of

-
61. Hunsucker, R.D. (1982) Atmospheric gravity waves generated in the high-latitude ionosphere: A review, *Rev. Geophys.* **20**:293-315.
 62. Mayr, H.G., Harris, I., Varosi, F., and Herrero, F.A. (1984a) Global excitation of wave phenomena in a dissipative multi-constituent medium, 1. Transfer function of the Earth's thermosphere, *J. Geophys. Res.* **89**:10929-10959.
 63. Mayr, H.G., Harris, I., Varosi, F., and Herrero, F.A. (1984b) Global excitation of wave phenomena in a dissipative multi-constituent medium, 2. Impulsive perturbations in the Earth's thermosphere, *J. Geophys. Res.* **89**:10961-10986.
 64. Hines, C.O. (1960) Internal atmospheric gravity waves at ionospheric heights, *Can. J. Phys.* **28**:1441-1481.
 65. Forbes, J.M. and Marcos, F.A. (1973) Thermosphere density variations associated with the auroral electrojet activity, *J. Geophys. Res.* **78**:3841-3847.
 66. Prolss, G.W. and von Zahn, U. (1976) Large and small scale changes in the disturbed upper atmosphere, *J. Atmos. Terr. Phys.* **38**:655-659.
 67. Potter, W.E., Kayser, D.C., and Mauersberger, K. (1976) Direct measurements of neutral wave characteristics in the thermosphere, *J. Geophys. Res.* **81**:5002-5012.

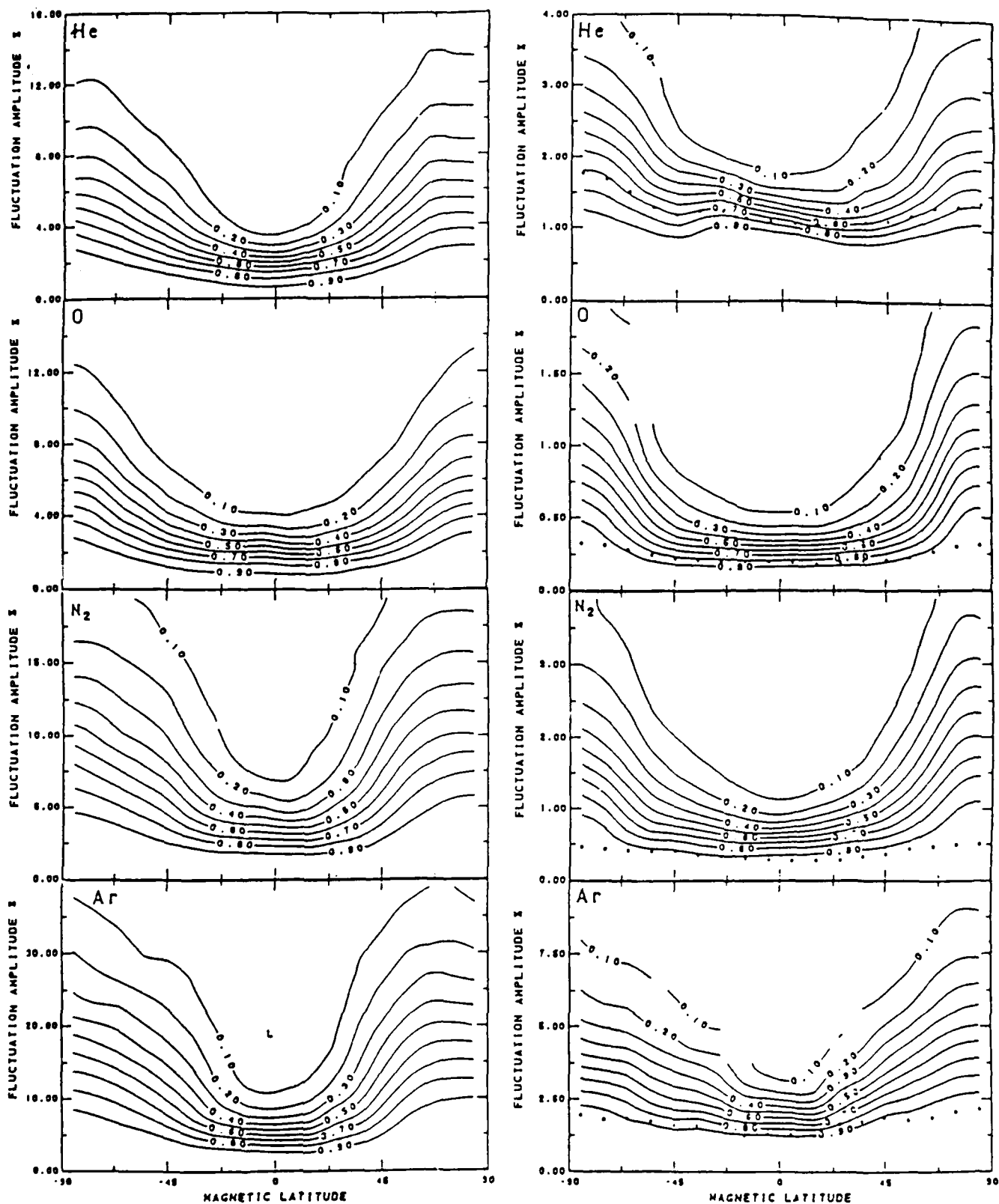


Figure 8. Contours giving the probability of occurrence of a fluctuation amplitude as large or larger than the ordinate at a particular magnetic latitude (abscissa) for a) long wavelength (400-4000 km) waves and b) short wavelength (40-400 km) waves. Figure is taken from Hedín and Mayr.⁹

NCAR TGCm 1-hour Impulse study Vertical wind perturbations (300km altitude)

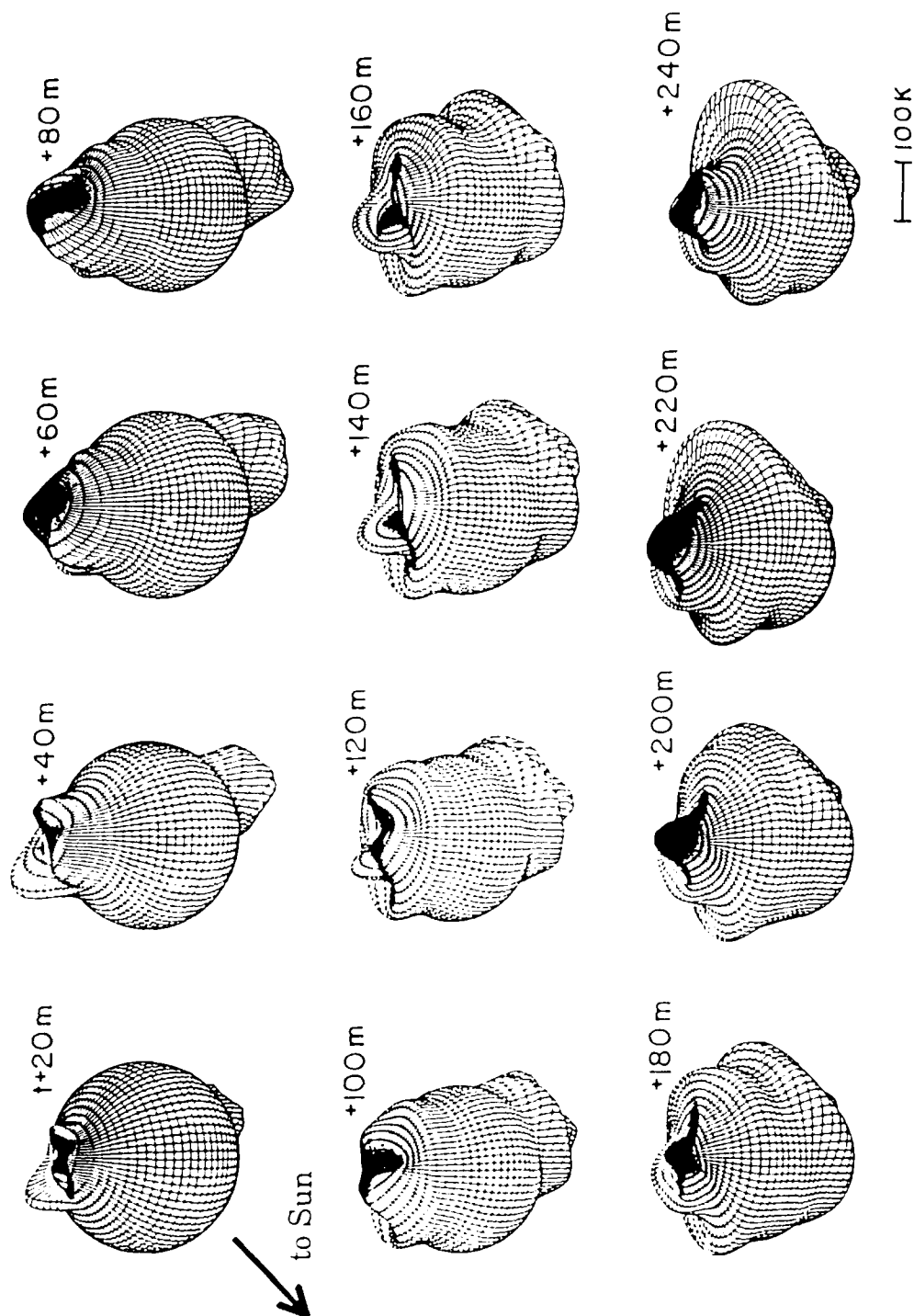


Figure 9. Calculated vertical wind perturbations at 300 km from the NCAR TGCm for a model run simulating a discrete geomagnetic storm. For this run impulsive high-latitude magnetospheric forcing was imposed of 1 hour duration (starting at time t , and stopping at time $t+60$ minutes). The vertical wind perturbations due to this impulsive forcing are plotted as deviations from the radius of the sphere shown in perspective plot. The scale for the vertical wind perturbations is given at lower right.

energy and momentum into the auroral thermosphere. The storm was initiated at t minutes and turned off at $t+60$ minutes and the vertical wind perturbations are plotted as departures from the radius of the sphere shown according to the scale at lower right. Thus, during the storm event (first three frames in top row), a large enhancement of the vertical wind in the auroral regions in the two opposite hemispheres can be noted. Maximum perturbations are associated with the dawn and dusk sectors of the auroral zone, where *in situ* Joule heating is particularly enhanced. As the model is run forward in time, the propagation of the disturbances to lower latitudes is evident, particularly in the northern hemisphere, where a nearly azimuthally-symmetric planetary-scale wave is seen to move towards the equator, ultimately interfering, at equatorial latitudes, with a similar wave propagating out of the southern hemisphere ~200 minutes after the simulated storm onset. The ability of the TGCM to simulate the entire spectrum of gravity waves is limited only by the resolution of the grid used (see below), since the gravity waves as well as the characteristics of the large-scale circulation are controlled by the same primitive equations solved by the model. This example illustrates the capability of the TGCM to simulate planetary-scale time-dependent disturbances. Other more realistic examples have been discussed by Roble et al.²⁷

The widespread occurrence of wavelike features in the observed thermospheric density has implications for how well models of any description can predict atmospheric densities and satellite drag. Two factors are of importance here. Firstly, the ability of any model to accurately specify the full spectrum of gravity waves is limited by the Nyquist frequency associated with the spatial resolution of the model. Secondly, the intrinsic stochastic nature of the generation of gravity waves in the thermosphere, and the complexity and variability of the sources may be expected to set an absolute limit on the accuracy with which models can predict the spatial and temporal details of the waves even within the allowed spatial frequency domain. At the higher spatial frequencies, in particular, it will be necessary to treat the wave spectrum in a probabilistic sense, that is, quantification of the probability of encountering density structures with a given amplitude in a given spatial frequency domain as a function of location and time (as per Figure 8).

To assess model limitations due to spatial resolution, density perturbations measured using the SETA AFGL accelerometer for a 21 day period have been analyzed to determine the nature of the measured gravity wave spectra. Figures 10 and 11 illustrate the nature of density perturbations measured using the SETA system at low latitudes for two orbits. In these plots, the density variations in specific spatial frequency intervals are shown using the following data analysis technique. The SETA measurements of total density were first reduced to a constant height (200 km) to remove the effects of changes in the satellite altitude, using an extrapolation with a scale height of 33.5 km, corresponding to a temperature of 800 K. The mean for the orbital segment was then subtracted from these data and a Behannon and Ness band pass least squares filter applied to the resulting time series to isolate the different scales as shown (latitude scale intervals as noted in figures). Using all available SETA measurements for Julian days 79094-5 and 79084, such data can be used to generate the density power spectra illustrated in Figures 12 and 13, respectively. These power spectra (spatial frequencies) have been calculated by passing a fast Fourier Transform through the spatial series. The resulting spectra for each orbital segment were averaged over one day to obtain the spectra shown in Figures 12 and 13. Lines have been drawn on the plots to indicate the spatial resolution afforded by the current versions of the NCAR-TGCM and the MSIS-86 semi-empirical model. These power spectra have been converted to integral representations, by calculating the percentage of power remaining at smaller

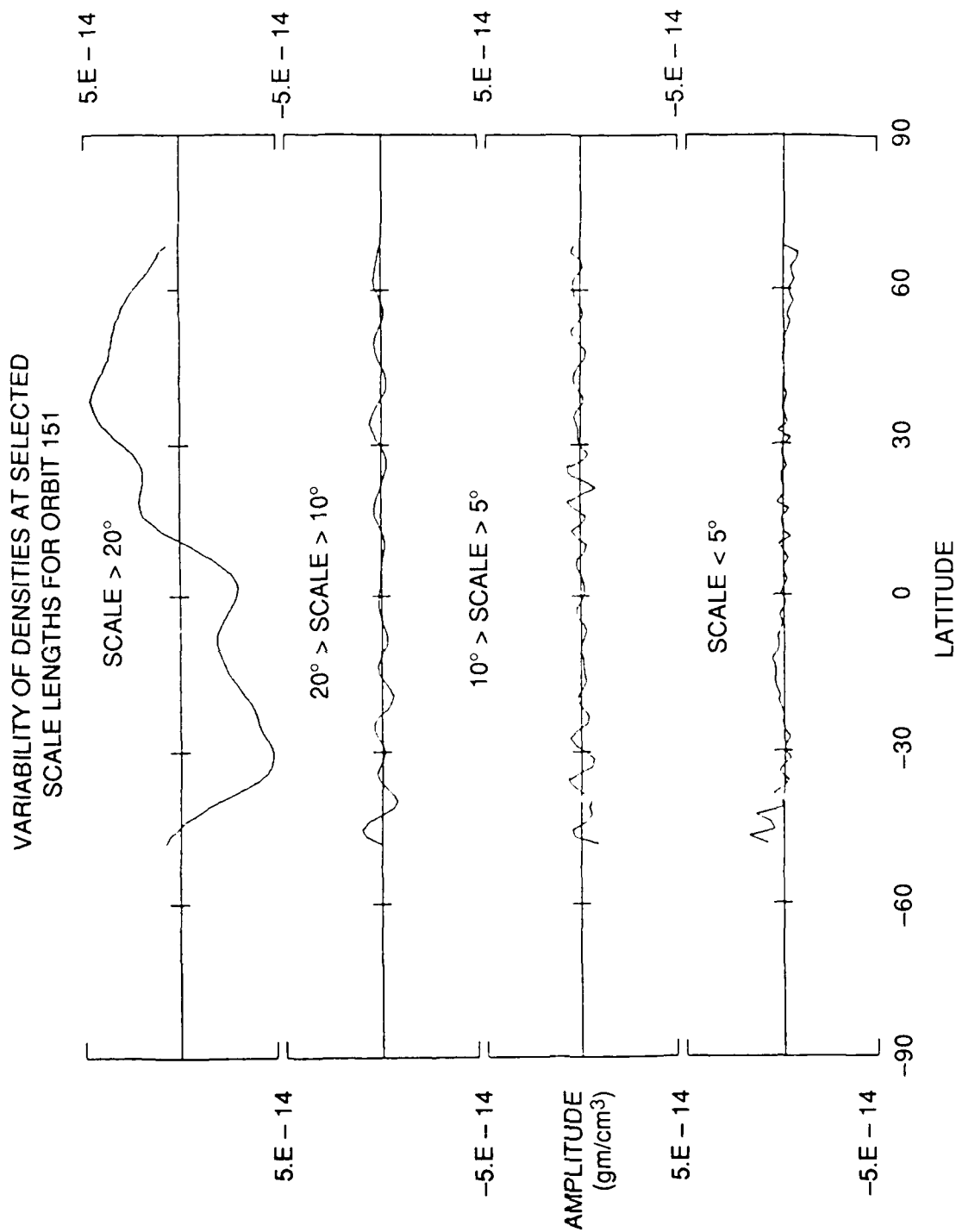


Figure 10. Measured variations in specific spatial scales as measured using the SETA instrument for orbit 151. Density variations in the specific spatial scale intervals were obtained by normalizing the data to 200 km and passing a Behannon and Ness least square filter through the spatial series.

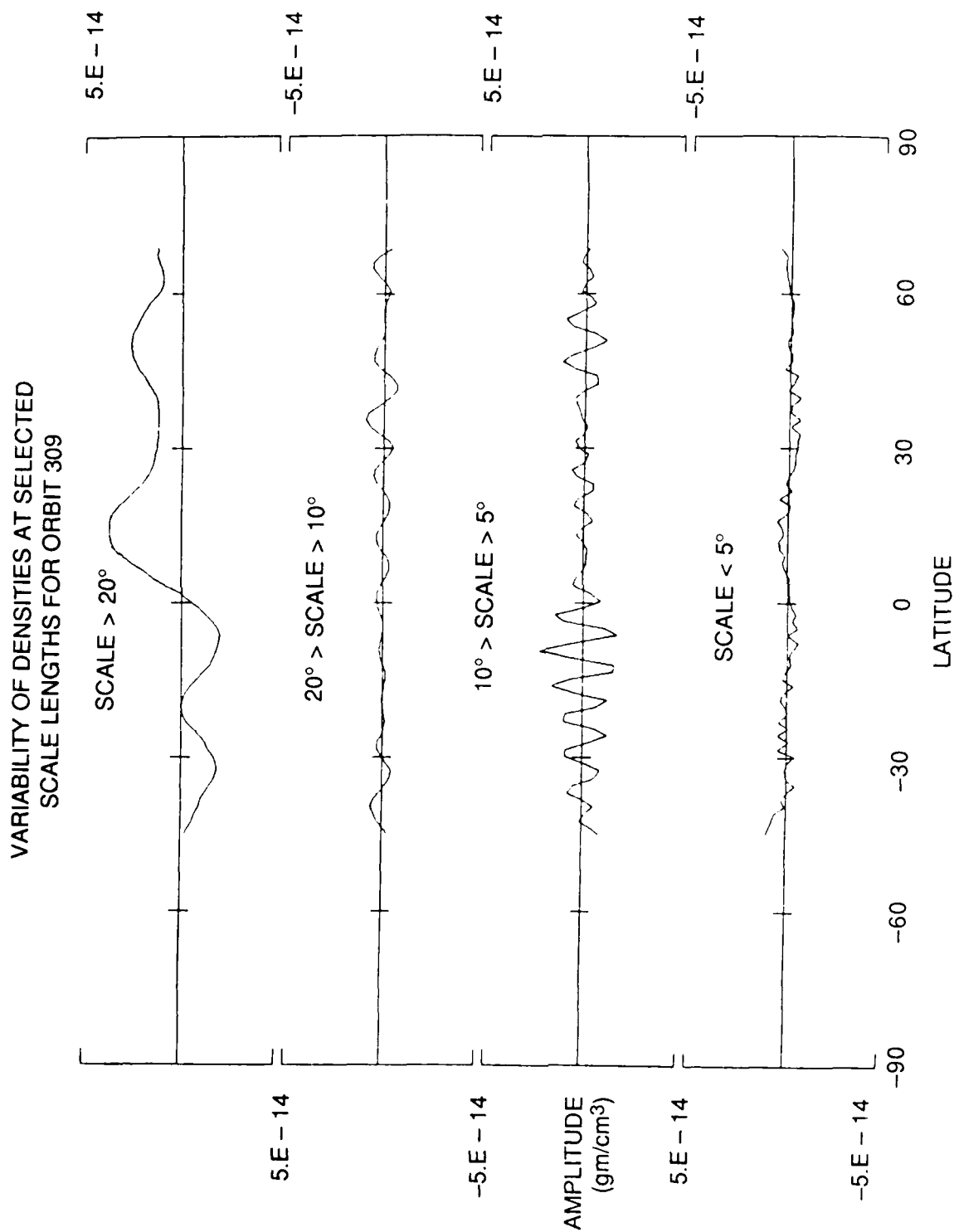


Figure 11. As for Figure 10, except for orbit 309.

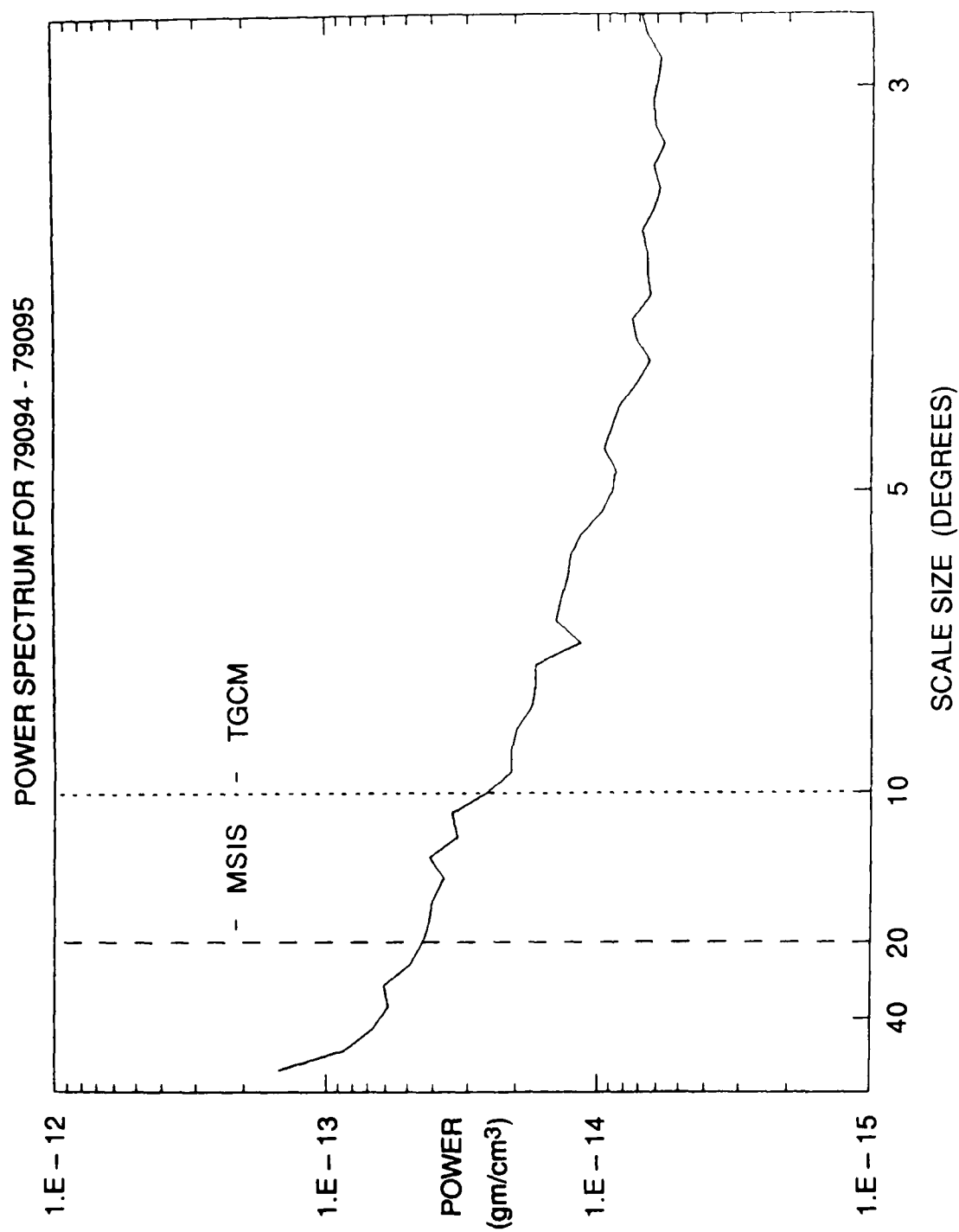


Figure 12. Power spectrum for SETA measured density fluctuations during Julian day 79094-95. Dashed and dotted vertical lines represent the spatial resolutions afforded by the current versions of the MSIS-86 and NCAR-TGCM models, respectively.

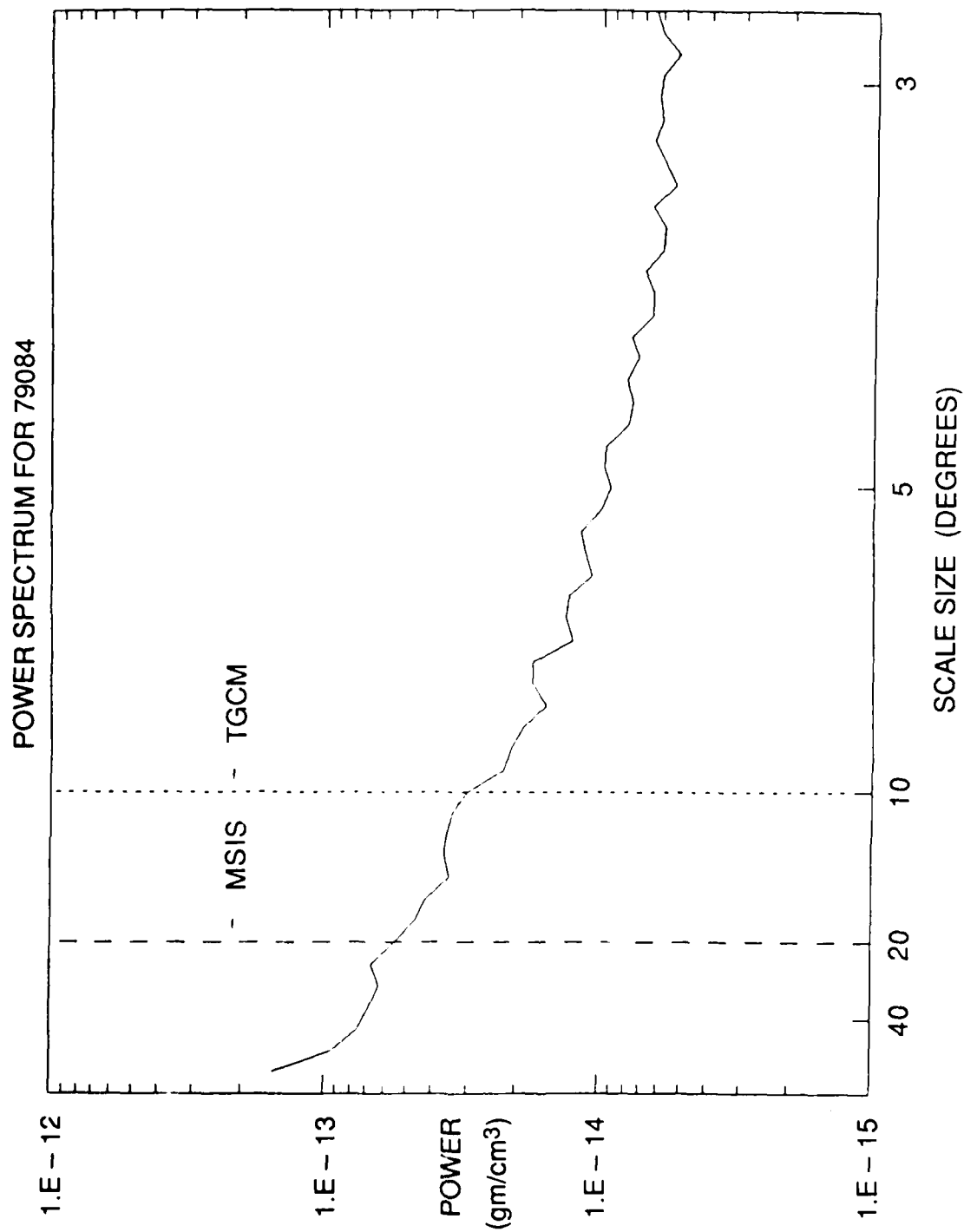


Figure 13. As for Figure 12, except for Julian day 79084.

scale sizes (Figures 14 and 15). The percentages were obtained by integrating under the power spectral curve at smaller scale sizes and dividing by the total area under the power spectral curve. The assumption was made here that fluctuations with spatial wavelengths less than $\sim 2.5^\circ$ were basically due to system noise. Lines were drawn on the integral plots to illustrate the percentage power in the measured density fluctuations that cannot be modeled using current TGCM and MSIS-86 resolutions. Thus, for example, Figure 14 shows that the MSIS resolution, roughly equivalent to a scale length of 20° latitude, allows only ~ 45 percent of the power in the measured waves to be modeled. The TGCM resolution, equivalent to 10° latitude, allows ~ 65 percent of the power to be modeled. The spatial resolution advantage of the TGCM is of significance for the specification of traveling disturbances, such as that shown in Figure 9.

From an examination of the information shown in Figures 10 - 15, we conclude that spatial resolution is important to enable modeling of important gravity wave spectral regions. Thus, the improvement in going from a 20° latitude resolution (MSIS-86) to a 10° resolution allows for significant improvements in the capability to model gravity wave features, even for the low latitude region used to provide the data shown in Figures 10 - 15. For higher latitudes, the improvement in modeling capability afforded by the higher spatial resolution model is even more significant. The move towards higher spatial resolution, however, is one that quickly leads to diminishing returns. A cursory examination of the spectra shown in Figures 12 and 13 illustrates that the decrease in power going from, for example, a 5° resolution to a 3° resolution is very modest and would not, therefore, lead to a significant improvement in modeling capability. The fluctuations at higher spatial frequencies are likely to be almost entirely due to stochastic noise due to small scale motions in the atmosphere.⁹

We conclude from this study that an improvement in the MSIS-86 intrinsic spatial resolution would be of significance to the modeling capability for thermospheric perturbations. Since semi-empirical models such as MSIS-86 are based on mean climatology, however, they cannot be expected to predict the type of time-dependent traveling waves shown in Figure 9. The current capability of the NCAR-TGCM is significantly better than that of MSIS in terms of the intrinsic spatial resolution. The TGCM also provides a possibility of specification of time-dependent phenomena, as well as mean climatology. Of course, to utilize the inherent modeling capability of a higher resolution model such as the NCAR-TGCM will require the generation of a new lower thermospheric data base and subsequent detailed validation tests to ensure that the geophysically significant perturbations are indeed modeled realistically.

The SETA study results discussed above are in basic agreement with the work of Hedin and Mayr⁹ who performed a recent statistical investigation of spatial variations in DE-2 composition data. These authors studied upper thermospheric atomic oxygen density fluctuations and found that the measured fluctuation amplitudes at high latitudes suggested that minimum possible rms deviations between oxygen density (or satellite drag) data and any semi-empirical model are about 6 percent and up to 10 percent at higher magnetic activities. Since overall deviations for current semi-empirical models under magnetically quiet conditions are of the order of 15 percent or higher, it would appear from this work and that of Hedin and Mayr⁹ that the stochastic nature of the shorter scale gravity waves is currently not the limiting factor in the capability of models to fit or predict oxygen (or satellite drag) data in the upper thermosphere. Wavelike density fluctuations will, however, provide a hard limit on accuracy that is not likely to be surpassed in the future. From the study presented in this report and the work of Hedin and Mayr, *we estimate that the best possible*

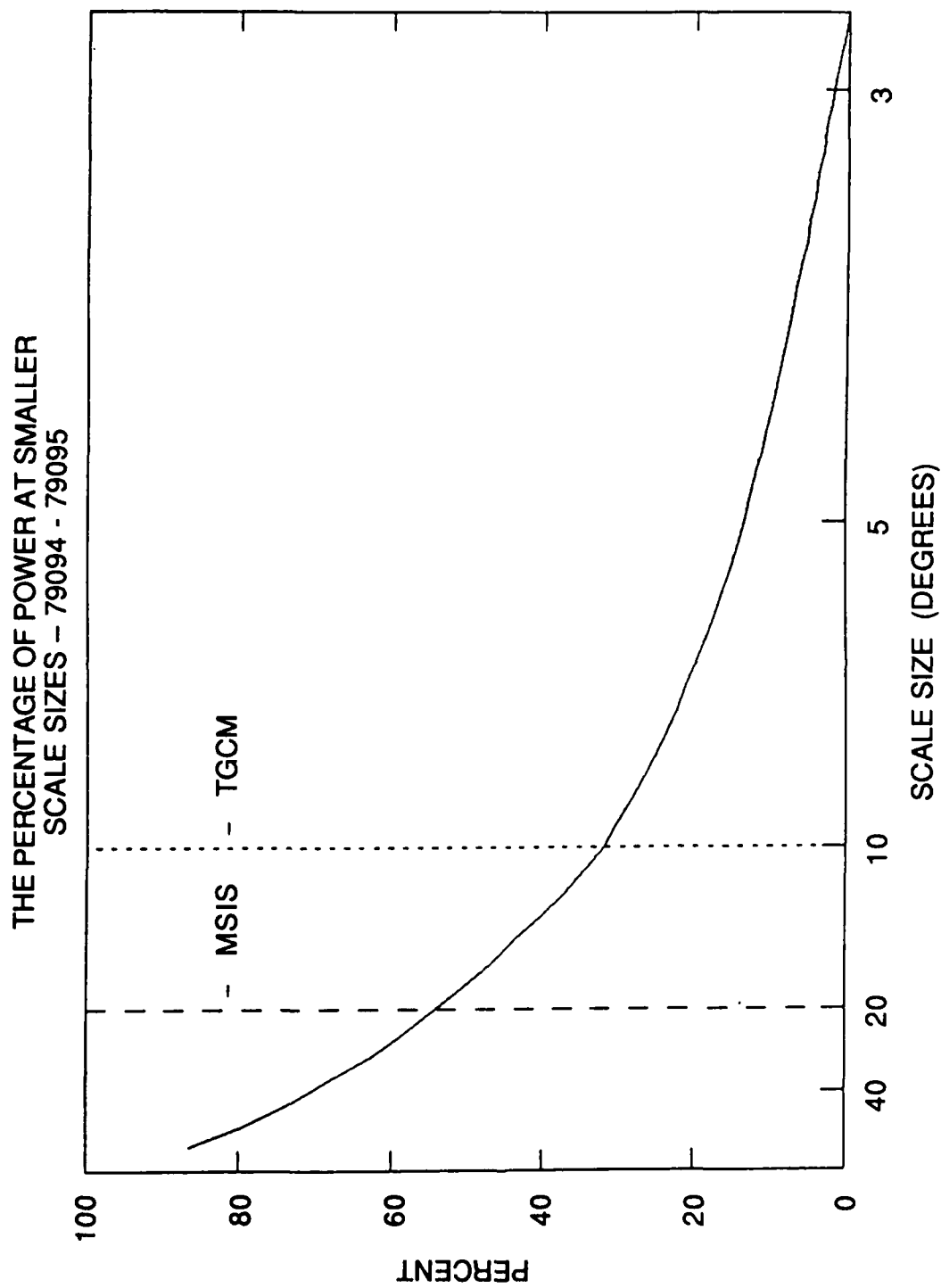


Figure 14. Integral power spectrum, illustrating the percentage power remaining at scales smaller than the abscissa for the SETA measurements from Julian day 79094-5. The dashed and dotted lines represent the MSIS-86 and TGCM spatial scales, respectively.

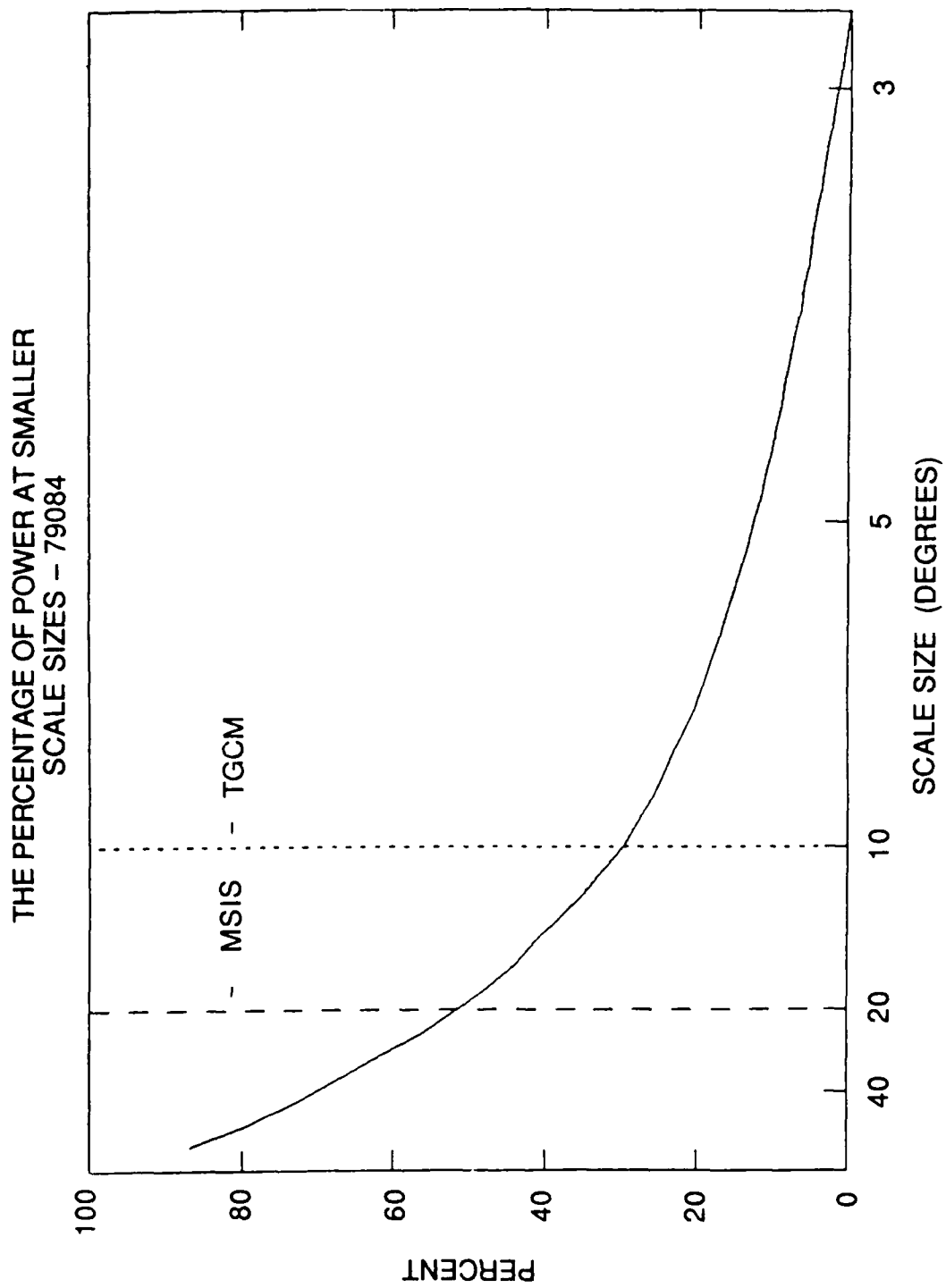


Figure 15. As for Figure 14, except for Julian day 79084.

accuracy for lower thermospheric density, taking into account the stochastic nature of the gravity waves, is of the order of 5 percent for mid- and low-latitudes and geomagnetically quiet times at high latitudes, rising to ~10 percent for geomagnetically active times at high latitudes. Further density specification beyond these limits will require the probabilistic approach mentioned above and illustrated in Figure 8.

The temporal resolution of models is also a subject of importance for the specification of time-dependent perturbations, such as those depicted by the simulations of Figure 9. In this case, and for numerous reported experimental measurements, significantly large perturbations occur on a time scale of ~tens of minutes. Current temporal resolution limitations to the MSIS-86 model, based on the use of 3-hour geomagnetic indices, implies that such rapid variations cannot be modeled adequately. In fact, semi-empirical models, which are of necessity dependent on climatological means for their construction, cannot be expected to ever be able to model traveling transient disturbances in the thermosphere. The TGCM, on the other hand, currently allows for greater temporal and spatial resolution than MSIS-86, and also enables rapid traveling disturbances, in principle, to be accurately modeled. To capitalize on the inherent advantages of the TGCM approach will require detailed experimental case study comparisons and validations in the domain of interest, namely the lower thermosphere. For the validation procedure to be successful, the best available indices will need to be used to characterize the energy, particle, and momentum inputs to the thermosphere discussed above and, even more importantly, a global scale data base of lower thermospheric densities, temperatures and winds will need to be established. An analogous effort, involving upper thermospheric winds and composition measurements from DE-2, has been carried out over the past several years and has led to a much improved capability of the TGCM to specify upper thermospheric winds (see Figure 6). The ADS spacecraft will provide the necessary measurements to validate the TGCM for the purpose of improved lower thermospheric density specification.

We conclude that the TGCM approach currently allows for greater temporal resolution than semi-empirical models. Upgrading of the semi-empirical models to allow for greater temporal resolution would be of benefit, but it should be recognized that this would not lead to a capability for prediction of traveling disturbances. In this regard, the TGCM provides a significant new capability, but its utility is tied to the accuracy with which the time dependent thermospheric forcings can be quantified and parameterized for use in the model. Careful validation procedures need to be employed based on direct experimental measurements of global-scale state parameters in the lower thermosphere from the ADS spacecraft.

2.5 Summary of the Theoretical Considerations Pertaining to Lower Thermosphere Density Specification

The density structure of the lower thermosphere is critically dependent on the nature and variability of the thermospheric energy and momentum sources and sinks and the resulting neutral wind systems of all scales. An improved physical understanding of the flow of energy and momentum through the lower thermosphere on a global scale is essential for improvements in density specification. This understanding requires the use of sophisticated theoretical tools capable of simulating the complex non-linear interactions of importance. One such tool is the NCAR-TGCM. This model affords better intrinsic temporal and spatial resolution than the semi-empirical MSIS-86

model, but requires extensive testing and validation as well as accurate prescriptions for the important time-dependent thermospheric inputs of energy, momentum and precipitating particles. The principal requirements for the enhancement of our physical understanding and description of the lower thermosphere state variables may be summarized as follows; specific recommendations are given in Section 7 of this report.

1) There is a serious need for a detailed and comprehensive experimental data base containing information on the lower thermosphere state variables: density, temperature, composition and wind. This data base should provide sufficient coverage to enable the local time, latitudinal, altitudinal, seasonal, Universal Time, and storm time dependencies of the state variables to be identified and quantified. To approach specification accuracies of 5 percent for thermospheric density, this data base will need to be collected using redundant, cross-calibrated and extremely accurate instrumentation. This requirement will be met by the ADS mission discussed below.

2) The tidal forcing of the lower thermosphere (phases and amplitudes of important tidal modes) needs to be quantified on a global basis using a combination of satellite (ADS) and ground-based (CEDAR) instrumentation and suitable theoretical analysis.

3) Extensive testing and case study activities need to be carried out using TGCM simulations and experimental measurements in the lower thermosphere to validate the theoretical framework and improve the formulation of the TGCM boundary conditions and inputs. An analogous validation procedure has been carried out successfully for upper thermosphere dynamics. Validation tests should include mean climatology as well as individual detailed case studies.

4) A detailed knowledge of globally-averaged thermospheric energy and momentum sources and sinks is required to define inputs to the TGCM. This knowledge will necessitate improved specifications of the solar UV-EUV fluxes using direct measurements if at all feasible, as well as the F10.7 cm proxy index. It will also require improved indices for the geomagnetic particle input, convection electric fields, and conductivities at high latitudes, incorporating data from the NOAA/TIROS and DMSP spacecraft and available auroral imagers.

5) Important aeronomic reaction rates, such as those involving atomic oxygen, need to be further quantified for use in the TGCM.

6) Further quantification of the prevalence and nature of gravity waves in the lower thermosphere is needed to determine the limits to accuracy governed by the stochastic nature of the shorter period waves and to derive probability distributions for the occurrence of thermospheric waves with given characteristics.

3. REVIEW OF MODELING TECHNIQUES FOR DENSITY (ABSOLUTE AND VARIABILITY)

3.1 Semi-Empirical Models

Semi-empirical models of the upper atmosphere can be divided into several series. The US Standard Atmosphere line of models provides altitude profiles of temperature and density for individual locations and for typical or average geophysical conditions. As such they are neither intended nor suitable for detailed comparison with satellite or rocket data taken globally and under a wide range of geophysical conditions. With the detection of atmospheric drag effects on early

artificial satellites, data became available that led to the well known series of Jacchia models. The J65 model was the earliest semi-empirical model to provide truly global coverage down to a lower altitude of 120 km. While drag based models use temperature and composition as intermediate parameters for the calculation of total density, these intermediate parameters may be in error since drag data provide no direct information on composition and temperature. The J77 model introduced separate pseudo-temperatures for each constituent, but this added complication did not lead to significant improvements in performance.

The OGO-6 satellite mass spectrometer launched in 1969 provided the first extensive measurements of the densities of the principal thermospheric constituents. Their sum provided an independent determination of total density. The observed variations in composition were quite different from Jacchia model predictions and led to a new approach to represent the observed variability. The ground-based incoherent scatter radar measurements of temperature were subsequently combined with the *in situ* composition measurements in the MSIS (Mass Spectrometer and Incoherent Scatter) models to provide composition and temperature as well as total density predictions of equivalent accuracy for various geographical, temporal, and solar conditions. The latest model, MSIS-86, contains extensive data from the Atmosphere Explorer and Dynamics Explorer missions (Table 2).

Table 2. Density Ratio to MSIS-86 for N₂, O and He when Ap<11

Data set	Altitude	N ₂		O		He	
		avg	sd	avg	sd	avg	sd
OGO-6	400-700	1.08	0.26	1.17	0.15	1.18	0.18
San Marco-3	190-250	1.08	0.21	0.93	0.16	1.10	0.15
Aeros-A NATE	200-500	1.12	0.43	1.16	0.30	1.16	0.36
AE-C NATE	190-400	1.04	0.29	0.89	0.18	0.69	0.15
AE-C OSS	135-160	0.97	0.15				
AE-C OSS	190-400	0.97	0.22	1.06	0.17	1.04	0.21
AE-D OSS	140-160	0.96	0.16				
AE-D OSS	190-400	0.88	0.22	0.99	0.18	0.79	0.21
AE-E NACE	140-160	1.01	0.12				
AE-E NACE	190-450	1.00	0.22	0.89	0.19	0.93	0.14
ESRO-4	200-350	0.87	0.32	0.83	0.24	0.86	0.32
DE-2 NACS	200-900	0.60	0.22	0.89	0.15	0.86	0.16
Rockets	100-120	0.83	0.36				
Rockets	110-160	0.89	0.26				
Rockets	190-300	0.89	0.26				
Arecibo	100-120	0.92	0.32				
Arecibo	110-135	1.16	0.52				

The MSIS-86 model has gained most acceptance from the scientific community and has been used most extensively in a great number of studies and experimental comparisons. It is continually updated and tested by Dr. A. E. Hedin of the Goddard Space Flight Center, who maintains an active

scientific thermospheric research program. Because of the continued interest in the development of the MSIS series of models and because it has been adopted by the International Committee on Space Research (COSPAR) as the new COSPAR International Reference Atmosphere (CIRA-88), we limit our discussions to a consideration of the current capabilities and possible future enhancements to the MSIS-86 model. Other semi-empirical models have been published, but these have not received as much critical scrutiny. The MSIS-86 model is based on a spherical harmonic (associated Legendre polynomial) expansion of the various fields to 5th order (spatial resolution ~20 degrees) with terms added to express various specific dependencies, such as magnetic activity, solar activity, longitudinal, etc.

Table 2 shows the present accuracy of the MSIS-86 model by presenting average departures and standard deviations of the individual data subsets used in generating the model.⁹ An additional critical comparison of the performance of the MSIS-86 model with an independent data set has been carried out by Marcos.⁸

The database from MSIS-86 (partial listing in Table 2) consists of composition, temperature, and density data from scientific satellites with *in situ* thermospheric measurements as well as rockets (for the lower thermosphere) and ground-based incoherent scatter stations. An examination of the MSIS-86 model illustrates the basic climatology of thermosphere density very well. Solar EUV flux, represented within the model by the average F10.7 cm flux, has the largest single influence on the thermosphere, giving a factor of 5 in total density from solar maximum to solar minimum. Thermospheric variations correlated with short term F10.7 variations (daily minus mean) are about one third as large. Magnetic activity variations can be almost as large as EUV variations. The differences between total densities at the pole and equator are relatively small. Under quiet magnetic activity conditions, latitude variations in the upper thermosphere are very small (5 percent). Global annual and semiannual variations are about ± 20 percent, but do not vary strongly with altitude. Daily variations in total density are of the same order of magnitude but change in amplitude and period with altitude so that semi-diurnal variations are more important in the lower thermosphere (seen also in the TGCM predictions shown earlier), whereas the diurnal amplitude grows with altitude. Pure seasonal variations are somewhat smaller than daily variations in the upper thermosphere. The magnetic pole rotating about the geographic pole produces UT variations on the order of 5 percent in total density, and longitudinal variations are the same order or smaller. In all cases, except the EUV and global annual/semiannual variations, the temperature and composition variations are much larger than the total density variations with the out of phase behavior (not realized before mass spectrometer measurements) of various constituents resulting in smaller net effects.

The present accuracy of the MSIS-86 and other semi-empirical models has been the subject of detailed recent studies by Marcos^{7,8} using an independent data base (from SETA measurements). The accuracy with which the MSIS-86 model reproduces the data used in its generation may be assessed by reference to Table 2. In general, the error of MSIS-86 is within 15 percent under quiet geomagnetic activity conditions, rising to ~30 percent or more at active times in the high-latitude region. Hedin (private communication, 1988) has recently shown that the MSIS-86 model is the best available semi-empirical model in terms of reproducing the thermospheric densities provided by the original Jacchia satellite drag data and the CACTUS satellite drag data from a French satellite. This unpublished work indicates that a slow improvement in the capability of semi-empirical models has indeed been sustained, although the gains of the past several years have been relatively minor and the rate of

improvement is such that significant advances are extremely unlikely without an infusion of new and highly reliable data.

The limitations on the accuracy of the MSIS-86 model (or any semi-empirical model) are set by a combination of several factors, including: 1) the inherent accuracy (or lack thereof) of the contributing sensors providing data for the model fitting procedures, 2) possible errors or inappropriate assumptions in the extrapolation procedures used to interpolate between data points and to extend the range of the empirical model to altitude regions where the data are sparse, 3) limited temporal and spatial resolution in the formulation of the empirical model (for example, MSIS-86 uses 3-hourly Kp values to determine the geomagnetic activity effect which observations show can be much more rapid in reality), 4) limited experimental coverage and/or unmodeled and unpredicted systematic variations, and 5) the inherent stochastic nature of atmospheric variability, which might be expected to provide a fundamental limit on the accuracy with which any given geophysical situation can be quantitatively modeled. We next discuss these various sources of inaccuracy in turn, outlining at the same time directions for improvement in density specification.

3.1.1. INHERENT ACCURACY OF CONTRIBUTING SENSORS

The accuracy with which a semi-empirical model represents thermospheric density depends on the accuracy of the primary experimental observations. Reference to Table 2 shows that individual average density ratios differ from unity by large values (regularly up to 15 percent), indicating that the experimental techniques used to generate the MSIS-86 model do not always provide self-consistent results. Inconsistencies between different data subsets, possible differences between techniques, and systematic errors for individual sensors are all possible contributors to a reduction in the overall MSIS density accuracy from the optimum. To take an extreme, but not altogether unlikely example, a large systematic (calibration) error for just one of the many satellite mass spectrometers contributing to MSIS-86 could have a significant impact on the overall model accuracy by skewing the model away from a true representation of thermospheric densities. The effect of such a calibration error would be to bias the model in favor of the erroneous measurements, leading to a deterioration in the overall level of model accuracy. In such a situation, the specific source of the additional error would be very difficult to recognize and correct for. In reality, it is likely that the data base used to generate MSIS-86 is composed of measurements subject to a continuum of systematic errors and defects.

To provide a direct example of inconsistencies among the sensors contributing to MSIS-86, we show in Figure 16 a comparison among data from the OSS, NATE and MESA instruments flown together on Atmosphere Explorer-C. In this figure, simultaneous observations of total density along the track of the satellite have been intercompared by plotting the ratio of a) NATE to MESA and b) OSS to MESA against MESA densities. Both the OSS (open source spectrometer) and the NATE (neutral atmosphere composition experiment) instruments were heavily used in the formulation of MSIS-86, while MESA (miniature electrostatic accelerometer) provides a third independent measure of density. If all three experiments had yielded identical total densities, all plotted points would fall on the horizontal line through unity. Instead, there are clearly systematic variations among the three instruments at the 15 percent level. For example, the OSS/MESA scatter plot illustrates a trend towards lower ratios at the higher measured densities. This trend could indicate a systematic error that was a function of altitude in either one or the other (or both) instruments. Similarly, the

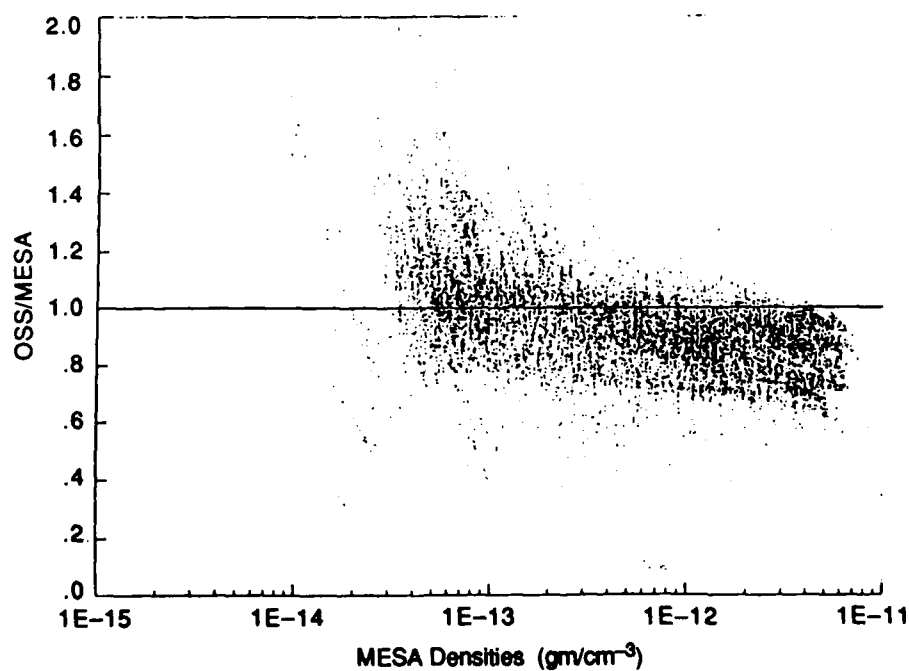
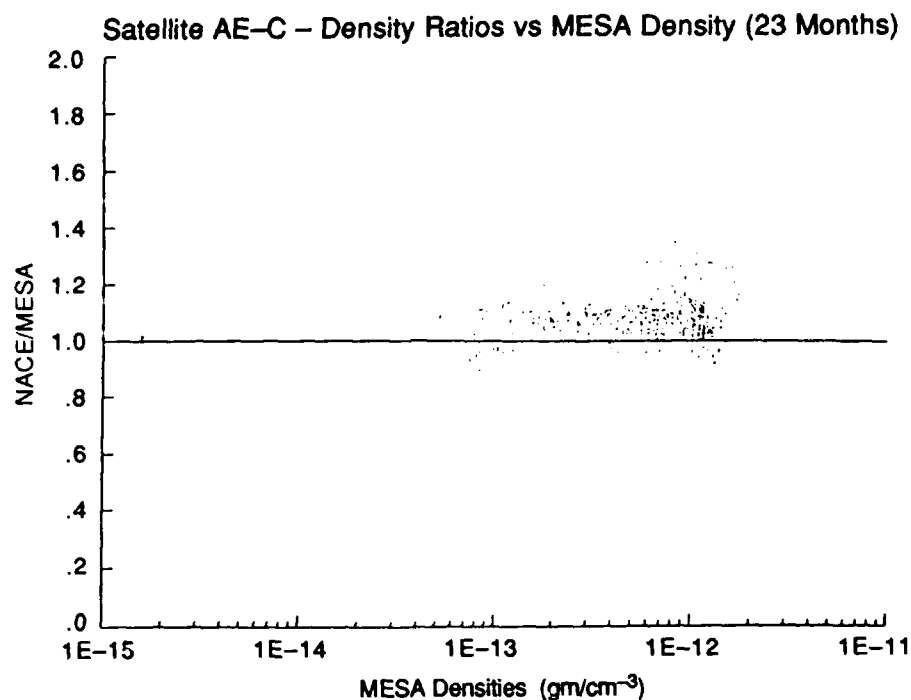


Figure 16. Comparison between measurements of total density on the AE-C spacecraft using the MESA, OSS and NACE instruments. a) The ratio of simultaneous measurements of density from NACE and MESA are plotted as a function of the total MESA density in a scatter plot form. b) the ratio of simultaneous measurements from OSS and MESA. Systematic differences between the individual techniques are evident; see text.

NACE/MESA ratios indicate that NACE measured systematically higher (by ~10 percent) than MESA at all altitudes. Clearly, to determine which are the operative systematic errors in such data sets several years after calibration and delivery of the instruments is a daunting task. However, a detailed intercomparison of the contribution of each individual experimental technique to the overall accuracy of MSIS-86 is a task that should be carried out. Ideally, of course, this difficult task would be made much more tractable if there were to exist a new, independent, and thoroughly intercalibrated data set that could act as a uniform standard to arbitrate among the more historical contributing data sets. *The ADS data base will fulfill this very important role. It is, of course, crucial that any new data base be designed to meet or surpass the required 5 percent accuracy for total density and corresponding accuracies for temperature and wind.*

Another source of systematic error common to many of the MSIS-86 contributing sensors is due to the effects of the neutral wind at the satellite location. As mentioned above, an in-track neutral wind can cause a significant error in the determination of density from either mass spectrometer or drag measurements. None of the data bases within MSIS-86 have been properly corrected for wind, since wind measurements were, in general, not available. An examination of the wind observations reported from Dynamics Explorer indicates that significant density errors can regularly occur at high- and mid-latitudes due to this effect. For example a 200 m/sec wind has a 5 percent effect on drag and a 2.5 percent effect on mass spectrometer density measurement. The differing effects of wind on the different techniques may explain some of the inconsistencies mentioned above. In any event, *it is important that the ADS density data base be appropriately corrected using direct wind measurements.*

3.1.2. ERRORS IN THE EXTRAPOLATION PROCEDURES

MSIS-86 uses the diffusive equilibrium profile to extrapolate between individual measurements. This is likely to be a fairly good assumption for quiet times and low latitudes, but is likely to break down for more active periods and at high latitudes.¹³ The degree of uncertainty introduced by the extrapolation procedure used in MSIS-86 is difficult to estimate, though it is probably smaller than the possible systematic errors or inter-technique differences discussed above. The best estimation of this source of error will come from detailed numerical modeling (TGCM) studies of the departures from diffusive equilibrium that can occur in the atmosphere. Such studies will involve the analysis of individual terms in the momentum equation solved by the TGCM²⁴ and should be carried out as part of the interpretive part of the density specification program.

3.1.3. LIMITED TEMPORAL AND SPATIAL RESOLUTION

The relatively limited spatial and temporal resolution afforded by MSIS-86 has been alluded to above. There are computational advantages to keeping the number of model coefficients within manageable limits but, on the other hand, there are clear disadvantages in terms of limits on the types of spatial and temporal structures that become amenable to realistic modeling. From the considerations discussed in Section 2.4, it is clear that a modest increase in the spatial resolution of MSIS (to ~10° resolution) would be advantageous and would enable significant climatological features to be better modeled, particularly in the high latitude region, where relatively small-scale density structures are known to persist.

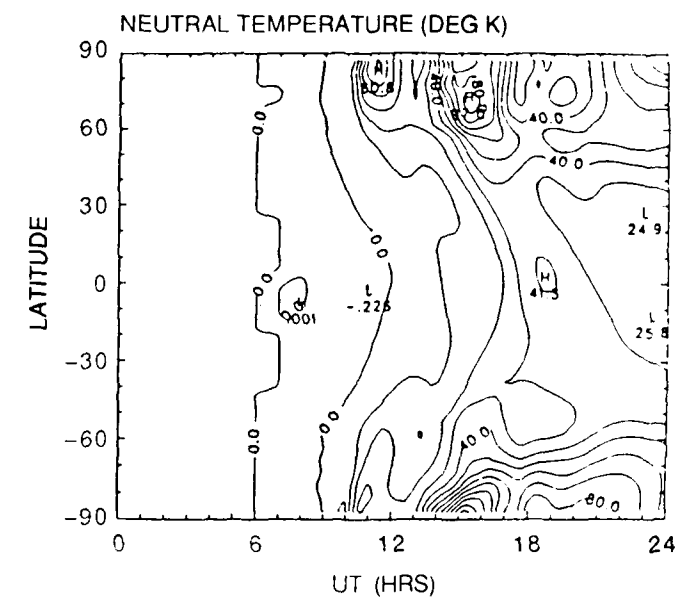
The temporal resolution of the model is limited in two ways. Firstly, the use of the 3-hour Kp geomagnetic index and the daily F10.7 solar flux index determines the maximum rate of change of perturbations depending strongly on solar and geomagnetic input that can be modeled accurately. Thus, for example although purely UT dependent changes can be followed at much higher temporal resolution, the relative changes in thermospheric density occurring due to geomagnetic storm-time perturbations can only be followed with a 3-hour resolution limit. Since the major perturbations in thermospheric density can be traced to geomagnetic and solar disturbances, the temporal resolution of the indexes used in the semi-empirical model places a significant restriction on its capability to track the more rapid perturbations in the thermosphere. Figure 17 shows a comparison of storm-time calculations of thermospheric temperatures at 120 km calculated using the NCAR-TGCM and the MSIS-83 model.²⁷ A simple comparison between the two perspective plots (Figure 17b for the NCAR-TGCM and Figure 17d for the MSIS-83 model) illustrates clearly the effect of the 3-hour temporal resolution for the MSIS model. The temperature predictions for the MSIS-83 case show "steps" at 3-hour intervals based on the updating of the appropriate Kp index, while the predictions of the NCAR-TGCM show a more smoothly varying response. In both cases, it should be noted that the geomagnetic perturbations in thermospheric temperature for this particular case maximize at high latitudes, but propagate significantly down through equatorial latitudes. It is considered that the 3-hour geomagnetic resolution element would be very difficult to improve upon in the foreseeable future, given the nature and availability of geomagnetic indexes covering the periods used to generate the model.

The second important limitation of an MSIS-class model in terms of its temporal resolution is more subtle and is one that also cannot be removed in the foreseeable future. Since any semi-empirical model is based on "climatological" records of experimental data, the model outputs for specific geomagnetically active periods can only represent the average or mean behavior of the thermosphere to similar but "generic" disturbances. Thus MSIS-class models cannot be expected to predict the phases and amplitudes of traveling disturbances in the thermosphere. In other words, semi-empirical models can only predict the "DC" response of the thermosphere. The TGCM, on the other hand, has the inherent capability to predict the "AC" response as well as the "DC" response. As discussed below, the accurate prediction of the *phases* of such AC disturbances will be a great challenge for the numerical model approach.

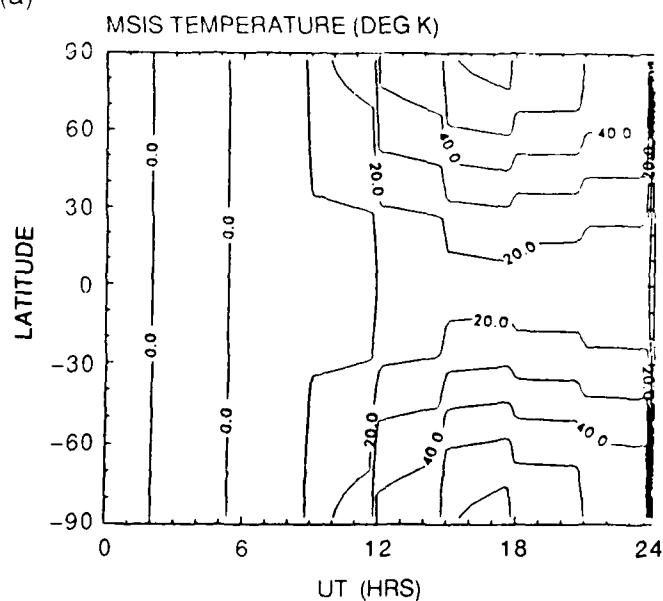
3.1.4. LIMITED EXPERIMENTAL COVERAGE AND/OR UNMODELED AND UNPREDICTED SYSTEMATIC VARIATIONS

The MSIS-86 model contains data from many previous experimental investigations, as discussed above. The coverage afforded by these previous techniques, however, was particularly limited at lower thermospheric altitudes. At the lower altitudes, reliance has been placed on an extremely limited (in terms of global coverage) rocket data set. The coverage at upper thermospheric altitudes is much better and various satellite missions have contributed large bodies of data providing a firm basis for the specification of the geographic, seasonal, and solar cycle dependencies. *There is a clear need to improve the direct experimental coverage of the lower thermosphere densities for use in semi-empirical models and this is one of the major goals of the ADS mission.*

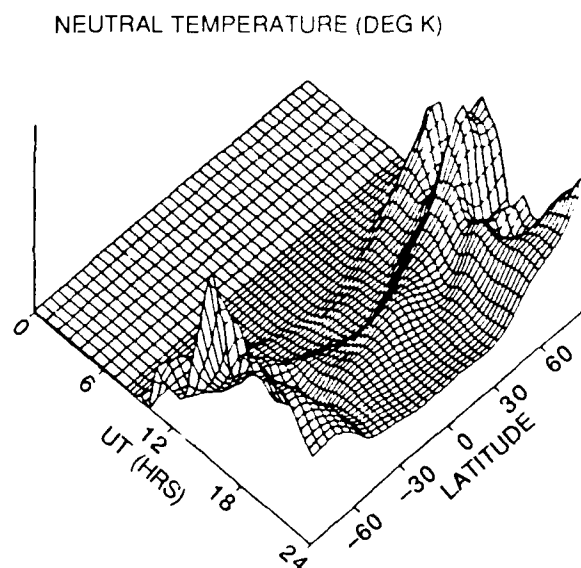
The existence of important, but as yet unrecognized, systematic variations in thermospheric density could be a cause for reduced accuracy of the semi-empirical models. To provide an example of



(a)

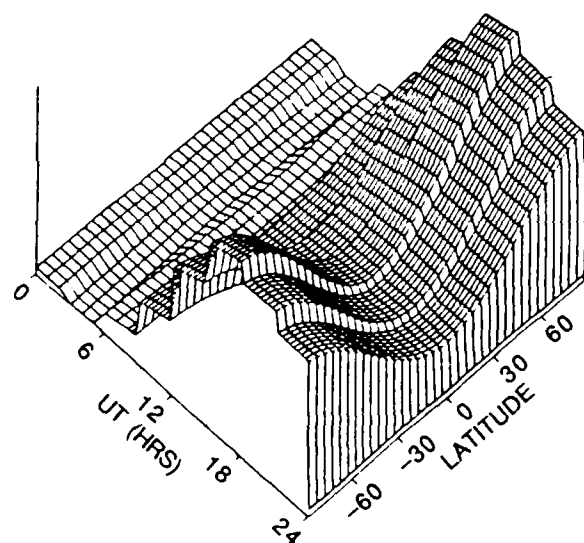


(c)



(b)

MSIS TEMPERATURE (DEG K)



(d)

Figure 17. Comparison between calculations from the NCAR-TGCM and the MSIS-83 models for the March 22, 1979 substorms.²⁷ The figure shows contours of the time variation of the zonally averaged temperature difference (degrees Kelvin). (a) TGCM-calculated temperature difference along the 120 km constant-height surface, (b) a perspective illustration of that temperature response, (c) MSIS-83-calculated temperature difference along the 120 km constant-height surface, and (d) a perspective illustration of that temperature response. Contour intervals are 10°K.

a variation not incorporated in the MSIS formulation, a significant systematic modulation of the semi-annual variation might be found that would reduce model errors. It is considered unlikely, however, that any single simple undiscovered systematic variation exists that could make a dramatic difference in our predictive capability, but a number of relatively small improvements could have a significant cumulative effect. *The discovery of additional systematic variations will necessitate continued and careful scrutiny of the MSIS data base by experienced scientists.* In this regard, the provision of the ADS data base would provide significant incentive to conduct such a careful search.

3.1.5 INHERENT STOCHASTIC NATURE OF ATMOSPHERIC VARIABILITY

This topic has also been discussed previously, leading to our estimation of a 5-10 percent "floor" on the predictive capability of MSIS-class models due to incoherent gravity waves. It is important to improve the estimate for this natural predictive limit by carefully extending studies such as the one discussed above, since without a long term study of this topic, unrealistic goals will be strived for, with the consequent waste of scientific and human resources. The ADS data base will provide the ideal data resource to determine the power spectra for thermospheric density perturbations under a variety of conditions. Although much can be done along these lines using existing data bases, the ADS data base will considerably improve the data resource for such studies in the lower thermosphere region.

3.1.6 SUMMARY OF FUTURE IMPROVEMENTS FOR SEMI-EMPIRICAL MODELS

The causes for the current accuracy limit in density predictions using MSIS-class models were discussed in Section 3.1. Wave activity will provide an ultimate floor on point predictions on the order of 5-10 percent in the upper thermosphere, depending on latitude and activity level, and to a more or less unknown degree in the lower thermosphere. *Significant improvement will only come from a multifaceted attack, involving further analysis of old measurements as well as new measurement programs since without new measurements of the required accuracy, there is no appropriate standard for model improvements.*

3.2 Dynamical Models - TGCMs

As discussed above, two thermospheric general circulation models (TGCMs) are in an advanced state of development. These are: 1) the NCAR TGCM of R.G. Roble and colleagues and 2) the University College London (UCL) TGCM of Fuller-Rowell and Rees. These models use the complete set of primitive equations to calculate the response of the thermospheric winds, temperatures, and compositional structures to a prescribed set of input boundary conditions and time-dependent forcings. In this report, we concentrate our attention on the NCAR model, since it is readily accessible from within the United States. The UCL model is almost entirely analogous to the NCAR model, though there are many differences in detail. The basic validity of the numerical scheme used in the NCAR-TGCM has been tested extensively through comparisons of model predictions with experimental data from DE-2 as well as other experimental techniques. In general, it may be considered that the set of equations solved by the NCAR-TGCM is adequate to represent the thermospheric response with a spatial resolution element of 10° latitude \times longitude (given by twice the grid spacing) and a temporal

resolution element of ~2 minutes (given by computer time limitations). It should always be remembered, however, that the TGCM calculations are only as reliable as the inputs used to define the boundary conditions and the time dependent forcings. *The capability of the TGCM to predict thermospheric densities is therefore entirely determined by the accuracy with which the important thermospheric forcings can be quantified and used as inputs to the model.* The principal external forcings that control the density structure are the solar UV/EUV flux, the magnetospheric convection electric field and auroral particle fluxes. Clearly, any dependence on TGCMs for density specification will require an ancillary program to determine these important forcings quantitatively.

The NCAR model uses a grid of $5^\circ \times 5^\circ$ in latitude and longitude, with calculations carried out on 24 constant-pressure surfaces from ~97 to ~500 km altitude. The time step for individual calculations is variable, but is typically ~1.5 minutes. Table 3 provides a summary of the inputs and outputs of the

Table 3. NCAR-TGCM Inputs and Outputs (Version 4)

Model	Parameterizations
Inputs:	
Lower Boundary winds, composition, and temperature	Tidal amplitudes and phases according to prescription of Fesen et al ²⁶ . Composition and density structure given by MSIS-86.
Magnetospheric convection electric field	Modified Heelis model linked to NOAA/TIROS activity index
Low latitude electric fields	Empirical model of Richmond
Ionosphere densities and conductivities	Self-consistent calculations
Cross-cap potential	Modified Reiff/Luhmann model linked to NOAA/TIROS activity index.
Solar UV/EUV fluxes	Hinteregger fluxes from AE measurements scaled by solar F10.7 cm index
Auroral input	Scaled to NOAA/TIROS activity index according to prescription of Roble and Ridley ²¹
Upper boundary condition	Standard zero derivative assumptions.
Outputs:	
Winds, temperatures, ion densities, composition, heights of constant-pressure levels, ion drifts, thermospheric densities.	Stored in History files at selected Universal Times

TGCM in its current configuration. Recent modifications have included the development of a scheme to calculate ionospheric parameters self-consistently with the neutral thermospheric parameters, using the same Eulerian scheme as the original TGCM. This important development eliminates the need for a reliance on the use of questionable empirical models to describe ionospheric densities and conductivities.

Much of the analysis of the scientific underpinnings for thermospheric density, discussed above, utilized results from the NCAR TGCM to illustrate the fundamental forcing processes and their influence on thermospheric density. In general, the TGCM provides very realistic calculations for

upper thermospheric state variables and these have been validated by means of extensive testing using the DE-2 and other data sets. The lower thermospheric calculations have not yet been tested in the same way against global-scale data sets and this would be one of the principal mission objectives for the ADS spacecraft.

3.2.1 CURRENT PERFORMANCE OF THE NCAR-TGCM FOR DENSITY SPECIFICATION

As discussed previously, the lower thermospheric TGCM predictions require further verification. However, it is possible to evaluate the capability of the NCAR-TGCM to calculate density structure at upper thermospheric altitudes. This section presents the results of a critical comparison between calculations of the NCAR-TGCM and the MSIS-86 models for: 1) a geomagnetically quiet period of 2 days, centered on Julian day 81325 and 2) a geomagnetically active period of 3 days, centered on Julian day 82328. In both cases, extensive density measurements are available from the DE-2 spacecraft at altitudes of ~300 - 400 km. Since the self-consistent version (number 4) of the TGCM has not yet been released for external use, we use the previous version (number 3) which contains a tidal forcing prescription, but does not contain the fully self-consistent prescription for thermosphere-ionosphere coupling. Version 3 of the model also is deficient in that insufficient thermospheric cooling due to NO and CO₂ radiation is incorporated and thus calculated thermospheric temperatures and densities are in general too large. This problem has been resolved in version 4, but, for the purposes of the comparisons presented here, the discrepancy between the NCAR-TGCM and MSIS-86 absolute total densities has been artificially removed by normalizing the median NCAR-TGCM density to the median density contained within MSIS-86. This procedure is reasonable, since the MSIS-86 total global mean density values are likely to be much more reliable than the point-to-point spatial variations under consideration here. Medians were used rather than means so that the comparisons illustrate better the capability of the two models to predict independently variations about the total global-mean density as a function of space and time. It is to be expected that significant improvements in model realism will be attained with version 4 of the TGCM and therefore these comparisons may be taken as biased unfavorably against the current capabilities of the TGCM.

For the comparisons, two types of data presentations are made, first to demonstrate the capability of the two models to predict the natural variability observed along the orbital track of the DE-2 spacecraft and, second, to determine the absolute accuracy with which density variations from the global mean are predicted in each case. Figures 18a and b show, respectively, the comparison for variability for the quiet and active periods. Density data for atomic oxygen (principal constituent at the altitude of the DE-2 measurements, namely ~350 km) was binned as a function of latitude along the DE-2 spacecraft track for about 20 orbital passes for the quiet days and about 30 for the active days. The TGCM was run using time-dependent inputs for the solar and magnetospheric energy and momentum inputs in each case and predicted density values were obtained by sampling the model output along the spacecraft orbital track. Similarly, the MSIS-86 model densities were obtained by using the appropriate geophysical indexes and evaluating the semi-empirical model along the orbital track. After binning and averaging the data and model predictions by latitude, the standard deviations about the medians were evaluated and plotted in histogram format in Figures 18a and b. The standard deviations calculated in this way illustrate both the natural variability contained within the real atmosphere at these altitudes (DE data) and the variability that can be predicted by the

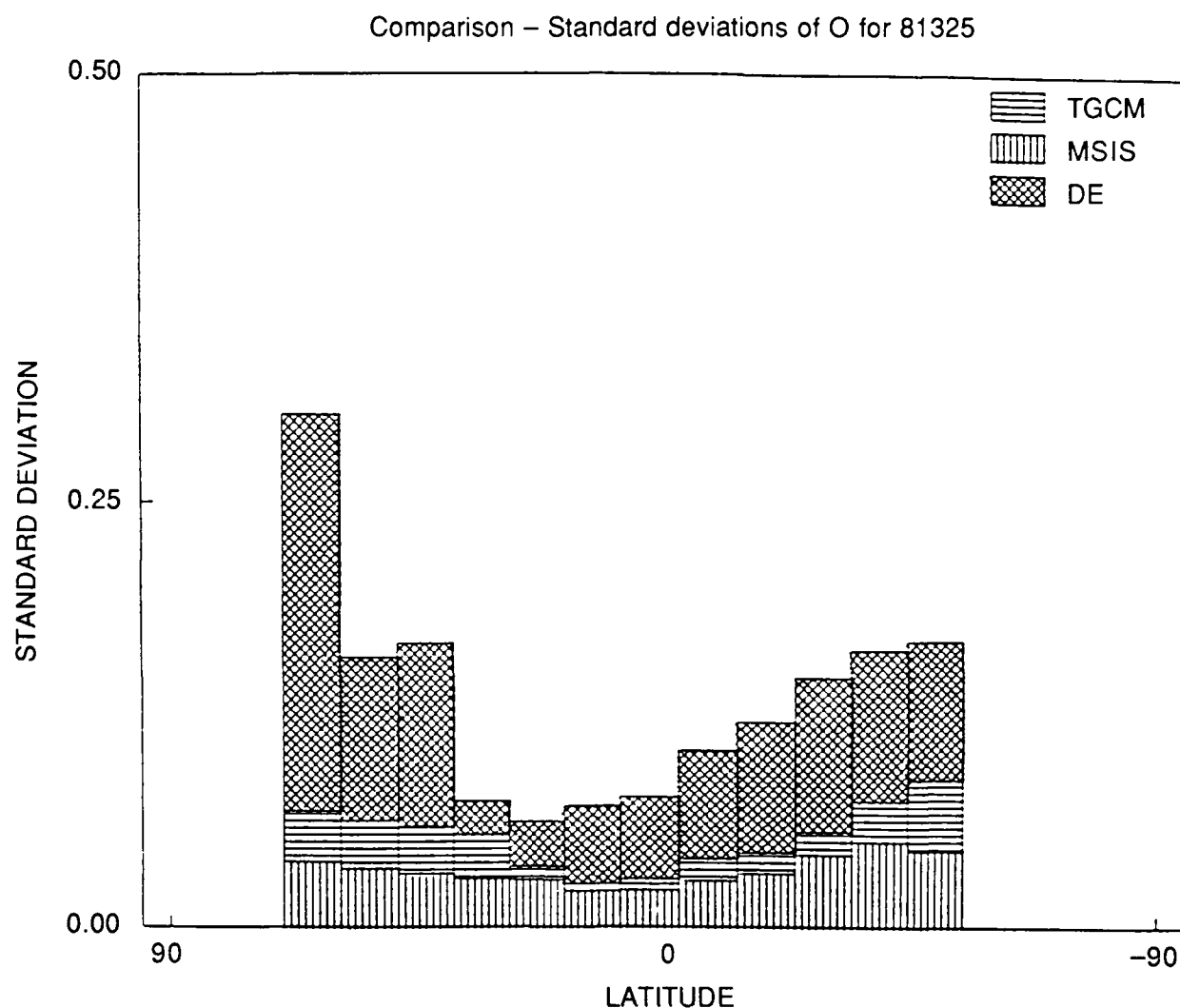


Figure 18a. Calculated standard deviations from the mean as a function of latitude for the geomagnetically quiet two-day period centered on Julian day 81325. Standard deviations from the atomic oxygen density measurements from the NACS instrument on DE-2 are compared with standard deviations obtained by evaluating the NCAR-TGCM and the MSIS-86 models along the orbital track of the spacecraft (see key at top right).

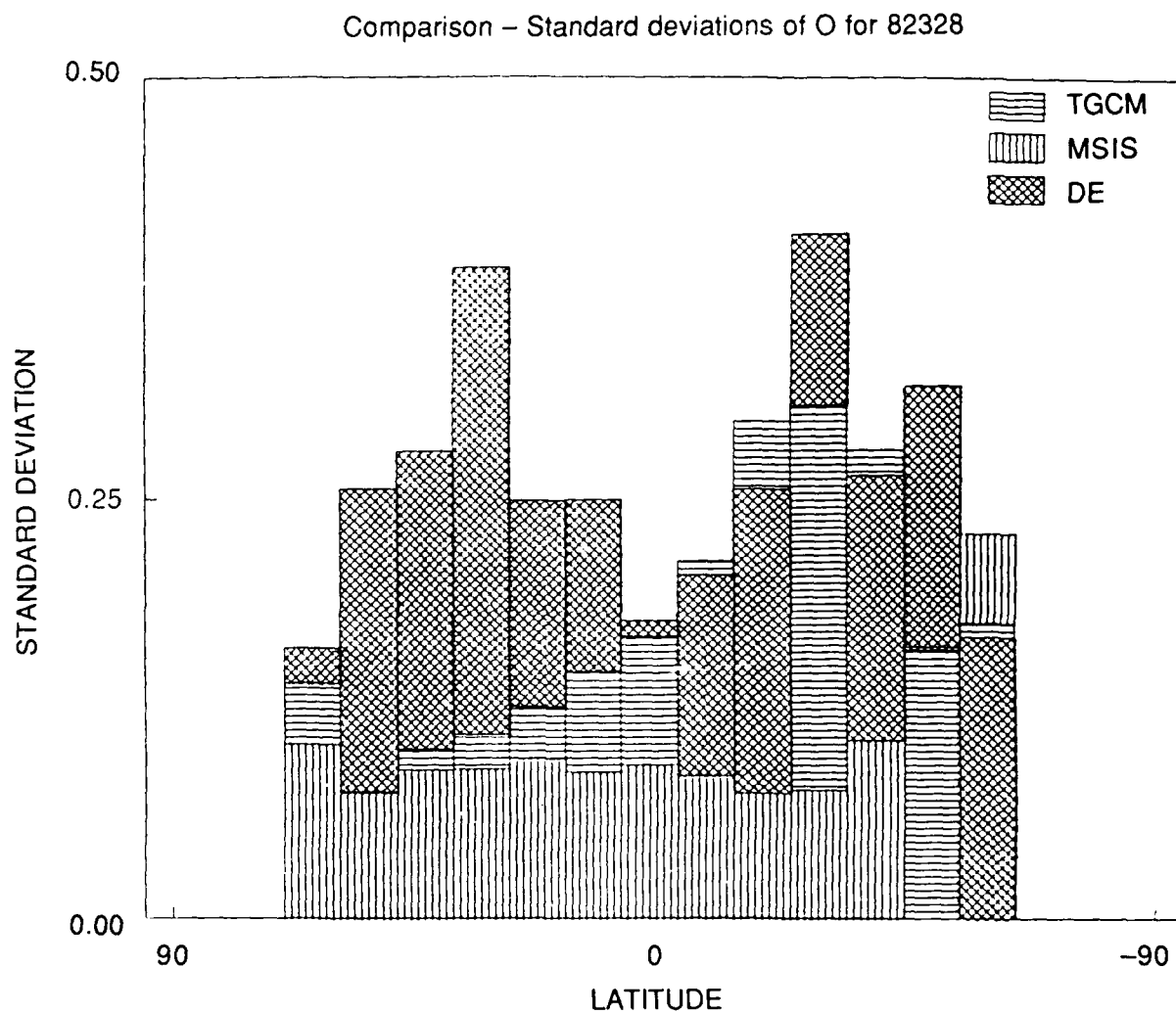


Figure 18b. Same comparison for the 3-day geomagnetically active period centered on Julian day 82328. The altitude range for the DE-2 observations is 300-400 km.

two types of models. Figure 18a indicates that the measured variability maximizes at the higher latitudes, as expected, reaching values of ~20 percent or greater for the quiet-time case. The MSIS-86 and the NCAR-TGCM standard deviations fall below the measured values, indicating that both models tend to underestimate the natural variability in the real atmosphere. In all cases, however, the TGCM model predicts greater variability than the MSIS model, as would perhaps be expected from the superior spatial and temporal resolution discussed above. The improvement is modest at low latitudes, but becomes significant at the higher latitudes. Figure 18b shows a similar comparison for the active period. While the histograms show much greater variability and a more complicated latitudinal variation for both the model predictions and the spacecraft measurements, the basic story is the same, with the TGCM capable of predicting more of the natural variability at all latitudes.

The comparisons shown in Figures 18a and b illustrate the capability of the two models to predict the natural variability that occurs in the atmosphere as a function of latitude. This type of comparison, however, does not tell us which model is superior for the actual prediction of density as a function of space and time. To compare density measurements and density predictions more directly, data from the same two periods were used to ratio the predictions of the models with the spacecraft measurements. These comparisons are similar to those reported in previous literature (Marcos⁷) and are shown in Figures 19a and b. For these plots, model predictions (after the median normalization discussed above) have been ratioed with the individual spacecraft measurements and the standard deviations of the ratios calculated for each latitudinal bin. The comparisons for the quiet and active periods indicate that the two models provide roughly commensurate relative errors. For the quiet case these errors are on the order of 15 percent when averaged over all latitudes, in agreement with previous work. For the active case, the errors are larger, as would be expected from the extreme geomagnetic conditions prevalent (large southward turning of the interplanetary magnetic field Kp in excess of 7). It can be seen, however, that there is not much to choose between the TGCM and MSIS predictions. In other words, version 3 of the TGCM seems to be roughly equivalent in accuracy to MSIS-86 for density specification. *These are extremely encouraging results, since they imply that the TGCM approach has already matched the density specification accuracy embedded within the most comprehensive semi-empirical model available and, moreover, that the TGCM is already superior for the prediction of levels of natural variability.* As mentioned above, this performance is for an already obsolete version of the TGCM. It is estimated that with recently achieved and planned improvements to the TGCM, the density specification accuracies should improve further, dependent of course on the precision with which thermospheric forcings can be prescribed.

4. AFGL DENSITY SPECIFICATION WORKSHOP RECOMMENDATIONS

A Density Specification workshop was held at the Air Force Geophysics Laboratory in October 1987 and was attended by over 100 participants from universities, government laboratories, and private corporations. After extensive discussions of many of the issues discussed above pertaining to absolute density specification, several overall conclusions were stated regarding the status of empirical models and possible future progress in this area. Since these conclusions are directly relevant to the present report, they are reiterated here.

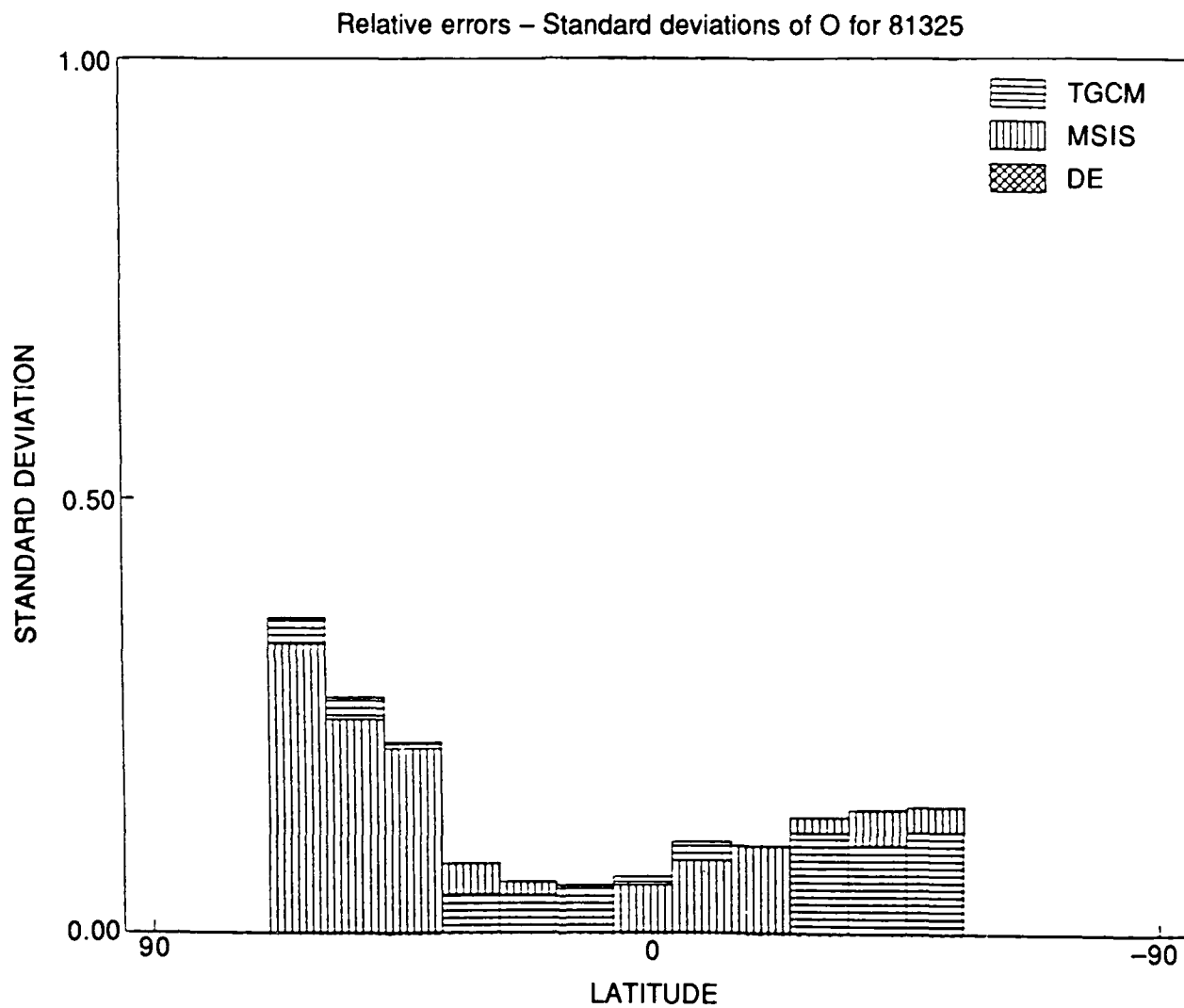


Figure 19a. Calculated relative errors obtained by ratioing the TGC and MSIS-86 model predictions to the measured atomic oxygen densities on a point-by-point basis, binning by latitude and obtaining the standard deviation about the mean ratio for each bin.

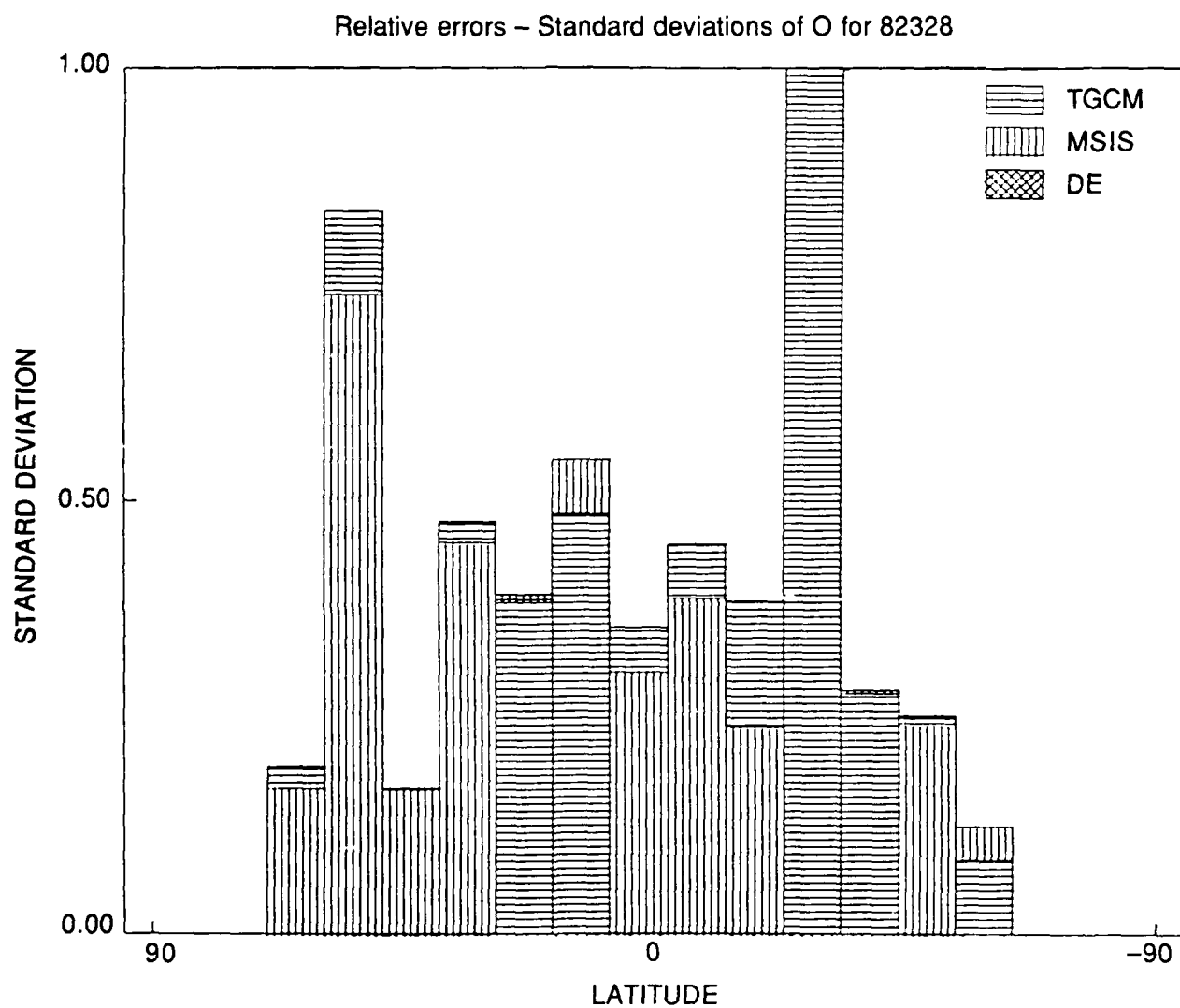


Figure 19b. Same comparison for the 3-day geomagnetically active period centered on Julian day 82328

4.1 Status of Empirical Models

The results of the workshop indicated that the density specification accuracy of semi-empirical models had reached a plateau of ~15 percent and that further significant improvement was likely to be at a slow rate. The requirements for further improvements were summarized as follows:

- 1) There is an important need for additional well-calibrated data sets to provide standard references for further comparisons, etc. Instruments need to be carefully optimized to allow for drifts, cross calibrations, ground-truth measurements, etc. There is a need for redundancy in measurement techniques.
- 2) Existing data sets used within semi-empirical models need to be critically tested to verify consistency. Poorly calibrated and inaccurate data should be excised from the models.
- 3) Data sets should be continually examined to determine whether unmodeled systematic variations occur in the atmosphere that can be incorporated explicitly into the semi-empirical models.
- 4) The effects of neutral wind motions should be taken into account when incorporating data into semi-empirical models.
- 5) Hybrid approaches involving the simultaneous use of semi-empirical techniques as well as numerical modeling calculations should be pursued.

4.2 Workshop Recommendation for Density Specification Program

The workshop participants felt that further work was required to determine the absolute limit on accuracy imposed by the stochastic nature of the thermospheric medium. They also felt that in the short term the tools existed to make significant inroads towards the provision of a more accurate density specification model. These tools include the TGCs, MSIS-86 model and hybrid schemes, such as the VSH approach of Killeen et al.⁵⁸ For the longer term, to break the current 15 percent barrier to density specification, it was felt that since the scientific problem is a multifaceted one, an attack on a broad front would be needed to improve the basic understanding of the region. This approach would involve both theoretical and experimental elements. It was therefore suggested that a coordinated program in density specification be initiated, involving scientists from several institutions. The elements of the program would be the following:

- 1) A density specification spacecraft mission, comprising redundant, well-calibrated instruments, together with supporting observations from DMSP and NOAA/TIROS, as well as ground-based measurements, such as LIDAR and incoherent scatter radar observations.
- 2) An investigation of gravity waves and tides to establish theoretically and experimentally the ground-floor variability.
- 3) An effort to compare and contrast TGC calculations with experimental observations, to validate the TGC in various regions of the atmosphere, leading to an improved theoretical understanding.
- 4) An effort to improve semi-empirical models through continued critical evaluation of the existing data resource and the incorporation of additional well-calibrated data from the ADS density specification mission.

5) An effort to improve the quantitative specification of magnetospheric and solar thermospheric forcings through observations and theory.

6) A science team approach to the interpretative problem, with focussed workshops.

The conclusions of the density specification workshop are in general accord with the recommendations of this report detailed below.

5. ADS MISSION PAYLOAD AND OBSERVABLES

The elements of the Atmospheric Density Specification (ADS) mission, described in this section, have been designed to respond to the challenge of improved neutral density specification discussed above. The mission payload and orbital considerations are discussed in this section. The instruments chosen for the ADS payload have all been flown successfully in previous missions and require no extensive development phase prior to spacecraft integration.

5.1 Instrumentation

The payload instrumentation complement is comprised of four core instruments and two additional desired capabilities - one an extra instrument and one an additional capability to a core instrument. These instruments and their observables are detailed in the following table:

Table 4. ADS Mission Complement

Instrument Name	Observations
Basic Payload:	
SETA - Satellite Electrostatic Triaxial Accelerometer	Density and crosstrack wind
QINMS - Quadrupole Ion/Neutral Mass Spectrometer	Density, high accuracy
CADS - Composition and Density Sensor	Density and intrack winds
FPI - Fabry-Perot Interferometer/IPD Photometer	Winds and temperatures
Enhanced Payload:	
EUVS - Extreme Ultra Violet Sensor	Solar UV and EUV fluxes
FPI - DENS	O ₂ density profiles from 60-90 km

5.1.1 SETA

The Satellite Electrostatic Triaxial Accelerometer, SETA, provides three axes of precise acceleration data from which density to ± 5 percent and cross-track winds to ± 50 m/s can be calculated.⁷ SETA, flown in 1979, is an upgraded version of MESA, the accelerometers flown

successfully on three Atmosphere Explorers.⁶⁸ A proof mass is electrostatically suspended in a 3-dimensional electric field. Acceleration in any axis causes force that is counteracted by an opposing electric field to keep the proof mass in its original position. The counteracting electric field provides a precise measure of the acceleration force on the proof mass.

5.1.2 QINMS

The Quadrupole Ion-Neutral Mass Spectrometer, QINMS, measures the neutral and ion densities in the mass range of 1 to 64 amu over an altitude range of 140 to greater than 500 km. From these measurements total neutral and ion densities can be determined (neutrals to ~5 percent). Ion energies are also determined. The QINMS is nearly the same as the instrument successfully deployed on STS-4 to measure ion and neutral spacecraft contamination. Three other instruments are currently awaiting further shuttle flights.

The QINMS consists of a self-contained vacuum system, an accommodation sphere surrounding the ion source, a moveable flag within the accommodation sphere to allow unperturbed measurement of the reactive gases, a switchable electron impact ion source, a total density sampling grid, a retarding potential analyzer, a quadrupole mass selection filter, a high sensitivity ion detector/electron multiplier combination and a wide dynamic range logarithmic electrometer amplifier. Instrument contamination is controlled by a protective cover that is opened on orbit. Mass sampling occurs at 100 times per second and is controlled by a ROM which is commandable from the ground. The ROM also controls all other instrument variables.

5.1.3 CADS

The Composition and Density Sensor, CADS, also measures ion and neutral densities but is specifically designed to determine temperature and wind using a retarding potential analysis of the ion energy. The CADS is similar to QINMS in that it utilizes a quadrupole mass/ion spectrometer. The important difference is that it is optimized to measure in-track winds with a retarding potential electrode in the ion source.

5.1.4 FPI

The Fabry-Perot Interferometer (FPI) measures the intensity and spectral location of visible atmospheric emissions in altitude regions centered at ~98, 185, and 225 km. From these measurements the primary FPI state variables, winds and temperatures, can be calculated to better than ± 5 m/s and 10 Kelvin. Secondary measurements are metastable atom densities to ± 10 percent. Density profiles can be obtained by using measured temperature profiles and the hydrostatic approximation, together with an *in situ* observation of density to normalize the profile. Since the FPI is a remote sensing instrument, measurements can be made continuously, however data will degrade at the higher altitudes of an elliptical orbit. The FPI was flown successfully on Dynamics Explorer 2.⁴⁵ Since the FPI is an instrument that has not been flown previously on an Air Force spacecraft and

68. Champion, K.S.W. and Marcos, F.A. (1973) The triaxial accelerometer system on the Atmosphere Explorer, *Radio Sci.* 8:197.

since it provides critical wind and temperature information needed for the modeling efforts, we discuss the instrument in greater detail than the *in situ* sensors described above.

5.1.4.1 FPI Instrument Description

The instrument is composed of three basic elements: the interferometer, an electronics package, and the telescope sub-assembly. A schematic of the optical path of the instrument designed to meet the requirements discussed above is shown in Figure 20 and the telescopes are shown in Figure 21. The basic simplicity of the instrument is evident here. Also, shown is the IPD Photometer which will be discussed in the following section.

Incoming light passes through both fore and aft telescopes. The telescopes are oriented at $\sim 45^\circ$ with respect to the satellite velocity vector. The two look directions provide two vector wind components and, since vertical winds are normally small compared to horizontal winds, this permits the measurement of the vector winds. A simple scan mirror in each look direction chooses the altitude. A fore/aft selector chooses which telescope signal will be passed through a simple relay optics system to the interferometer. The telescopes are copies of the DE-FPI design.

Two line-to-circle convertors provide entry to the FPI/IPDPH. The line input matches the need to provide a narrow, horizontal sample of the horizon. In this way, good vertical resolution can be obtained while retaining good sensitivity using a broader horizontal field of view. The line shape is then converted to the circular input required by both the FPI and the IPDPH. Additionally the line inputs can be located close enough together so that they can share telescopes and operate simultaneously, sampling slightly different altitude regimes.

The light from the line-to-circle convertor is then partially collimated to pass through a dielectric interference filter mounted in a filter wheel. The interferometer light beam is then expanded and further collimated to meet theoretical requirements of the fixed-gap, high-resolution etalon. The etalon objective telescope then images the light, which now contains spectral information in an axially concentric pattern, onto the image plane detector. Figure 22 shows the basic interferometer output in the form of a high resolution 12-channel spectrogram which contains the wind, temperature, and brightness information.

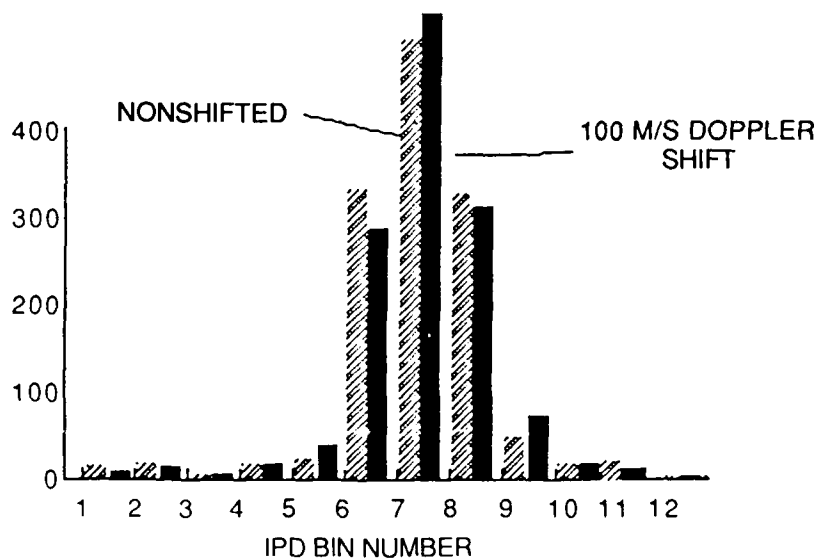
The optical throughput or etendue is held constant throughout the optical system to maximize sensitivity and minimize size. The etendue is controlled by the spectral resolution and instrument size constraints. Folded optics are used to minimize size as well as to avoid mechanical and thermal distortions.

5.1.4.2 Fabry-Perot Interferometer

The heart of the instrument is the Fabry-Perot interferometer that performs the high resolution spectral analysis of light emitted from the earth's atmosphere. The interferometer is a single, fixed gap etalon system with a folded optics objective telescope and a 12-channel image plane detector. The interferometer section is made up entirely of flight-spare hardware and optics from the Dynamics Explorer program.

The etalon and etalon mount are the products of the development effort leading to the successful DE-FPI instrument. The etalon has three zerodur spacers glued to two fused silica end plates on whose inner surfaces are deposited the semi-reflecting dielectric coatings. The etalon is mounted in a fully

INTERFEROGRAMS OBTAINED WITH THE HE/NE LASER AND DE ETALON AND DETECTOR. A PRESSURE STEP WAS TAKEN TO SIMULATE A 100 M/S NEUTRAL WIND.



INTERFEROMETER SPECTROGRAM OUTPUT
FIGURE 4.1.4.3

Figure 22. ADS Fabry-Perot interferometer spectrogram output. The peak detected by the multichannel IPD contains the Doppler information necessary to calculate, winds, temperature, and volume emission rates. The effect of a 100 m/sec wind on the spectrum is illustrated.

kinematic mount designed to provide isolation from stresses due to temperature gradients, etc., while maintaining optical alignment and instrumental ruggedness.⁶⁹

The image plane detector (IPD) is similarly a product of the DE development program and is a 12-channel concentric ring anode device incorporating a micro-channel plate electron multiplication stage and an S-20 photocathode. Each anode ring is single-photon-counting and measures one spectral element. The IPD effectively "scans" the etalon in angle without the need to mechanically change any etalon parameter. It also detects light in all spectral elements simultaneously, thereby enhancing instrument sensitivity over conventionally scanned interferometers. The IPD is identical to that used successfully on DE-FPI.⁷⁰

5.1.4.3 Scanning Telescope Optical Design

The telescope is shown schematically in Figure 21. Two look directions at 45° with respect to the velocity vector are provided to obtain full vector wind measurements. The basic telescope design is the

-
- 69. Killeen, T.L., Hays, P.B., Kennedy, B.C., and Rees, D. (1982) Stable and rugged etalon for the Dynamics Explorer Fabry-Perot interferometer, 2, Performance, *Applied Optics* **21**:3903-3912.
 - 70. Killeen, T.L., Kennedy, B.C., Hays, P.B., Symanow, D.A., Ceckowski, D.H. (1983) An image plane detector for the Dynamics Explorer Fabry-Perot interferometer, *Applied Optics* **22**:3503-3513.

same as DE-FPI consisting of a protective cover, light shielding baffle, and horizon scan mirror. For this mission, an optical switch selects fore and aft views.

5.1.4.4 Electronics

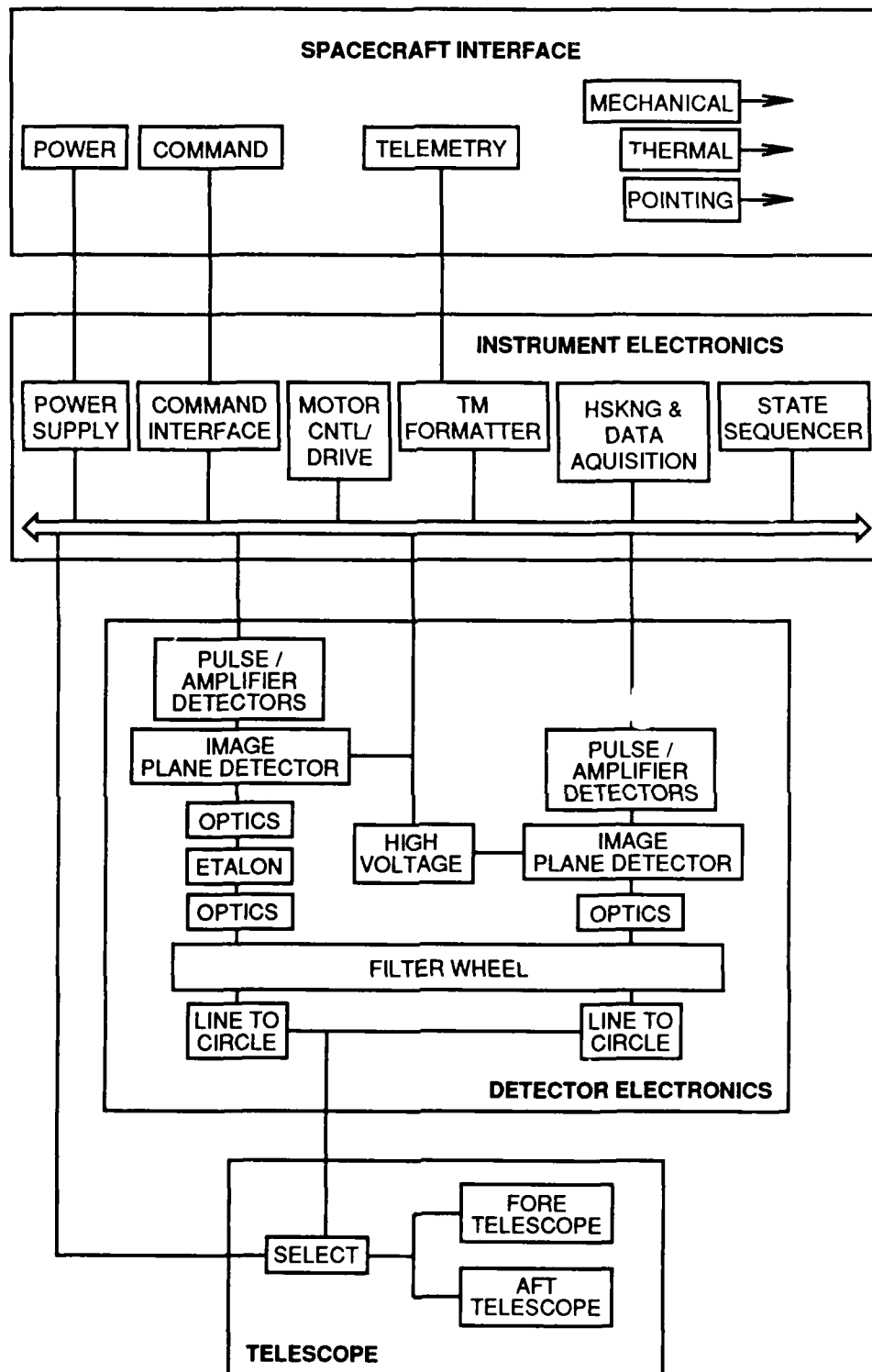
The electronics block diagram is shown in Figure 23. The instrument is functionally divided into four sections: telescope, detector, instrument electronics, and satellite interface. The telescope drive consists of two stepper motors for horizon scan and another stepper motor for fore and aft selection. Scan will be controlled by a state sequencer similar to that flown on DE-FPI. The detector electronics are a basic copy of those flown on DE-FPI and consist of a HV supply for the IPD, 12 channels of analog and pulse detection of the IPD output signals, calibration sources, and filter wheel drive and position. The IPDPH detector electronics are identical to the FPI detector electronics. The instrument electronics sub-system distributes supply voltages, commands, and timing signals to the other instrument blocks. Instrument monitors such as temperature measurements, high voltage monitors, scan position decoder outputs, etc., enter this section for transmission to the telemetry stream. The satellite interface section is designed to provide simple interfaces to facilitate testing, integration and flight operations and to minimize interconnects. The electronics design is almost entirely a carryover from the DE-FPI and AE-VAE systems with minor updates from the HRDI/UARS currently in final assembly and test.

5.1.5 FPI SENSITIVITY

The Low Altitude Doppler Interferometer instrument described in the previous sections has the inherent high throughput of the Fabry-Perot interferometer and has the spectral selectivity to measure winds and temperatures in the earth's atmosphere. The basic instrument sensitivity is shown in Table 5.

Table 5. ADS-FPI Instrument Sensitivity

System transmission, T_0 (all elements coated)	0.1
Quantum efficiency, Q_e	0.1
Etendue ($A\Omega$)	$1.815 \times 10^{-3} \text{ cm}^2 \text{ ster}$
$\Delta\nu$ (ring)	$0.045 \text{ cm}^{-1} (5577 \text{ \AA})$ $0.0327 \text{ cm}^{-1} (7650 \text{ \AA})$
Spectral response:	
C_i (counts per sample)	
$\frac{A\Omega}{4\pi} T_0 Q_e \times 10^6 \Delta t \int_0^\infty T_{FP}(\nu) R(R/\text{cm}) d\nu$	
5200 \AA	$0.22 \Delta t R_i$
5577 \AA	$0.20 \Delta t R_i$
5896 \AA	$0.14 \Delta t R_i$
6300 \AA	$0.10 \Delta t R_i$
7650 \AA	$0.03 \Delta t R_i$



FPI ELECTRONICS BLOCK DIAGRAM

Figure 23. Electronic Functional Block Diagram for the ADS Fabry-Perot Interferometer

5.1.6 FPI ERROR ANALYSIS

5.1.6.1 Statistical Errors

Statistical errors in the measurements of winds, temperatures and emission line brightnesses are dependent on the integration time period and the brightness of the given emission. We have modified the full DE-FPI simulator computer program to calculate statistical measurement precisions for the ADS-FPI. These calculations involved the simulation of spectrograms using a measured instrument function and the analysis of the spectrograms using the DE-FPI flight analysis routines. The accuracies are depicted in Figure 24. It can be seen that for typical daytime brightnesses for the 5577Å emission, accuracies of 5 m/sec and 10 K are obtained with integration periods of 1 second. For typical nighttime brightnesses, these accuracies are degraded to 20 m/sec and 50 K respectively. These errors are sufficiently small to enable the generation of vector altitude profiles as required for the proposed investigations.

5.1.6.2 Systematic Errors

Systematic errors may occur due to instrument spectral drift. Experience with exhaustive laboratory calibrations and spaceflight for the DE-FPI have indicated that a combination of continuous etalon temperature measurements to 0.01° and periodic in-flight spectral calibrations are sufficient to provide knowledge of instrument drifts to ~1 m/sec. Two further types of systematic error are of importance. These are due to uncertainties in the attitude and velocity of the instrument with respect to the earth and due to calibration uncertainties in the instrument discussed below.

The spacecraft has an inherent orbital velocity of about 7 km/sec which appears as a large DC background shift on any spectral signal attached to the earth. In our worst case, looking at 45° with respect to the spacecraft one finds that an attitude uncertainty of 0.05° leads to a 5 m/sec error in the deduced wind. This is a very important point and clearly the wind measurements become degraded for large uncertainties in the attitude. The accuracy of the post-flight knowledge of attitude is therefore a matter of importance to the wind measurement and is of greater concern than errors in the determination of the satellite velocity itself. Several considerations, however, mitigate the negative impact of large attitude errors on the proposed science.

- 1) It is straightforward to use the Rayleigh scattered light signal from the lower atmosphere during the day and the 5577Å emission during the night to provide for a rapid and accurate in-flight determination of the instrument zenith angle using simple discrimination electronics to optimize the field of view.

- 2) The volume emission rate altitude profiles and the kinetic and rotational altitude profiles are insensitive to errors in attitude and much of the science is therefore unaffected.

- 3) Many of the interesting science problems related to the dynamics of the mesosphere/lower thermosphere involve "AC" rather than "DC" wind systems (for example, gravity waves, eddies, etc.) and therefore relative measurements of winds, which are largely unaffected by attitude errors, are sufficient for many purposes.

- 4) The wind measurements themselves (for example in the upper thermosphere at low latitudes where the wind field is known to be smoothly varying) will provide an in-flight indication of the magnitude of the attitude drift for later comparison.

ADS-FPI: TYPICAL 'ONE SHOT' INTEGRATION TIMES FOR SPECIFIED ACCURACY

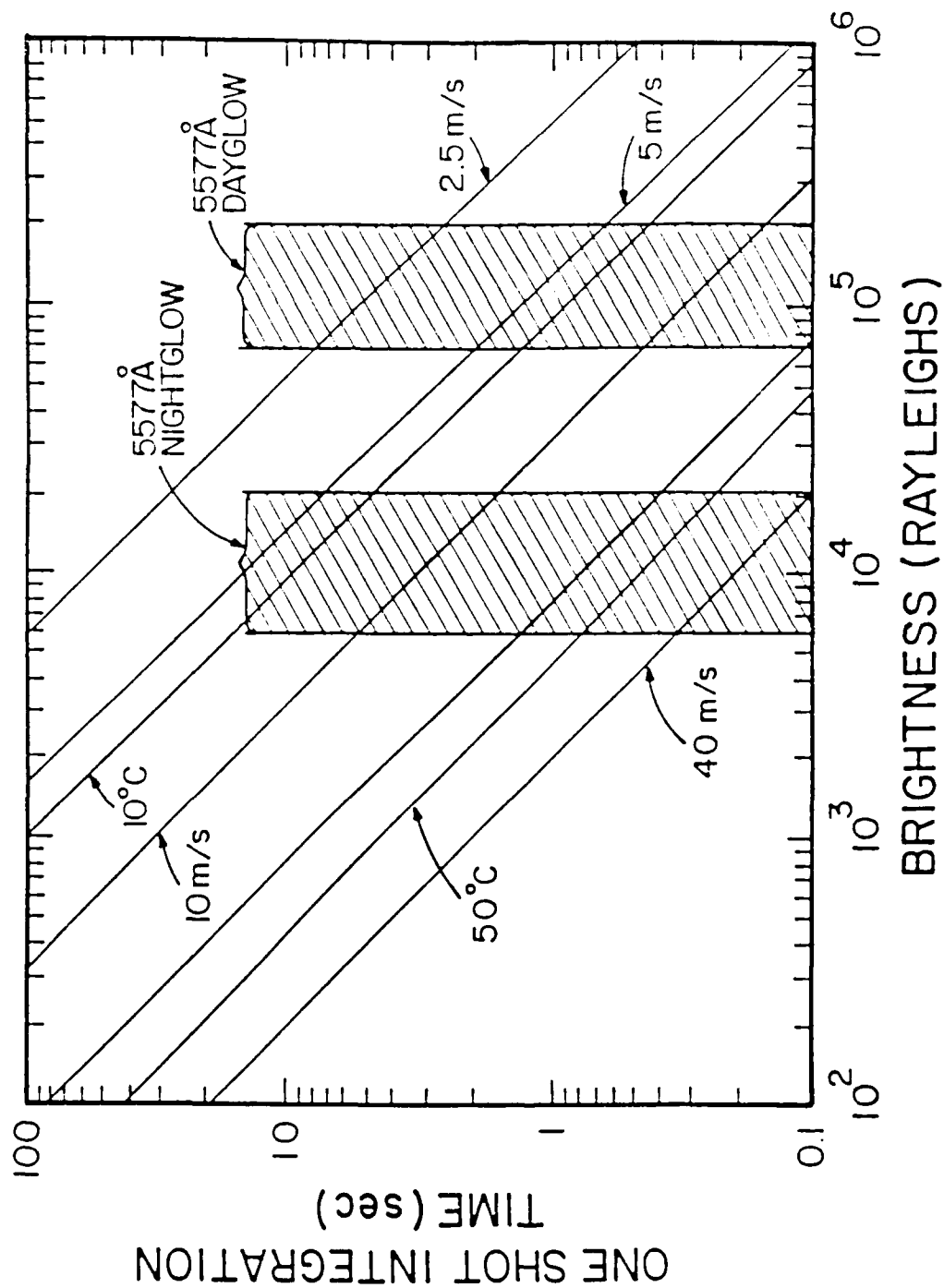


Figure 24. Errors on derived winds and temperatures for the ADS Fabry-Perot interferometer.

5.1.7 IPDPH

The Image Plane Detector Photometer, IPDPH, is shown in Figure 20. The IPDPH is an integral part of the ADS-FPI package which shares the telescope, filter wheel, and many of its electronics with the FPI. Also, the IPD and its electronics are direct copies of the DE-FPI IPD. Additional elements are a second line-to-circle convertor and three simple lenses. The IPDPH complements the measurement package by providing for accurate rotational temperature measurements from 90 - 120 km using the O₂ (0-0) atmospheric band emission and direct O₂ density measurements from 60 to 120 km using the method of oxygen fluorescence. Rotational temperature measurements are obtained to very high precision by detecting the spectral changes in the shape of the O₂ atmospheric band (Figure 25). Figure 26 illustrates the accuracies with which rotational temperatures can be measured as a function of altitude in the daytime thermosphere by using a combination of the observations from the FPI and IPDPH channels of the ADS remote sensing instrument. As can be seen, rapid measurements of the temperature profile to accuracies of $\sim 1^\circ$ can be obtained in the altitude region 90 - 120 km. The technique is limited below 90 km by the increasing optical depth of the (0-0) emission and above 120 km by the fall-off in O₂ density. In this region, however, the hydrostatic law can be used to derive O₂ density profiles.

5.1.8 ENHANCEMENT TO ADS: EUVS

An Extreme Ultraviolet Spectrometer, EUVS, is recommended for inclusion on the ADS payload to provide very important direct measurements of the solar UV/EUV fluxes. As discussed above, knowledge of these fluxes is crucial for the theoretical and/or semi-empirical modeling of the thermosphere. Without such an instrument, reliance will have to be placed on the use of the indirect F10.7 cm radio flux index (see discussion above). The specific instrument has not been selected at this time; however, suitable instruments have flown, for example, on Atmosphere Explorer.⁷¹

5.1.9 ENHANCEMENT TO ADS: FPI-DENS

Rotational temperatures, as discussed above, can be remotely sensed by the baseline FPI instrument package. Since density measurements below 90 km are desirable, it is recommended that enhancement of the FPI package be considered, to enable absolute density measurements of O₂ in the optically-thick region from 60 - 90 km. This enhancement would involve the addition of filters and a modified detection system to enable the optically thin (0-1) atmospheric band emission of molecular oxygen (8640Å) to be observed as well as the (0-0) optically thick band. This technique has been described in a University of Michigan report to AFGL and will not be discussed in detail here. The technique relies on the normalization of the unabsorbed (0-0) band intensities to the measured optically thin (0-1) band intensities. Once the unattenuated (0-0) band intensities are estimated, the degree of absorption by O₂ in the (0-0) band along the line of sight of the instrument can be calculated and tomographic inversions used to determine the altitude profile of density. The enhancement to the

71. Hinteregger, H.E., Bedo, D.E., and Manson, J.E. (1973, April) The EUV spectrophotometer on Atmosphere Explorer, *Radio Science* 8(No. 4):349.

O_2 ATMOSPHERIC (O-O) BAND

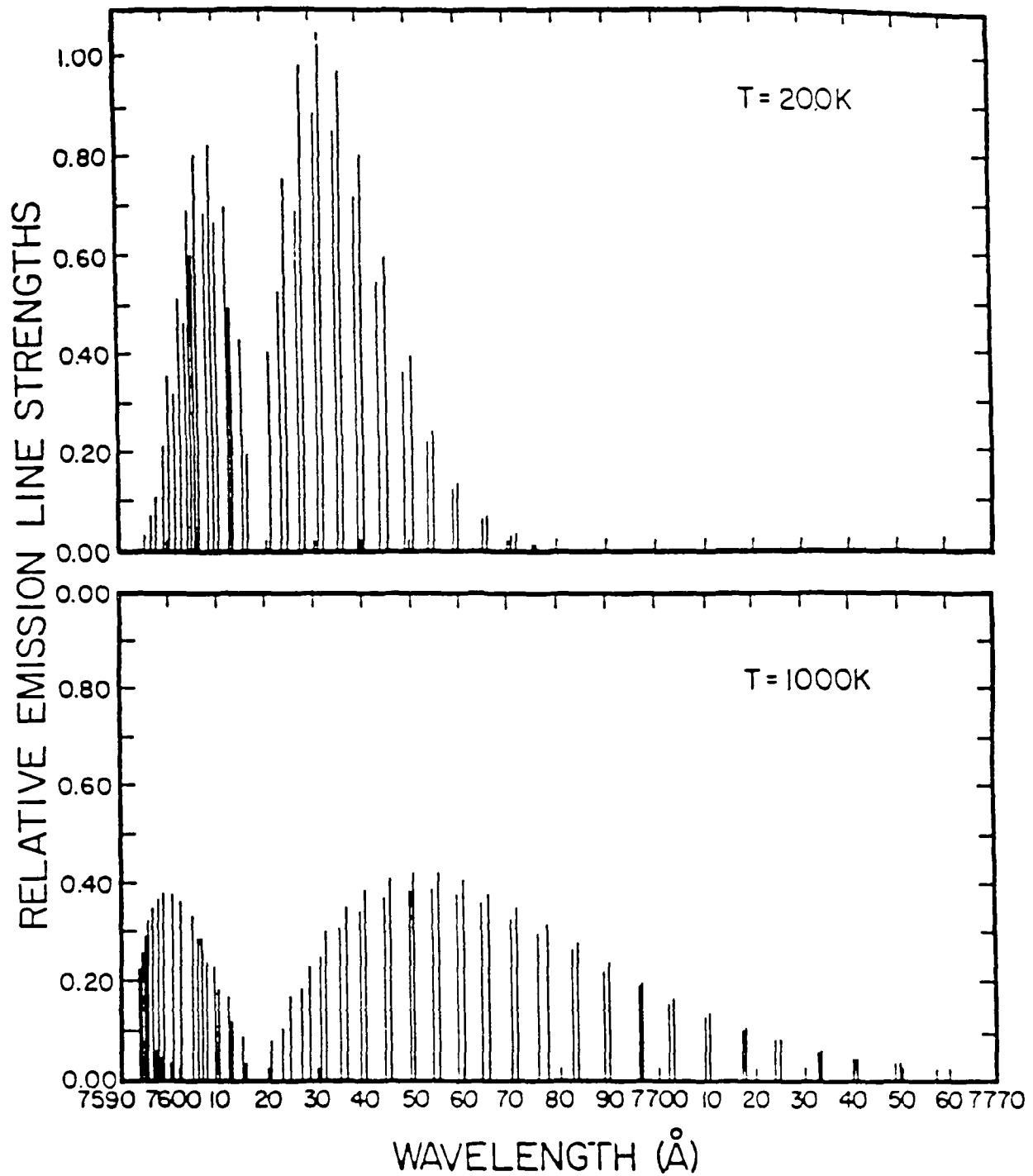


Figure 25. Changes in spectral signature of the O_2 (O-O) atmospheric band due to changes in rotational temperature. The rotational temperature can be measured by using two relatively low spectral resolution measurements with FPI and IDPPH channels.

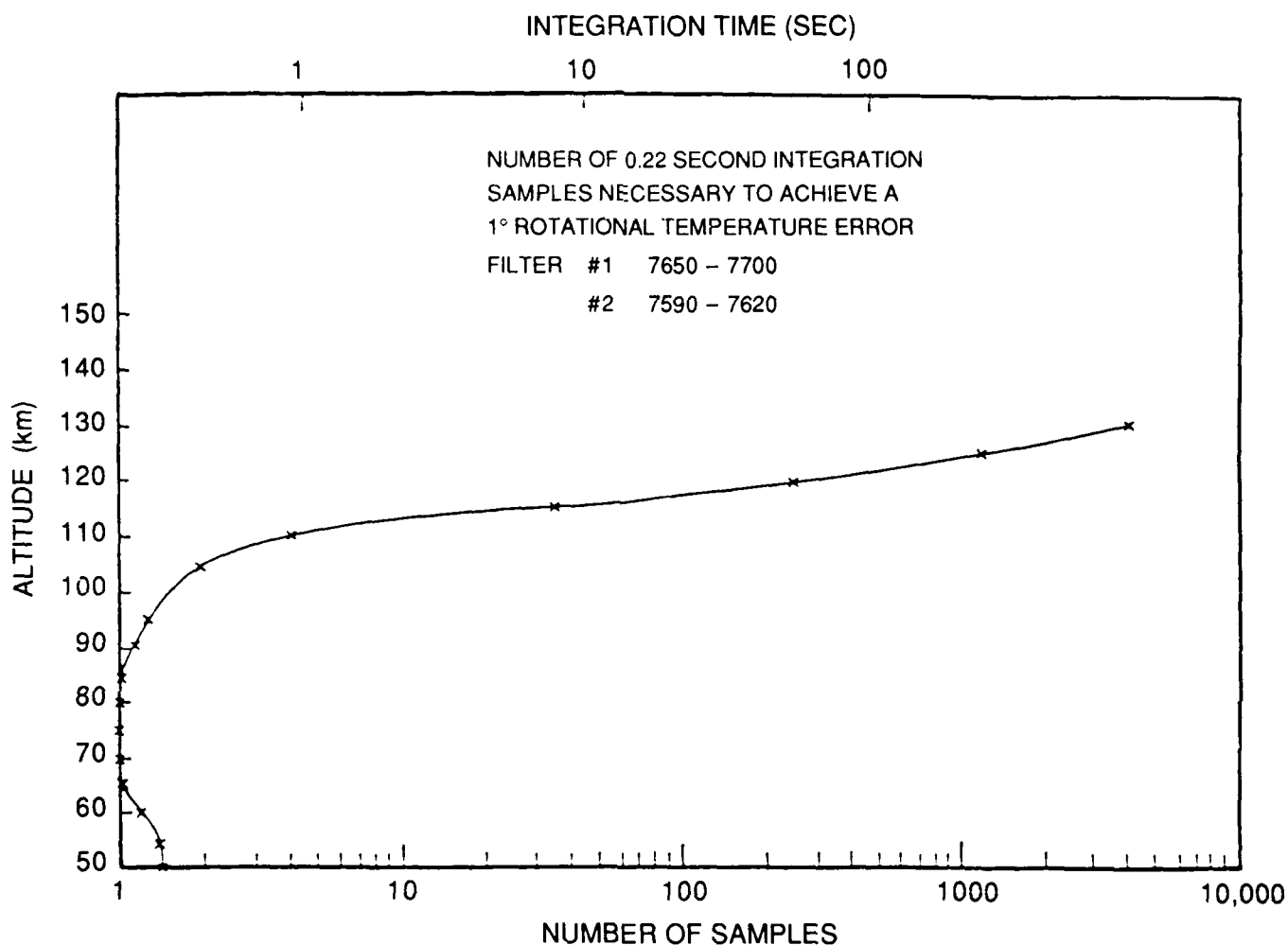


Figure 26. Number of 0.22 second integration times necessary to achieve a 1° rotational temperature error in the daytime thermosphere as a function of altitude using the ADS-FPI. ADS-FPI sample time and integration period for a statistical error of one degree on a measurement of rotational temperature from the O₂ (0-0) atmospheric band. Below ~70 km, the optical depth of the emission limits the measurement (although the technique can be somewhat extended into the optically deep region using algorithms such as those developed for the UARS/HRDI program, Hays, private communication).

baseline FPI package would involve some additional expense but would enable the density structure of the mesosphere to be probed at high accuracy.

5.2 Spacecraft and Orbital Parameters

Table 6 summarizes the basic spacecraft and orbital parameters. Further discussion of the optimum orbital lifetime and geometry is given in a later section.

Table 6. Spacecraft and Orbit Parameters

Orbit (see Section 5.4)	~150 × 500 km, 70° inclination			
Lifetime	1.5 years (with propulsion)			
Nominal size and layout	Figure 27			
Weight	41.3 kg			
Power	53 W nominal			
Duty cycle	60% typical			
Pointing		Accuracy	Knowledge	Jitter
	Roll	1.0°	0.05°	0.05°
	Pitch	0.5°	0.05°	0.05°
	Yaw	0.5°	0.05°	0.05°
Ephemeris	< 5 km in-track, 1 km cross-track, .5 km altitude, normal ECI vector data			
Data rate	7 kbits/sec			
Orbital data storage	27 Mb			
Data duty cycle	Same as power			
Commands	8 power 20 pulse or relay 1 kbps digital			

5.3 Cross Calibration

An important factor in instrument selection is the ability to cross calibrate, both on the ground and on-orbit, to determine differences that may occur between ground calibrations and on-orbit conditions. The mass spectrometers that measure similar parameters are differently optimized and, consequently, can provide cross checks. Except for EUVS, all the instruments provide measurements of density with differing techniques and accuracies. Therefore, the primary measurement can be cross calibrated at various times during the mission.

5.4 Orbit Selection

Optimal orbit selection is a complex process involving the coverage needs dictated by the scientific requirements, to some extent the accuracies of the measurements, and satellite lifetime controlled by

the cost of on board propulsion. Good latitude coverage is obtained with a polar orbit. A sun-synchronous polar orbit provides constant local time so that seasonal variations can be examined if mission life is long enough. A polar orbit also gives good coverage of auroral activity and consequently information related to solar activity.

An equatorial orbit provides good diurnal coverage which is of great interest for tidal motions. However, low inclinations provide such poor latitude coverage that they are usually not chosen for a single satellite mission. One compromise was the 68.4° inclination of Atmosphere Explorer C.⁷² For this case perigee precesses about two days in a year. This choice provides a local time seasonal comparison but prevents *in situ* measurements at the poles. Since the FPI has the ability to remotely sense the atmosphere over the poles, an inclination of 70° is probably a reasonable compromise for the ADS mission, providing reasonable latitudinal and local time coverage. Note that AE-C, the first of three AE satellites was inclined at 68.4, whereas D and E were at 98 and 22.5° respectively. *The recommended inclination for ADS is in the range 66-70°.*

5.4.1 ORBITAL MOTION

Many texts are available that describe satellite motion in an orbit as are many sophisticated computer programs. A simple, first order analysis can be found in Danby.⁷³ Since the earth is oblate, it can be shown that the orbital forces are such that the orbit precesses in inertial space. As a consequence, launch time and apogee and perigee selection provide a degree of control over the orbital motion. The relevant equations describing these perturbations are:

$$d\varpi_s = - \frac{3nJ_2}{2a^2(1-e^2)^2} \left(\frac{5}{2} \sin^2 i - 2 \right) dt$$

$$d\Omega_s = - \frac{3nJ_2}{2a^2(1-e^2)^2} \cos i dt$$

$$dM_s = n dt \left\{ 1 - \frac{3J_2}{2a^2(1-e^2)^2} \left(\frac{3}{2} \sin^2 i - 1 \right) \right\}$$

Where:

ϖ_s = Argument of perigee, angle from ascending node to perigee

72. Dalgarno, A., Hanson, W.B., Spencer, N.W., and Schmulling, E.R. (1973, April) The Atmosphere Explorer mission, *Radio Science* 8 (No. 4):263-266.

73. Danby, J.M.A. (1962) Fundamentals of celestial mechanics, MacMillan, NY.

Ω_S = Longitude of ascending node referenced to the vernal equinox
 dM_S = Change in period due to oblate earth
 e = eccentricity
 i = inclination
 a = semimajor axis
 n = mean motion, $\frac{2\pi}{\text{Period}}$
 J_2 = Coefficient of gravity potential

$$R_{\text{apogee}} = \left(\frac{1+e}{1-e} \right) R_{\text{perigee}}$$

$$\langle R_{\text{earth}} \rangle = 6370 \text{ km}$$

Here, we see e.g. that in a polar orbit, $i = 90^\circ$, $d\Omega_S$, is zero and the longitude of the ascending node is fixed. For $i = 0^\circ$, an equatorial orbit, $\cos i = 1$ and longitude and consequently local time variations are maximized for otherwise equal orbits.

5.4.2 SATELLITE LIFETIME

It is beyond the scope of this study to run detailed lifetime-cost-data coverage analyses. Some simple guidelines will be presented.

The calculation of satellite lifetime is relatively simple in principle, being the result of atmospheric drag on a moving body, coupled to the orbital motion equations. In practice, however, predictions with useful practical accuracies are quite difficult. Figure 27 shows the rapidity with which a circular orbit decays and the error in predicting reentry with two of the earlier atmospheric models.⁷⁴ Note the factor of 2 in lifetime prediction. Figure 28 shows the effect of eccentricity and initial perigee, h_p , on lifetime.⁷⁴ Note that for this particular model, ARDC 1959, a one year lifetime requires about a 160 km perigee and 4000 km apogee. It is also important to note that not only is the quality of the model crucial, but solar activity significantly affects the density profile of the atmosphere and in turn adds further uncertainty to satellite life predictions. It is clear that higher and more eccentric orbits increase lifetime. For example, increasing perigee from ~150 to 400 km, (Figure 28), can increase lifetime by about 100. Figure 28 shows the orbital life of Dynamics Explorer 2, which would be typical for an ADS satellite, lasted about 13 months with an initial apogee of 1000 km and perigee of 300 km. Atmosphere Explorer C, which was nearly identical to Dynamics Explorer 2, was able to operate with a 150 km perigee using on board propulsion. Clearly, a 140 km perigee requires on board propulsion to provide a significant lifetime.

The scientific requirements to provide seasonal, local time (for tidal analysis) and latitudinal coverage imply that a lifetime in excess of one year is essential. The longer the lifetime the better, but less than full seasonal coverage would seriously limit the mission objectives. *It is therefore*

74. Jensen, J., Towsend, G., Kork, J., and Kraft, D. (1962) Design Guide to orbital flight, McGraw-Hill pp. 252-253.

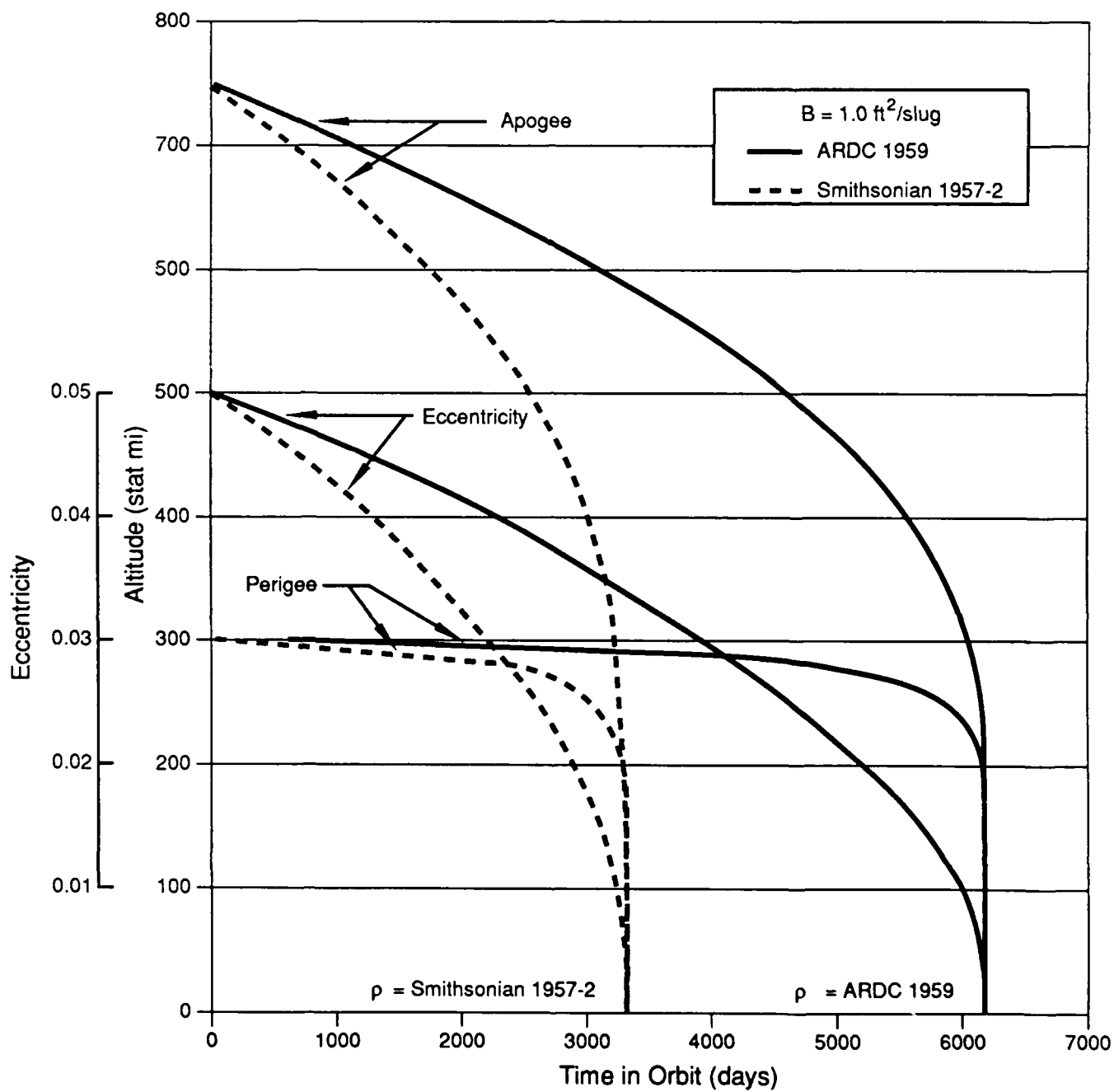


Figure 27. Orbital Decay Histories

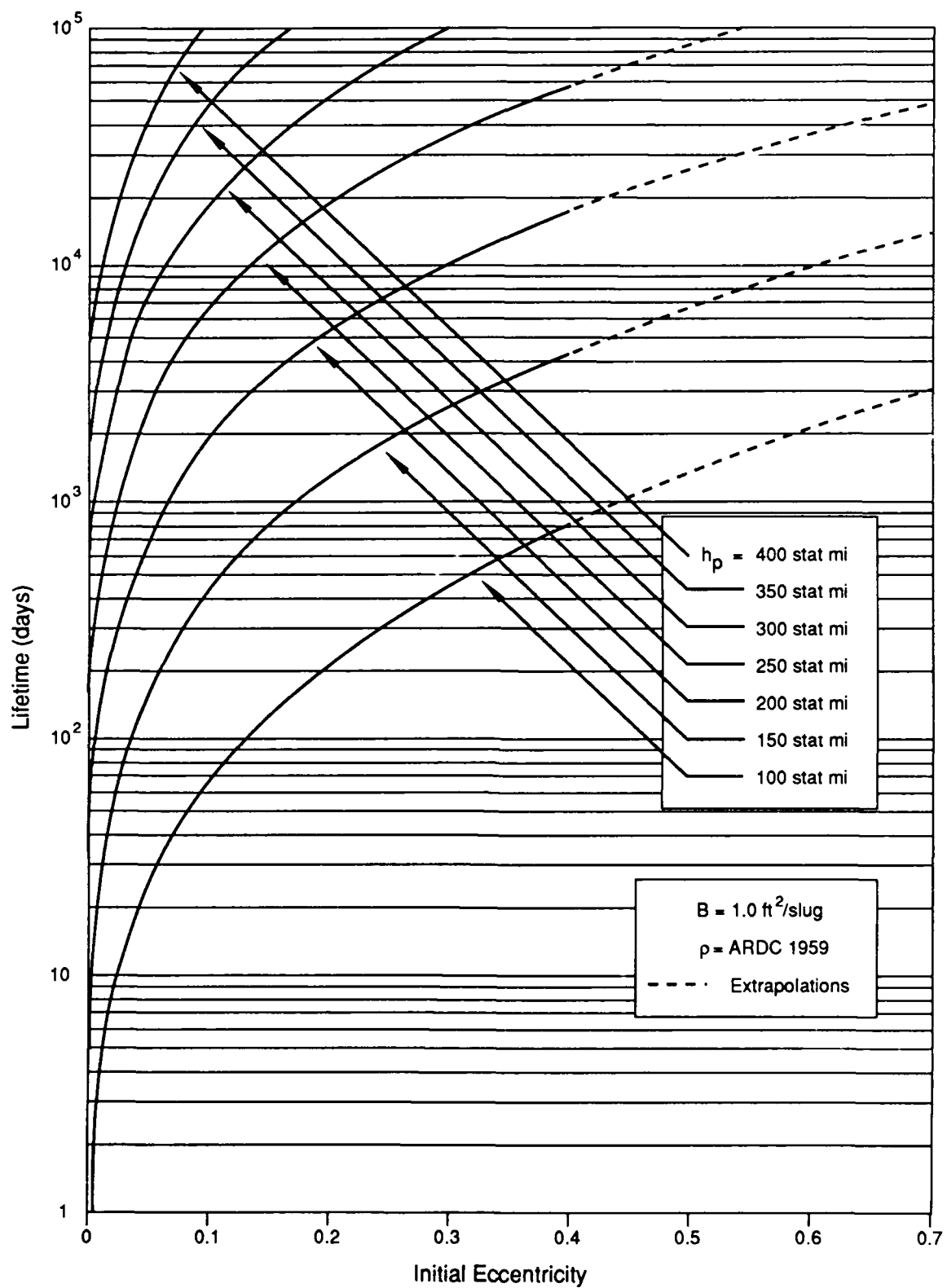


Figure 28. Satellite Lifetime Versus Initial Eccentricity

recommended that on-board propulsion be added to the ADS spacecraft payload to enable a lifetime in excess of 18 months. A perigee of 140 km would be optimum, but this might have to be increased to 160 km depending on spacecraft systems considerations. With such propulsion, the duration of *in situ* measurements below 200 km would be optimized by judicious orbital station keeping.

Figure 29 illustrates schematically the ADS mission payload (enhanced).

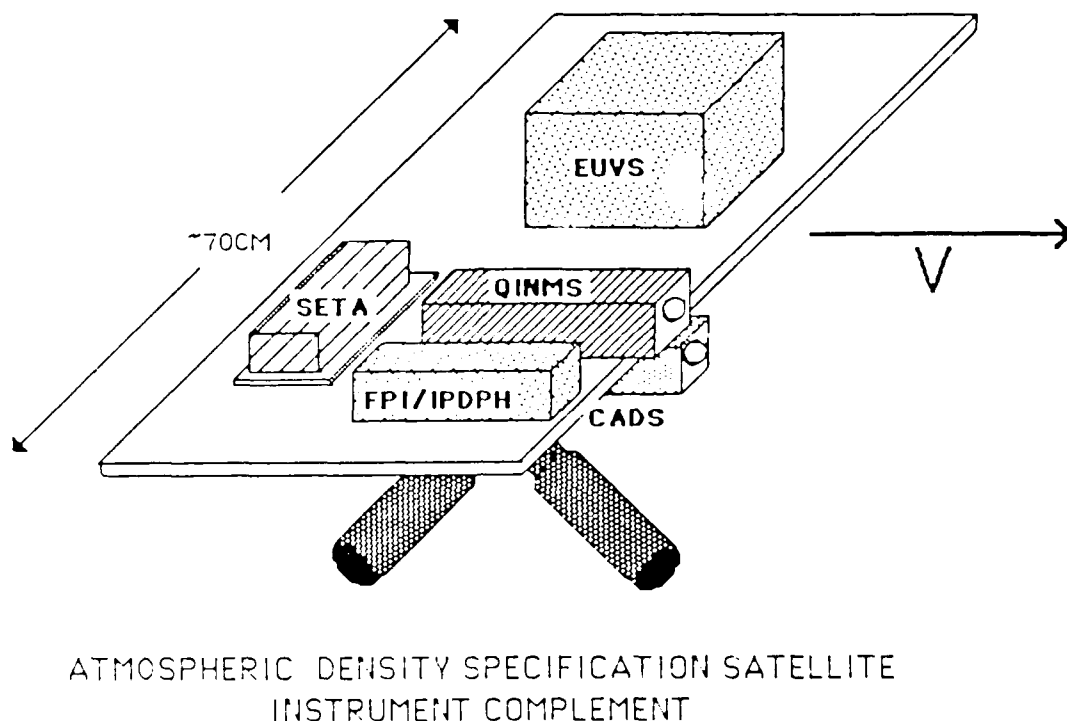


Figure 29. Instrument schematic.

6. DATA RESOURCE AND UTILITY

The previous sections have provided the scientific and technical rationale for the ADS mission and associated scientific activities involving theoretical and semi-empirical modeling. In this section, a brief description of the data base to be collated from the ADS program is provided together with a short discussion on the utility of the proposed data base for future density specification.

The ADS mission will provide absolutely calibrated and redundant measurements of total neutral density, satellite drag, vector wind and temperature in the lower thermosphere. *In situ* measurements of density, cross-track wind, neutral and ion composition, temperature, and satellite drag will be obtained down to a possible (preferred) perigee of 140 km. The remote sensing observations from the FPI package will extend the neutral measurements down to 90 km (60 km with the enhanced system discussed in Section 5.1.9). Altitude profiles of neutral temperature, O₂ densities,

and the vector wind obtained by the remote sensing technique will allow for extension of the measurements and resultant modeling capabilities into the upper mesosphere. Sufficient coverage of these state variables will enable the following dependencies to be quantitatively determined in the lower thermosphere and upper mesosphere:

- 1) Seasonal dependence
- 2) Altitude dependence
- 3) Latitudinal and Universal time dependencies
- 4) Tidal phases and amplitudes in the lower thermosphere
- 5) Local time and storm time dependencies

These multi-instrument data will be collated in a central location, merged with orbit/altitude data from the spacecraft and accessed using a relational data base management system. For optimum return on the investment, it is recommended that the data be analyzed and interpreted by a team of government and university scientists to accomplish the following central tasks:

- 1) Provide a calibration standard against which other density techniques may be compared.
- 2) Incorporate ADS data into the semi-empirical models, thus vastly enhancing the present coverage of lower thermosphere density.
- 3) Provide a set of case studies as well as climatological means for detailed comparison with the TGCs. These comparisons will essentially validate the TGCs in the lower thermosphere and allow for significantly improved theoretical understanding of the region.
- 4) Provide a standard for testing of the various versions of the Air Force's operational models of the thermosphere and mesosphere

While the ADS data base alone will make an important contribution to the progress in both the semi-empirical modeling and numerical modeling areas, additional efforts will be required to supplement the data resource. The major requirements have been discussed in previous sections of this report and may be summarized as follows:

- 1) Improved quantification of solar fluxes and magnetospheric forcings - this will require the availability of DMSP data, available auroral imaging data as well as solar flux measurements.
- 2) Ground-truth measurements of density and wind - this will require LIDAR, optical, and incoherent scatter and high-frequency radar measurements. Measurements of this type are planned within the National Science Foundation's CEDAR program.
- 3) Extended coverage for tides - this will involve the NSF CEDAR chain of optical and radar instruments.

7. CONCLUSIONS

We have reviewed the current scientific and technical issues related to the limitations on the accuracy of operational models for the absolute density of the Earth's thermosphere and upper mesosphere. The central conclusion of the study is that a multi-faceted attack involving both modern theoretical and experimental techniques is now feasible that would lead to a significant improvement in the current accuracy. It is anticipated that such an effort would lead to a reduction in the specification accuracy for absolute density approaching the estimated best attainable accuracies (based on considerations of the stochastic nature of the atmosphere). These estimates are ~5 percent at

mid- and low latitudes and for geomagnetically quiet times at high latitudes, rising to ~10 percent for geomagnetically active times at high latitudes.

A specific approach has been evaluated that involves use of the most sophisticated available modeling tools, coupled with a dedicated satellite mission to provide a comprehensive, well calibrated data resource. The central components of the program are: 1) the Atmosphere Density Specification (ADS) mission designed to provide the comprehensive measurement standard and 2) a 3-dimensional, time dependent model (TGCM), with inputs specified by ancillary measurements of solar, auroral and magnetospheric processes. We first list the essential requirements for the approach and then describe our basic recommendations for an implementation plan.

7.1 Requirements

The principal requirements for improvements in density specification may be stated as follows:

1) The problem of accurate density specification in the thermosphere and mesosphere is non-trivial and has resisted many previous efforts to enhance significantly the performance of the semi-empirical models. Only a multi-faceted attack, involving both theoretical and experimental techniques will provide realistic chances for significant improvements. A science team approach similar to that used for successful NASA missions is therefore espoused, involving the active participation of specialists from both government and university research groups.

2) To make significant improvements, a detailed scientific understanding of the interplay among all important atmospheric state variables - not just density itself - is essential. These variables are density, composition, temperature, and wind. In addition, perturbations in these state variables must be quantified and understood at a variety of spatial and temporal scales. A full description of seasonal, altitudinal, local time, universal time, geomagnetic storm time etc. dependencies is required, with as comprehensive a geographic coverage as possible. Density measurements are required to accuracies better than ~5 percent, temperature measurements to better than ~20 - 50 K, and wind measurements to better than ~15 - 20 m/sec.

3) The phases and amplitudes of the tidal wind structures (diurnal, semidiurnal, terdiurnal) in the mesosphere and lower thermosphere and their variations must be adequately quantified. This requires coordinated ground-based and spacecraft observations of winds and temperatures.

4) A time-dependent specification of magnetospheric energy, particle and momentum inputs is required to determine the thermospheric response to variations in the important forcings.

5) Continued efforts to extend and improve the utility of the proxy variables for the solar UV and EUV fluxes are required.

6) Continued efforts to improve the accuracy of semi-empirical models of the thermosphere are needed. These efforts will involve the critical evaluation of individual subsets of the available data and the identification of additional, as yet unmodeled, dependencies.

7) Continued efforts to validate and develop the 3-dimensional, time-dependent models of the thermosphere are required. These efforts will lead to the necessary improved theoretical understanding of the domain and will enable more realistic and higher temporal and spatial resolution predictions for thermospheric perturbations.

7.2 Implementation Recommendations

A concerted attack on the experimental and theoretical issues involved in leading to an improved predictive and specification capability for thermosphere and upper mesosphere dynamics is obviously required. Based on the results of the present study, the following elements are recommended:

- 1) Flight of the Atmosphere Density Specification (ADS) mission containing the mission payload described above is recommended. This mission will allow for all the important atmospheric state variables to be determined experimentally with comprehensive coverage in the domain of interest. The baseline instrument complement of the ADS mission includes an ion/neutral mass spectrometer capable of determining absolute neutral densities to ~5 percent (QINMS), an electrostatic triaxial accelerometer for satellite drag and cross-track wind determination (SETA), a Fabry-Perot interferometer for the determination of altitude profiles of vector winds, temperatures and composition (FPI), and an ion mass spectrometer capable of determining neutral winds and ion and neutral constituent abundances (CADS). An enhanced payload would include a solar EUV flux monitor (EUVS) and the density profilometer attachment to the FPI (FPI-DENS). The baseline instruments are all of the *in situ* variety, with the exception of the Fabry-Perot interferometer which is a remote sensing instrument. The FPI is essential for a successful program and provides the necessary vector wind and temperature altitude profiles. Extensive cross calibration among the various instruments is required to provide confidence in the absolute accuracy of the various measurements. The recommended lifetime of the mission is >18 months and the recommended orbital inclination is 66 - 70°. The recommended perigee is ~140 km, which implies a need for an on-orbit propulsion capability. The optimum orientation would be 3-axis stabilized, with a spin rate equivalent to one spin per revolution about the earth. This would ensure that all the *in situ* sensors remained pointed towards the ram direction.

- 2) We recommend that important ancillary data be made available and used in the interpretation of the ADS data resource. Such ancillary data sets include the auroral particle data from DMSP and NOAA/TIROS, available solar flux and geomagnetic activity information, available ground-based optical, radar and LIDAR observations of atmospheric state variables from the NSF CEDAR program, and available global auroral images.

- 3) We recommend that the ADS data base be incorporated into the semi-empirical models. Specifically the data should be used as a standard against which to compare other individual data sets.

- 4) We recommend use of the ADS data for extensive validation and testing of the current version of the TGCM. The TGCM should be used to predict and specify absolute densities and perturbations.

- 5) We recommend that the ADS data base be used for testing and validation of the Air Force operational model of the thermosphere and mesosphere.

In summary, it is our opinion that a well designed and focused mission to determine all the thermospheric and upper mesospheric state variables with high absolute accuracy and the appropriate geophysical coverage, together with a parallel modeling and theoretical effort, will lead to a significantly improved specification capability for atmospheric density. As a corollary to this, it is also our opinion that a program that falls short of the concerted effort described in this report is destined for failure, given the intrinsic difficulties and current lack of full understanding of upper atmospheric physics. We therefore caution against a piecemeal approach involving less than

adequate experimental coverage and/or the absence of strong theoretical support. It is clear that significant resources will be required to enable the program described here to be successful. These resources are needed to support the tasks associated with the ADS mission itself as well as the ancillary activities described.

References

1. Hedin, A.E. (1983) A revised thermospheric model based on mass spectrometer and incoherent scatter data: MSIS-83, *J. Geophys. Res.* **88**:10170-10188.
2. Hedin, A.E. (1987) MSIS-86 thermospheric model, *J. Geophys. Res.* **92**:4649-4662.
3. Hedin, A.E. (1988) CIRA-88, Chapter 1, The empirical model atmosphere: Atmospheric model in the region 90 to 2000 km, *in press*, Pergamon Press.
4. Jacchia, L.G. (1964) Static diffusion models of the upper atmosphere with empirical temperature profiles, *Smithsonian Astrophys. Obs. Spec. Rpt. No. 170*, also published in *Smithsonian Contrib. Astrophys.* **8**:215-257, 1965.
5. Jacchia, L.G. (1971) Revised static models of the thermosphere and exosphere with empirical temperature profiles, *Smithsonian Astrophys. Observ. Spec. Rpt. No. 332*.
6. Jacchia, L.G. (1977) Thermospheric temperature, density and composition: New models, *Smithsonian Astrophys. Obs. Spec. Rpt. No. 375*.
7. Marcos, F.A. (1985) Requirements for improved thermospheric neutral density models, Paper AAS85-312, AAS/AIAA Astrodynamics Specialist Conference Proceedings, Vail, CO.
8. Marcos, F.A. (1987) Accuracy of satellite drag models, Paper AAS 87-552, AAS/AIAA Astrodynamics Specialist Conference Proceedings, Kalispell, MO.
9. Hedin, A.E. and Mayr, H.G. (1987) Characteristics of wavelike fluctuations in Dynamics Explorer neutral composition data, *J. Geophys. Res.* **92**:11159-11172.
10. Schunk, R.W. (1975) Transport equations for Aeronomy, *Planet. Space Sci.* **23**:437.
11. Mayr, H.G., Harris, I., and Spencer, N.W. (1978) Some properties of upper atmosphere dynamics, *Rev. Geophys. and Space Phys.* **16**:539.
12. Burns, A.G., Killeen, T.L., and Roble, R.G. (1989) Processes responsible for the compositional structure of the thermosphere, *J. Geophys. Res.* **94**:3670-3686.
13. Rees, D., Fuller-Rowell, T.J., and Rishbeth, H. (1988) The use of mass spectrometer measurements to derive thermospheric temperature and density, *Planet. Space Sci.* **36**: 281-290.
14. Dickinson, R.E., Ridley, E.C., and Roble, R.G. (1984) Thermospheric general circulation with coupled dynamics and composition, *J. Atmos. Sci.* **41**:205-219.

15. Johnson, H.S. (1968) Gas phase kinetics of neutral oxygen species, NBS-NSRSDS-20, U.S. Government Printing Office, Washington, DC.
16. Campbell, I.M. and Gray, C.N. (1973) Rate constants for $O(^3P)$ recombination and association with $N(^4S)$, *Chem. Phys. Lett.* **18**:607-609.
17. Colegrove, F.D. (1966) Atmospheric composition in the lower thermosphere, *J. Atmos. Terr. Phys.* **37**:1563-1570.
18. Dickinson, R.E., Ridley, E.C., and Roble, R.G. (1981) A three-dimensional, time-dependent general circulation model of the thermosphere, *J. Geophys. Res.* **86**:1499-1512.
19. Roble, R.G., Dickinson, R.E., and Ridley, E.C. (1982) Global circulation and temperature structure of the thermosphere with high-latitude plasma convection, *J. Geophys. Res.* **87**:1599-1614.
20. Roble, R.G., Dickinson, R.E., Ridley, E.C., Emery, B.A., Hays, P.B., Killeen, T.L., and Spencer, N.W. (1983) The high latitude circulation and temperature structure of the thermosphere near solstice, *Planet. Space Sci.* **31**:1479-1499.
21. Roble, R.G. and Ridley, E.C. (1987) An auroral model for the NCAR thermospheric general circulation model, *Annales Geophysicae* **5**:369-382.
22. Fuller-Rowell, T.J. and Rees, D. (1980) A three-dimensional, time-dependent global model of the thermosphere, *J. Atmos. Sci.* **37**:2545-2657.
23. Fuller-Rowell, T.J., Quegan, S., Rees, D., Moffett, R.J., and Bailey, G.J. (1987) Interactions between neutral thermospheric composition and the polar ionosphere using a coupled ionosphere-thermosphere model, *J. Geophys. Res.* **92**:7744-7748.
24. Killeen, T.L. and Roble, R.G. (1984) An analysis of the high latitude thermospheric wind pattern calculated by a thermospheric general circulation model, 1, Momentum forcing, *J. Geophys. Res.* **89**:7509-7522.
25. Killeen, T.L. and Roble, R.G. (1986) An analysis of the high latitude thermospheric wind pattern calculated by a thermospheric general circulation model, 2, Neutral Parcel trajectories, *J. Geophys. Res.* **91**:11291-11307.
26. Fesen, C.S., Dickinson, R.E., and Roble, R.G. (1986) Simulation of thermospheric tides at equinox with the NCAR thermospheric general circulation model, *J. Geophys. Res.* **91**:4471-4489.
27. Roble, R.G., Forbes, J.M., and Marcos, F.A. (1987) Thermospheric dynamics during the March 22, 1979 magnetic storm, *J. Geophys. Res.* **92**:6045-6068.
28. Forbes, J.M., Roble, R.G., and Marcos, F.A. (1987) Thermospheric dynamics during the March 22, 1979, Magnetic storm 2. Comparisons of model predictions with observations, *J. Geophys. Res.* **92**:6069-6081.
29. Roble, R.G., Killeen, T.L., Carignan, G.R., Spencer, N.W., Heelis, R.A., Reiff, P.H., Winningham, J.D., and Evans, D.S. (1988) Thermospheric dynamics during 21/22 November 1981: Dynamics Explorer measurements and TGCM predictions, *J. Geophys. Res.* **93**:209.
30. Killeen, T.L. (1987) Energetics and dynamics of the earth's thermosphere, *Rev. Geophys.* **25**:433-454.
31. Roble, R.G., Ridley, E.C., and Dickinson, R.E. (1987) On the global mean structure of the thermosphere, *J. Geophys. Res.* **92**:8745-8758.
32. Hinteregger, H.E. (1981) Representations of solar EUV fluxes for aeronautical applications, *Adv. Space Res.* **1**:39.
33. Hinteregger, H.E., Fukui, K., and Gilson, B.R. (1981) Observational, reference and model data on solar EUV, from measurements on AE-E, *Geophys. Res. Lett.* **8**:1147.
34. Lean, J. (1987) Solar-Ultraviolet irradiance variations: A review, *J. Geophys. Res.* **92**:839-868.
35. Foster, J.C., Holt, J.M., Musgrave, R.G., and Evans, D.S. (1986) Ionospheric convection associated with discrete levels of particle precipitation, *Geophys. Res. Lett.* **13**:656-659.
36. Fuller-Rowell, T.J., and Evans, D.S. (1987) Height integrated Pedersen and Hall conductivity patterns inferred from the TIROS/NOAA satellite data, *J. Geophys. Res.* **92**:7606.

37. Rees, D., Fuller-Rowell, T.J., and Smith, R.W. (1980) Measurements of high latitude thermospheric winds by rocket and ground-based techniques and their interpretation using a three-dimensional time-dependent dynamical model, *Planet. Space Sci.* **28**:919-932.
38. Rees, D., Fuller-Rowell, T.J., Gordon, R., Killeen, T.L., Hays, P.B., Wharton, L.E., and Spencer, N.W. (1983) A comparison of wind observations of the upper thermosphere from the Dynamics Explorer satellite with the predictions of a global time-dependent model, *Planet. Space Sci.* **31**:1299-1314.
39. Rees, D., Gordon, R., Fuller-Rowell, T.J., Smith, M., Carignan, G.R., Killeen, T.L., Hays, P.B., and Spencer, N.W. (1985a) The composition, structure, temperature and dynamics of the upper thermosphere in the polar regions during October to December, 1981, *Planet. Space Sci.* **33**:617-666.
40. Rees, D., Fuller-Rowell, T.J., Smith, M.F., Gordon, R., Killeen, T.L., Hays, P.B., Spencer, N.W., Wharton, L.E., and Maynard, N.C. (1985b) The westward thermospheric jet-stream of the evening auroral oval, *Planet Space Sci.* **33**:425-456.
41. Rees, D., Fuller-Rowell, T.J., Gordon, R., Heppner, J.P., Maynard, N.C., Spencer, N.W., Wharton, L.E., Hays, P.B., and Killeen, T.L. (1986) A theoretical and empirical study of the response of the high-latitude thermosphere to the sense of the "Y" component of the interplanetary magnetic field, *Planet. Space Sci.* **34**:1-40.
42. Rees, D., Fuller-Rowell, T.J., Quegan, S., Moffett, R.J., and Bailey, G.J. (1987) Thermospheric dynamics: Understanding the unusual disturbances by means of simulations with a fully-coupled global thermosphere/high-latitude ionosphere model, *Annales Geophysicae* **5**:303-328.
43. Roble, R.G., Emery, B.A., Dickinson, R.E., Ridley, E.C., Killeen, T.L., Hays, P.B., Carignan, G.R., and Spencer, N.W. (1984) Thermospheric circulation, temperature and compositional structure of the Southern Hemisphere polar cap during October-November, 1981, *J. Geophys. Res.* **89**:9057-9068.
44. Roble, R.G., Emery, B.A., Reid, G.C., Solomon, S., Garcia, R.R., Evans, D.S., Killeen, T.L., Hays, P.B., Heelis, R.A., Hanson, W.B., Winningham, J.D., Spencer, N.W., and Brace, L.H. (1987c) Joule heating in the mesosphere and lower thermosphere during the 13 July 1982 solar proton event, *J. Geophys. Res.* **92**:6083-6090.
45. Hays, P.B., Killeen, T.L., Spencer, N.W., Wharton, L.E., Roble, R.G., Emery, B.E., Fuller-Rowell, T.J., Rees, D., Frank, L.A., and Craven, J.D. (1984) Observations of the dynamics of the polar thermosphere, *J. Geophys. Res.* **89**:5597-5612.
46. Hardy, D.A., Gussenhoven, M.S., Ratstrick, R., and McNeil, W.J. (1987) Statistical and functional representations of the pattern of auroral energy flux, number flux, and conductivity, *J. Geophys. Res.* **92**:12275-12294.
47. DeVries, L.L. (1972) Structure and motion of the thermosphere shown by density data from the Low-G Accelerometer Calibration System (LOGACS), *Space Res.* **12**:867-879.
48. Wu, S.T., Matsushita, S., and DeVries, L.L. (1974) An analysis of the upper atmospheric wind observed by LOGACS, *Planet. Space Sci.* **22**:1036.
49. Straus, J.M. (1978) Dynamics of the thermosphere at high latitudes, *Rev. Geophys. Space Phys.* **16**:183-194.
50. Marcos, F.A. and Forbes, J.M. (1985) Thermospheric winds from the satellite electrostatic triaxial accelerometer (SETA) system, *J. Geophys. Res.* **90**:6543-6552.
51. Killeen, T.L. and Roble, R.G. (1988) Thermosphere Dynamics: Contributions from the first five years of the Dynamics Explorer Program, *Rev. Geophys.* **26**:329-367.
52. Hernandez, G. and Killeen, T.L. (1987) Optical measurements of winds and temperatures in the upper atmosphere, in CIRA-86, *COSPAR International Reference Atmosphere*, Pergamon Press, in press.
53. Killeen, T.L., Smith, R.W., Spencer, N.W., Meriwether, J.W., Rees, D., Hernandez, G., Hays, P.B., Cogger, L.L., Sipler, D.P., Biondi M.A., and Tepley, C.A. (1986) Mean neutral circulation in the winter polar F-region, *J. Geophys. Res.* **91**:1633-1649.

54. Wharton, L.E., Spencer, N.W., and Mayr, H.G. (1984) The Earth's thermospheric superrotation from Dynamics Explorer 2, *Geophys. Res. Lett.* **11**:531-533.
56. Manson, A.H., et al. (1985) Mean winds of the upper middle atmosphere (60-110 km): a global distribution from radar systems (MF, meteor, VHF), Handbook for MAP, 16, 239-253.
57. Heppner, J.P. and Miller, M.L. (1982) Thermospheric winds at high latitudes from chemical releases, *J. Geophys. Res.* **87**:2633-2647.
58. Johnson, R.M. and Luhmann, J.G. (1985a) Neutral wind spectra at the auroral mesopause: Geomagnetic effect?, *J. Geophys. Res.* **90**:1735-1743.
59. Johnson, R.M. and Luhmann, J.G. (1985b) High-latitude mesopause neutral winds and geomagnetic activity: A cross-correlation analysis, *J. Geophys. Res.* **90**:8501-8506.
60. Johnson, R.M., Wickwar, V.B., Roble, R.G., and Luhmann, J.G. (1987) Lower thermospheric winds at high-latitude: Chatanika radar observations, *Annales Geophysicae* **5**:383-405.
61. Hunsucker, R.D. (1982) Atmospheric gravity waves generated in the high-latitude ionosphere: A review, *Rev. Geophys.* **20**:293-315.
62. Mayr, H.G., Harris, I., Varosi, F., and Herrero, F.A. (1984a) Global excitation of wave phenomena in a dissipative multi-constituent medium, 1, Transfer function of the Earth's thermosphere, *J. Geophys. Res.* **89**:10929-10959.
63. Mayr, H.G., Harris, I., Varosi, F., and Herrero, F.A. (1984b) Global excitation of wave phenomena in a dissipative multi-constituent medium, 2, Impulsive perturbations in the Earth's thermosphere, *J. Geophys. Res.* **89**:10961-10986.
64. Hines, C.O. (1960) Internal atmospheric gravity waves at ionospheric heights, *Can. J. Phys.* **28**:1441-1481.
65. Forbes, J.M. and Marcos, F.A. (1973) Thermosphere density variations associated with the auroral electrojet activity, *J. Geophys. Res.* **78**:3841-3847.
66. Prolss, G.W. and von Zahn, U. (1976) Large and small scale changes in the disturbed upper atmosphere, *J. Atmos. Terr. Phys.* **38**:655-659.
67. Potter, W.E., Kayser, D.C., and Mauersberger, K. (1976) Direct measurements of neutral wave characteristics in the thermosphere, *J. Geophys. Res.* **81**:5002-5012.
68. Champion, K.S.W. and Marcos, F.A. (1973) The triaxial accelerometer system on the Atmosphere Explorer, *Radio Sci.* **8**:197.
69. Killeen, T.L., Hays, P.B., Kennedy, B.C., and Rees, D. (1982) Stable and rugged etalon for the Dynamics Explorer Fabry-Perot interferometer, 2, Performance, *Applied Optics* **21**:3903-3912.
70. Killeen, T.L., Kennedy, B.C., Hays, P.B., Symanow, D.A., Ceckowski, D.H. (1983) An image plane detector for the Dynamics Explorer Fabry-Perot interferometer, *Applied Optics* **22**:3503-3513.
71. Hinteregger, H.E., Bedo, D.E., and Manson, J.E. (1973, April) The EUV spectrophotometer on Atmosphere Explorer, *Radio Science* **8**(No. 4):349.
72. Dalgarno, A., Hanson, W.B., Spencer, N.W., and Schmerling, E.R. (1973, April) The Atmosphere Explorer mission, *Radio Science* **8** (No. 4):263-266.
73. Danby, J.M.A. (1962) Fundamentals of celestial mechanics, MacMillan, NY.
74. Jensen, J., Townsend, G., Kork, J., and Kraft, D. (1962) Design Guide to orbital flight, McGraw-Hill pp. 252-253.